ผลกระทบของท่อนาโนไทเทเนียมไดออกไซด์ที่เติมด้วยเลดซัลไฟด์ควอนตัมดอทเพื่อเป็นชั้นส่งผ่านอิเล็กตรอนต่อประสิทธิภาพของเซลล์แสงอาทิตย์ชนิดเพอรอฟสไกต์

นายณัฐภัทร รัตนวิชัย

จุฬาลงกรณ์มหาวิทยาลัย
Chulalongkorn University

บทคัดย่อและแฟ้มข้อมูลฉบับเต็มของวิทยานิพนธ์ตั้งแต่ปีการศึกษา 2554 ที่ให้บริการในคลังปัญญาจุฬาฯ (CUIR)
เป็นแฟ้มข้อมูลของนิสิตเจ้าของวิทยานิพนธ์ ที่ส่งผ่านทางบัณฑิตวิทยาลัย
The abstract and full text of theses from the academic year 2011 in Chulalongkorn University Intellectual Repository (CUIR)
are the thesis authors' files submitted through the University Graduate School.

วิทยานิพนธ์นี้เป็นส่วนหนึ่งของการศึกษาตามหลักสูตรปริญญาวิศวกรรมศาสตรมหาบัณฑิต
สาขาวิชาวิศวกรรมเคมี ภาควิชาวิศวกรรมเคมี
คณะวิศวกรรมศาสตร์ จุฬาลงกรณ์มหาวิทยาลัย
ปีการศึกษา 2560
ลิขสิทธิ์ของจุฬาลงกรณ์มหาวิทยาลัย

Effects of PbS Quantum Dot doped TiO_2 Nanotubes as Electron Transporting Layer on the Efficiency of Perovskite Solar Cells

Mr. Natthapat Rattanawichai

จุฬาลงกรณ์มหาวิทยาลัย
CHULALONGKORN UNIVERSITY

A Thesis Submitted in Partial Fulfillment of the Requirements

for the Degree of Master of Engineering Program in Chemical Engineering

Department of Chemical Engineering

Faculty of Engineering

Chulalongkorn University

Academic Year 2017

Copyright of Chulalongkorn University

Thesis Title	Effects of PbS Quantum Dot doped TiO_2 Nanotubes as Electron Transporting Layer on the Efficiency of Perovskite Solar Cells
By	Mr. Natthapat Rattanawichai
Field of Study	Chemical Engineering
Thesis Advisor	Paravee Vas-Umnuay, Ph.D.

Accepted by the Faculty of Engineering, Chulalongkorn University in Partial Fulfillment of the Requirements for the Master's Degree

.....Dean of the Faculty of Engineering

(Associate Professor Supot Teachavorasinskun, Ph.D.)

THESIS COMMITTEE

.....Chairman

(Varun Taepaisitphongse, Ph.D.)

.....Thesis Advisor

(Paravee Vas-Umnuay, Ph.D.)

.....Examiner

(Associate ProfessorTawatchai Charinpanitkul, D.Eng.)

.....External Examiner

(Pisist Kumnorkaew, Ph.D.)

จุฬาลงกรณ์มหาวิทยาลัย
CHULALONGKORN UNIVERSITY

ณัฐภัทร รัตนวิชัย : ผลกระทบของท่อนาโนไทเทเนียมไดออกไซด์ที่เติมด้วยเลดซัลไฟด์ควอนตัมดอทเพื่อเป็นชั้นส่งผ่านอิเล็กตรอนต่อประสิทธิภาพของเซลล์แสงอาทิตย์ชนิดเพอรอฟสไกต์ (Effects of PbS Quantum Dot doped TiO_2 Nanotubes as Electron Transporting Layer on the Efficiency of Perovskite Solar Cells) อ.ที่ปรึกษาวิทยานิพนธ์หลัก: อ. ดร.ปารวี วาศน์อำนวย, 85 หน้า.

การสังเคราะห์ท่อนาโนไทเทเนียมไดออกไซด์ด้วยวิธีไฮโดรเทอร์มอลจากอนุภาคไทเทเนียมไดออกไซด์ขนาดแตกต่างกันดังนี้ 5, 25 และ 50 นาโนเมตร เพื่อให้ได้ท่อนาโนไทเทเนียมไดออกไซด์ที่มีพื้นที่ผิวสัมผัสมากที่สุดซึ่งเหมาะสำหรับใช้เป็นชั้นส่งผ่านอิเล็กตรอนในเซลล์แสงอาทิตย์ชนิดเพอรอฟสไกต์ พบว่าขนาดอนุภาคของไทเทเนียมไดออกไซด์ตั้งต้นขนาด 25 นาโนเมตรสังเคราะห์ได้ท่อนาโนไทเทเนียมไดออกไซด์ที่มีพื้นที่ผิวสัมผัสมากที่สุดประมาณ 312.39 ตารางเมตรต่อกรัม อย่างไรก็ตามไทเทเนียมไดออกไซด์นั้นมีข้อจำกัดที่ว่าจะดูดกลืนแสงที่มีความยาวคลื่นน้อยกว่าความยาวคลื่นแสงอาทิตย์หรือแสงที่มองเห็นได้และมีค่าแถบช่องว่างพลังงานที่กว้าง ดังนั้น จึงมีการเติมเลดซัลไฟด์ควอนตัมดอทลงในท่อนาโนไทเทเนียมไดออกไซด์ที่มีพื้นที่ผิวสัมผัสมากที่สุดเพื่อปรับปรุงการดูดกลืนแสงและค่าแถบช่องว่างพลังงาน โดยวัดค่าแถบช่องว่างพลังงานได้ 2.97 อิเล็กตรอนโวลต์ซึ่งมีค่าน้อยลง ท่อนาโนไทเทเนียมไดออกไซด์และท่อนาโนไทเทเนียมไดออกไซด์ที่เติมด้วยเลดซัลไฟด์ควอนตัมดอทถูกนำไปประยุกต์ใช้เป็นชั้นส่งผ่านอิเล็กตรอนในเซลล์แสงอาทิตย์ชนิดเพอรอฟสไกต์โดยถูกนำไปเติมลงในไทเทเนียมไดออกไซด์(นาโนเทค)ที่ความเข้มข้นแตกต่างกัน ผลสรุปว่าท่อนาโนไทเทเนียมไดออกไซด์ที่เติมด้วยเลดซัลไฟด์ควอนตัมดอทที่ความเข้มข้น 0.3 มิลลิกรัมต่อมิลลิลิตรให้ค่าประสิทธิภาพการแปลงพลังงานของอุปกรณ์เซลล์แสงอาทิตย์มากที่สุด คือ 14.95 เปอร์เซ็นต์ ซึ่งมีค่าสูงกว่าเซลล์แสงอาทิตย์ที่ไม่ได้มีการเติมท่อนาโนไทเทเนียมไดออกไซด์ที่เติมด้วยเลดซัลไฟด์ควอนตัมดอทถึง 15 เปอร์เซ็นต์ เพราะฉะนั้น ชั้นส่งผ่านอิเล็กตรอนรูปร่างแบบท่อขนาดเล็กเป็นการเพิ่มพื้นที่ผิวสัมผัสซึ่งทำให้ช่วยส่งผ่านอิเล็กตรอนได้ดีขึ้นในเซลล์แสงอาทิตย์ชนิดเพอรอฟสไกต์ นอกจากนี้การเติมเลดซัลไฟด์ควอนตัมดอทลงในชั้นส่งผ่านอิเล็กตรอนเป็นการปรับปรุงประสิทธิภาพของเซลล์แสงอาทิตย์และแถบช่องว่างพลังงานให้มีความเหมาะสมกับเซลล์แสงอาทิตย์ชนิดเพอรอฟสไกต์

ภาควิชา วิศวกรรมเคมี ลายมือชื่อนิสิต .....

สาขาวิชา วิศวกรรมเคมี ลายมือชื่อ อ.ที่ปรึกษาหลัก .....

ปีการศึกษา 2560

5870335921 : MAJOR CHEMICAL ENGINEERING

KEYWORDS: TIO2 NANOTUBES / ELECTRON TRANSPORTING LAYER / PEROVSKITE SOLAR CELL / LEAD SULFIDE QUANTUM DOTS / ENERGY BAND GAP

NATTHAPAT RATTANAWICHAI: Effects of PbS Quantum Dot doped TiO_2 Nanotubes as Electron Transporting Layer on the Efficiency of Perovskite Solar Cells. ADVISOR: PARAVEE VAS-UMNUAY, Ph.D., 85 pp.

TiO_2 nanotubes (TNTs) are used as an excellent electron transporting layer for high efficiency perovskite solar cells. In this work, TNTs were synthesized via hydrothermal process from different particle sizes of TiO_2 nanoparticle precursors as follows: 5 nm, 25 nm, and 50 nm. The highest surface area of 312.39 m^2/g of TNTs was obtained from TiO_2 precursor with particle size of 25 nm and was used to dope with lead sulfide quantum dots (PbS QDs). Due to a large band gap and poor conductivity of TNTs which limits the efficiency to transport electrons in the perovskite solar cell, PbS QDs doped TNTs were prepared to modify the valence and conduction energy bands of TNTs which can enhance the power conversion efficiency of perovskite solar cells. A slight decrease in the energy band gap of PbS QDs doped TNTs to about 2.97 eV was obtained. Both pure TNTs and PbS QDs doped TNTs were deposited onto the perovskite layer as the ETL with various concentrations of TNTs and PbS QDs doped TNTs in TiO_X. The best power conversion efficiency (PCE) of the perovskite device prepared from the concentrations of 0.3 mg/ml of PbS QDs doped TNTs in TiO_X is 14.95%, which is about 15% higher than that of perovskite solar cell with pure TNTs in TiO_X. As a consequence, ETL in nanotube structure has proved to be an efficient structure for transporting electrons in the perovskite solar cell. Moreover, high surface area TNTs offer the enhanced interfacial area for doping with PbS QDs, which ultimately improved the property of ETL and resulted in the enhanced PCE as a consequence of appropriate band gap.

จุฬาลงกรณ์มหาวิทยาลัย
Chulalongkorn University

Department:	Chemical Engineering	Student's Signature	.....
Field of Study:	Chemical Engineering	Advisor's Signature	.....
Academic Year:	2017		

ACKNOWLEDGEMENTS

First of all, the author would like to convey my sincere thanks to my advisor, Dr. Paravee Vas-Umnuay, Department of Chemical Engineering, Chulalongkorn University, for introducing me to this interesting project with the greatest advice, deep discussion and constant encouragement throughout this project including the instructing for developing the self-learning.

Moreover, the author also would like to express my grateful thanks to my thesis examiners, Dr. Varun Taepaisitphongse, Associate Professor Dr. Tawatchai Charinpanitkul, and Dr. Pisist Kumnorkaew for their useful comments, recommendation and participation as the thesis committee.

Further, the author would like to acknowledge the full support to Dr. Pisist Kumnorkaew, Dr. Chalita Ratanatawanate, Dr. Tanyakorn Muangnapoh and Mr. Khathawut Lohawet, National Nanotechnology Center (NANOTEC) for financial support, experimental preparation, analysis instrument and recommendation.

In addition, the author would like to thank all member of Center of Excellence in Particle Technology for their kind, friendship and helpful suggestions which support me to achieve this goal.

จุฬาลงกรณ์มหาวิทยาลัย
CHULALONGKORN UNIVERSITY

Last but not least, I would like to express my greatest thanks to my family and my friend for their encouragement and total support. Without their encouragement, this achievement would not have been possible.

CONTENTS

Page

THAI ABSTRACT iv

ENGLISH ABSTRACT v

ACKNOWLEDGEMENTS vi

CONTENTS vii

LIST OF TABLES xi

LIST OF FIGURES xii

CHAPTER 1 INTRODUCTION 1

1.1 Introduction 1

1.2 Objectives of Research 5

1.3 Scope of research 6

1.3.1 Characterization of TNTs. 8

1.3.2 Characterization of PbS QDs doped TNTs. 9

1.3.3 Characterization of perovskite solar cells. 10

CHAPTER 2 THEORY AND LITERATURE REVIEW 11

2.1Solar cells. 11

2.1.1 Principle of solar cells. 12

2.1.2 Types of solar cells. 13

2.2 Perovskite Solar Cells and device structure. 16

2.2.1 Perovskite crystal structure. 16

2.2.2 Planar structure of Perovskite Solar Cells. 17

2.2.3 Principles of Perovskite Solar Cells. 20

2.2.4 Solution processing techniques. 22

จุฬาลงกรณ์มหาวิทยาลัย
Chulalongkorn University

Page

2.2.4.1 Spin-coating technique. 22
2.2.4.2 Dip-coating technique. 23
2.2.4.3 Rapid convective deposition. 24
2.2.5 Solution process fabrication of perovskite layer. 25
2.3 Titanium dioxide (TiO_2) 26
2.3.1 Properties and applications of Titanium dioxide. 26
2.3.2 Phases structure of Titanium dioxide. 28
2.3.3 Morphologies and Nanostructures of Titanium dioxide. 30
2.3.4 Typical methods to synthesize TiO_2 nanotubes. 32
2.3.4.1 Template-assisted method. 32
2.3.4.2 Sol–gel process. 33
2.3.4.3 Electrochemical anodic oxidation. 34
2.3.4.4 Hydrothermal treatment. 34
2.3.5 Formation mechanism of TiO_2 nanotubes. 35
2.4 Lead Sulfide Quantum Dots (PbS QDs). 36
2.4.1 PbS QDs doped TNTs. 37
2.5 Performance Characteristics. 38
2.5.1 Current-voltage (I-V) characteristics. 38
2.5.2 External quantum efficiency (EQE). 39
2.6 Literature review. 40
CHAPTER 3 EXPERIMENTAL 44
3.1 Preparation of TNTs. 44

จุฬาลงกรณ์มหาวิทยาลัย
Chulalongkorn University

Page

3.1.1 Materials. 44

3.1.2 Synthesis of TNTs. 44

3.2 Deposition of PbS QDs onto TNTs. 45

3.3 Fabrications of perovskite solar cells. 45

3.3.1 Device Preparation. 46

3.3.2 Fabrication of conventional planar perovskite solar cell by one-step deposition. 47

3.4 Analytical instruments. 47

3.4.1 Characterization of TNTs. 48

3.4.2 Characterization of PbS QDs doped TNTs. 48

3.4.3 Characterization of Perovskite Solar Cells. 48

CHAPTER 4 RESULTS AND DISCUSSION 50

4.1 Synthesis of TNTs via hydrothermal process 50

4.1.1 Morphology and structure of TNTs. 50

4.1.2 Phase structure of TNTs. 53

4.1.3 Particle size distributions of synthesized TNTs. 54

4.1.4 Surface area of TNTs. 55

4.1.5 UV-vis absorption spectrum and energy band gap of TNTs. 56

4.2 Deposition of PbS QDs onto TNTs. 58

4.2.1 Morphology and structure of PbS QDs doped TNTs. 58

4.2.2 Phase structure of PbS QDs doped TNTs. 60

4.2.3 The elemental and chemical composition of PbS QDs doped TNTs. 61

จุฬาลงกรณ์มหาวิทยาลัย
CHULALONGKORN UNIVERSITY

Page

4.2.4 Comparison of UV-vis absorption spectra and energy band gap of pure TNTs and PbS QDs doped TNTs. 62

4.3 Fabrications of perovskite solar cells by one-step deposition solution processes. 64

4.3.1 Morphology and microstructure of perovskite film with PbS QDs doped TNTs as ETL. 65

4.3.2 UV-Vis spectrum and energy band gap of TiO_x: PbS QDs doped TNTs thin film with various concentrations. 66

4.3.3 Photovoltaic properties of perovskite solar cells 71

CHAPTER 5 CONCLUSION 81

5.1 Conclusions 81

5.2 Recommendations for the future work. 82

REFERENCES 83

VITA 85

จุฬาลงกรณ์มหาวิทยาลัย
CHULALONGKORN UNIVERSITY

LIST OF TABLES

Table 2.1 Physical properties of crystal structure of Titanium dioxide……..30

Table 2.2 BET surface areas and band gap for TiO_2 nanoparticle (NP), nanotube (NT), nanofiber (NF), nanowire (NW) and Degussa P-25 nanostructured samples……..32

Table 4.1 The average surface area of TiO_2 nanoparticles and TiO_2 nanotubes (TNTs) prepared from different sizes of TiO_2 precursors……..55

Table 4.2 The energy band gap of TNTs prepared from different sizes of TiO_2 precursors……...58

Table 4.3 The elemental and chemical composition of the synthesized PbS QDs doped TNTs……...62

Table 4.4 The energy band gap of TNTs without PbS QDs and PbS QDs doped TNTs……64

Table 4.5 Energy band gaps of ETL with various concentrations of PbS QDs doped TNTs in TiO_x……...71

Table 4.6 The performance of perovskite devices with difference ETL……..73

Table 4.7 The performance of perovskite devices with difference ETL……..77

จุฬาลงกรณ์มหาวิทยาลัย
CHULALONGKORN UNIVERSITY

LIST OF FIGURES

Figure 1.1 The developments of different kinds of solar cells are depicted……3

Figure 1.2 The device structure of perovskite solar cell……..4

Figure 1.3 Scope of research……...6

Figure 1.4 Preparation of electron transporting layer……...7

Figure 1.5 Characterization of TiO_2 nanotubes……...…8

Figure 1.6 Characterization of PbS QDs doped TNTs……9

Figure 1.7 Characterization of perovskite solar cells……10

Figure 2.1 A solar cell to a PV system ……..…...11

Figure 2.2 Basic operating principle of solar cells……12

Figure 2.3 Diagram of type of solar cells classified by generation……..15

Figure 2.4 Crystalline and amorphous silicon solar cell……15

Figure 2.5 Unit cell of basic ABX_3 perovskite structure……16

Figure 2.6 The device structure of perovskite solar cell……18

Figure 2.7 Schematic diagram of planar heterojunction solar cells……19

Figure 2.8 Principles of Perovskite Solar Cells……20

Figure 2.9 Energy level diagram of the materials used in perovskite solar cells……..21

Figure 2.10 Schematic of the spin-coating process……...23

Figure 2.11 Schematic of the dip-coating process……23

Figure 2.12 Schematic showing rapid convective deposition experimental setup……...24

จุฬาลงกรณ์มหาวิทยาลัย
Chulalongkorn University

Figure 2.13 Two general deposition methods for preparing perovskite active layers…..26

Figure 2.14 Applications of TiO_2 photo catalysis……27

Figure 2.15 Schematic illustration of the formation of photogenerated ……..28

Figure 2.16 Crystalline structures of titanium dioxide……29

Figure 2.17 TEM images of TiO_2 nanostructures……31

Figure 2.18 Illustration of two different types of hard templates……..33

Figure 2.19 Schematic drawing of the exfoliation and scrolling mechanism of nanotubes formation……36

Figure 2.20 Preparation of PbS QDs on TiO_2 nanotubes……...37

Figure 2.21 I-V characteristics of photovoltaic module……..38

Figure 2.22 The quantum efficiency of a silicon solar cell ……40

Figure 3.1 The conventional (n-i-p) planar perovskite solar cells……46

Figure 4.1 TEM images of TNTs synthesized via hydrothermal process from TiO_2 precursor with particle size of 5 nm……..50

Figure 4.2 TEM images of TNTs synthesized via hydrothermal process from TiO_2 precursor with particle size of 25 nm……51

Figure 4.3 TEM images of TNTs synthesized via hydrothermal process from TiO_2 precursor with particle size of 50 nm……51

Figure 4.4 TEM images of High magnification of outer diameter and inner diameter of the TNTs……..52

Figure 4.5 XRD patterns of TNTs synthesized via hydrothermal process from different particle sizes of TiO_2 nanoparticle precursors……53

จุฬาลงกรณ์มหาวิทยาลัย
Chulalongkorn University

Figure 4.6 Particle size distributions from DLS measurement of TNTs prepared from NaOH hydrothermal treatment with different sizes of TiO_2 precursors……54

Figure 4.7 UV-vis absorption spectra of as-prepared TNTs via hydrothermal process from different particle sizes of TiO_2 nanoparticle precursors 5, 25 and 50 nm……..56

Figure 4.8 The energy band gap of TNTs as-prepared via hydrothermal process from particle sizes of TiO_2 nanoparticle precursors 5, 25 and 50 nm……..57

Figure 4.9 TEM images of TNTs synthesized via hydrothermal process from TiO_2 precursor with particle size of 50 nm with low magnification……59

Figure 4.10 a).TEM images of a). PbS QDs inside and outside TNTs b). The average particles size of PbS QDs……60

Figure 4.11 XRD patterns of (a) standard TiO_2 with crystal structure of anatase from JCPDS 71-5576, (b) TNTs synthesized via hydrothermal process after annealing, (c) PbS QDs doped TNTs and (d) Galena (PbS) from JCPDS 05-0592……61

Figure 4.12 UV-vis absorption spectra of TNTs without PbS QDs and PbS QDs doped TNTs……63

Figure 4.13 The energy band gap of TNTs without PbS QDs and PbS QDs doped TNTs……...63

Figure 4.14 Cross-sectional SEM image of perovskite solar cell using one-step deposition method……65

Figure 4.15 Transmittance spectra of ETL with various concentrations of PbS QDs doped TNTs in TiO_X……..67

Figure 4.16 UV-Vis absorption spectra of ETL with various concentrations of PbS QDs doped TNTs in TiO_X……..68

จุฬาลงกรณ์มหาวิทยาลัย
CHULALONGKORN UNIVERSITY

Figure 4.17 Energy band gaps of ETL with various concentrations of PbS QDs doped TNTs in TiO_X.....68

Figure 4.18 The energy level alignment in the hybrid perovskite solar cell.....70

Figure 4.19 Energy diagram of TiO_2 and CQDs/TiO_2 as ETL in perovskite solar cells....70

Figure 4.20 Photovoltic performance of perovskite devices with various concentrations of TNTs in TiO_X as ETL.....73

Figure 4.21 Power conversion efficiency of perovskite devices with various concentrations of TNTs in TiO_X as ETL.....74

Figure 4.22 TNTs suspension with various concentrations of TNTs in TiO_X 74

Figure 4.23 The conventional (n-i-p) planar perovskite solar cells.....75

Figure 4.24 Photovoltic performance of perovskite devices with various concentrations of PbS QDs doped TNTs in TiO_X as ETL.....76

Figure 4.25 Power conversion efficiency of perovskite devices with various concentrations of PbS QDs doped TNTs in TiO_X as ETL.....78

Figure 4.26 PbS QDs doped TNTs suspension with various concentrations of PbS QDs doped TNTs in TiO_X (mg/ml).....78

Figure 4.27 External Quantum efficiency curves of the best perovskite solar cells prepared with different in ETL.....79

Figure 4.28 Power conversion efficiency of the best perovskite solar cells prepared with different in ETL.....80

จุฬาลงกรณ์มหาวิทยาลัย
Chulalongkorn University

CHAPTER 1
INTRODUCTION

1.1 Introduction

Electrical energy is the most essential and useful for human being and it is also one of the fundamental factors for manufacturing industries. Most of electrical energy is produced from fossil fuels, such as petroleum, natural gas and coal, which are non-renewable energy. The use of energy from fossil fuel combustion gives excessive greenhouse gas emissions, which causes air pollution, acid rain and leads to global warming. Because of limitation of fossil fuels and the hazard to the environment, researchers have been attempting to find new alternative energies to produce electricity and reduce the use of energy from fossil fuels [1].

Clean and renewable energies, for instance, wind energy, biomass, hydro energy, water wave energy, tidal power, geothermal energy and solar energy are basically defined as the energy that can be collected from natural resources around us which cannot be exhausted. They can be constantly renewed in short time without any negative effects to the environment [2].

จุฬาลงกรณ์มหาวิทยาลัย
Chulalongkorn University

Solar energy is one of the most important and the first choice renewable energy sources, which is the most abundant, widely distributed all around the world, not limited, pollution free and clean. Solar cells are electrical device, made from semiconductor, which can convert solar energy into electrical energy directly [3]. Solar cells can be classified into 3 main generations [4] ; the first generation solar cells are crystalline silicon solar cell made from crystalline silicon materials, such as single crystalline (sc-Si) and multi crystalline (mc-Si). The second generation solar cells are thin film solar cell made from amorphous silicon materials and compound semiconductors, such as amorphous silicon solar cell (a-Si), copper indium gallium diselenide solar cells (CIGS), cadmium telluride solar cells (CdTe) and copper zinc tin sulphide solar cells (CZTS). Both of the first and second generation solar cells are produced from inorganic materials, which have

high power conversion efficiency (PCE) and stability, but manufacturing of these cells is still too expensive, complicated process to produce with high technology and hazardous for health and environment [5]. Currently, researchers are searching and developing the new generation solar cells, which are produced from organic materials, such as dye sensitized solar cell (DSSC), organic photovoltaic cell (OPV), quantum dot solar cell, and hybrid materials solar cell. The DSSC and OPV have low cost of materials and a simple fabrication process but they have low power conversion efficiency as compared to those of the first and second generation solar cells. Furthermore, their long-term stability and durability is still limited [6].

Consequently, the hybrid materials solar cells have been developed, which are fabricated from a combination of organic and inorganic semiconducting materials. The advantages of these solar cells consist of a high power conversion efficiency, low cost, lightweight and easy fabrication [7].

Perovskite solar cells are one of the most promising hybrid materials due to their high power conversion efficiency, low cost, light weight, superb light-harvesting characteristics, easy improve energy band gap and simple fabrication process at low temperature. [8] Perovskite is the crystal structure with a general chemical formula of ABX_3, where A is cation, such as $CH_3NH_3^+$, or $NH_2CHNH_2^+$), B is metal cation, such as Pb^{2+}, Sn^{2+} and X is halide anions, such as Cl^-, Br^-, or I^- [9]. In 2009, Miyasaka and colleagues incorporated perovskite semiconductors into photovoltaic devices and obtained a power conversion efficiency (PCE) of 3.81% [10]. The power conversion efficiency of perovskite solar cells have been increasing from approximately 4% to over 20% in the past few years , as shown in Figure1.1.[11]

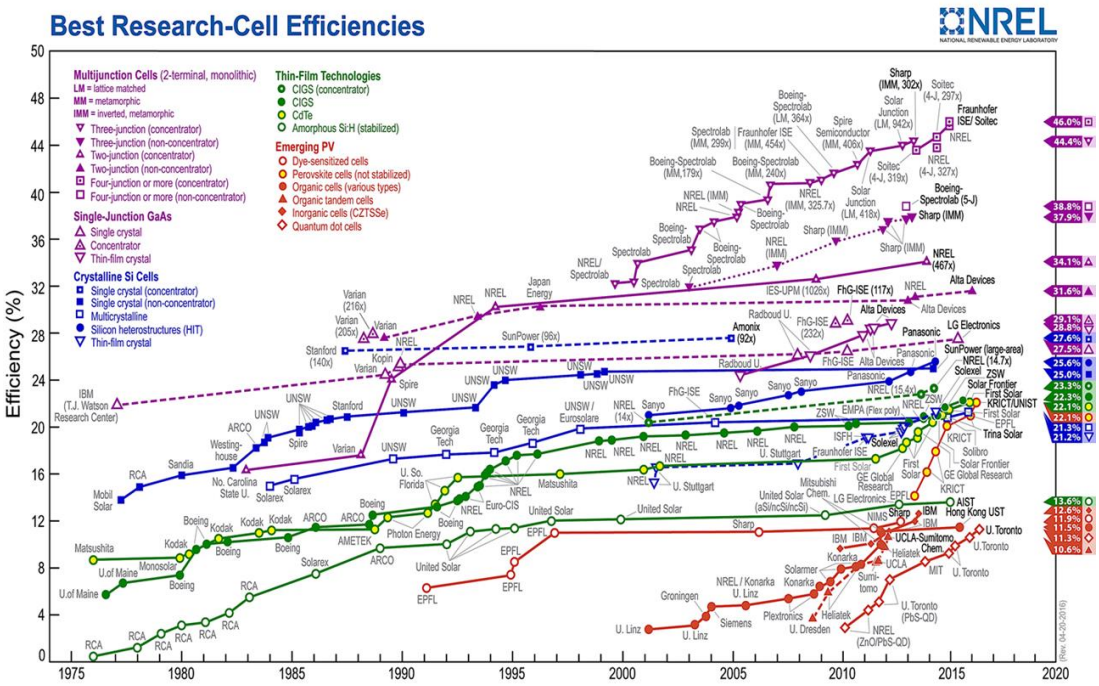

Figure 1.1 The developments of different kinds of solar cells are depicted [2].

The device structures of perovskite solar cell are respectively depicted in Figure 1.2. [11] The transparent conductive oxide (TCO) layer, for instance, Indium tin oxide (ITO) and fluorine-doped tin oxide (FTO), is usually coated on a substrate such as glass, which makes it as the transparent electrode of the solar cell. Electron transporting layer (ETL) is thin film of a semiconductor coated on the substrate which helps to transfer electrons from the perovskite layer. Perovskite layer or absorber layer is a layer which absorbs the sun light and transfers electron and hole to the next layer. Hole transporting layer (HTL) is another important layer for preventing the contact between the metal and perovskite layers so, it can reduce the problem of recombination between electrons and holes. Also, it helps to transfer a hole to the next layer. Metal is a counter electrode which will receive hole and makes a completely electric circuits. Normally, it is made from Au and Al [12] .

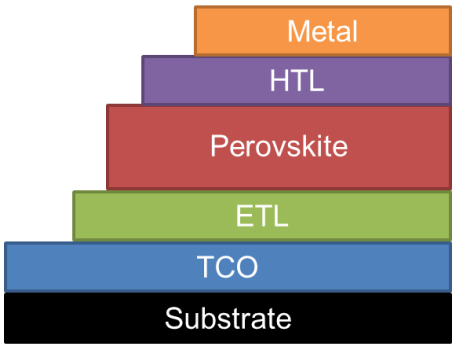

Figure 1.2 The device structure of perovskite solar cell.

Preparation methods for perovskite solar cells consist of two main methods, including one-step deposition method and two-step deposition method. For one-step deposition method, a precursor solution is prepared by mixing CH_3NH_3I (MAI) or $CH(NH_2)_2I$ (FAI) and PbI_2 in polar aprotic solvents such as Dimethylacetamide (DMA) or gamma-butyrolactone (GBL). After that spin-coating the precursor solution on the substrate, then drying and heating at low temperatures (70°C ~ 170°C). For two-step deposition method, a precursor solution is prepared by mixing PbI_2 and N,N – dimethylformamide (DMF), which is first coated on the substrate by spin-coating and then Iso-propyl alcohol (IPA) of CH_3NH_3I (MAI) or $CH(NH_2)_2I$ (FAI) is spun on the PbI_2 film, then dry and heat at low temperatures (70°C ~ 170°C) [13].

Titanium dioxide (TiO_2) is a well-known n-type semiconductor with good photocatalytic activities and great potential in many other areas, including converting sunlight to electricity (solar cell), environmental purification, photovoltaic and gas sensors. Furthermore, TiO_2 can be used as an electron transporting layer for perovskite solar cells which helps to transfer electrons from perovskite layer [14].

Gratzel and colleagues [15] used one-step and two-step deposition methods onto the TiO_2 film for perovskite solar cells, which resulted in power conversion efficiency (PCE) of 7.5% and 13.9%, respectively. Dongqin Bi's group [16] used a two-step deposition method for preparing $CH_3NH_3PbI_3$ perovskite solar cells onto ZrO_2 and TiO_2 mesoporous layer, resulting in power conversion efficiency (PCE) of 10.8% and 9.5%, respectively.

Kang- Du et al [17] improved the efficient absorption of solar energy from the sun light and modified the energy band gap of TiO_2 nanotubes (TNTs) by depositing PbS QDs into anodized TiO_2 nanotube via ultrasonic-assisted dip coating approach. The absorption spectra of TNTs decorated with PbS QDs have been extended to the visible light and enhanced the photocurrent of TiO_2 nanotubes.

However, TiO_2 possesses a large band gap which limits the efficiency of energy conversion [18]. In this research, TiO_2 nanotubes (TNTs) were synthesized via hydrothermal process. Then, lead sulphide (PbS) quantum dots (QDs) are applied to modify the band gap of TiO_2 to match with the solar spectrum. Perovskite solar cells will be fabricated and developed by one-step solution processes via spin coating and rapid convective deposition processes and investigated to find the optimized operating conditions. Characterization of physical and electrical properties of the obtained cell will be investigated in order to achieve high power conversion efficiency.

1.2 Objectives of Research.

1. To investigate the effect of different sizes of TiO_2 precursors to prepare TiO_2 nanotubes as the electron transporting layer on the morphology, surface area and crystal structure.

2. To investigate and compare the effect of bare TiO_2 nanotubes and PbS quantum dot doped TiO_2 nanotubes, as the electron transporting layer (ETL), in perovskite solar cells in terms of the absorption spectrum and solar cell performance.

3. To investigate and find the optimized operating condition based on various concentrations of TiO_2 nanotubes and PbS quantum dot doped TiO_2 nanotubes, which will be added in TiO_X as the electron transporting layer for conventional planar perovskite solar cells in terms of the solar cell performance.

จุฬาลงกรณ์มหาวิทยาลัย
Chulalongkorn University

1.3 Scope of research

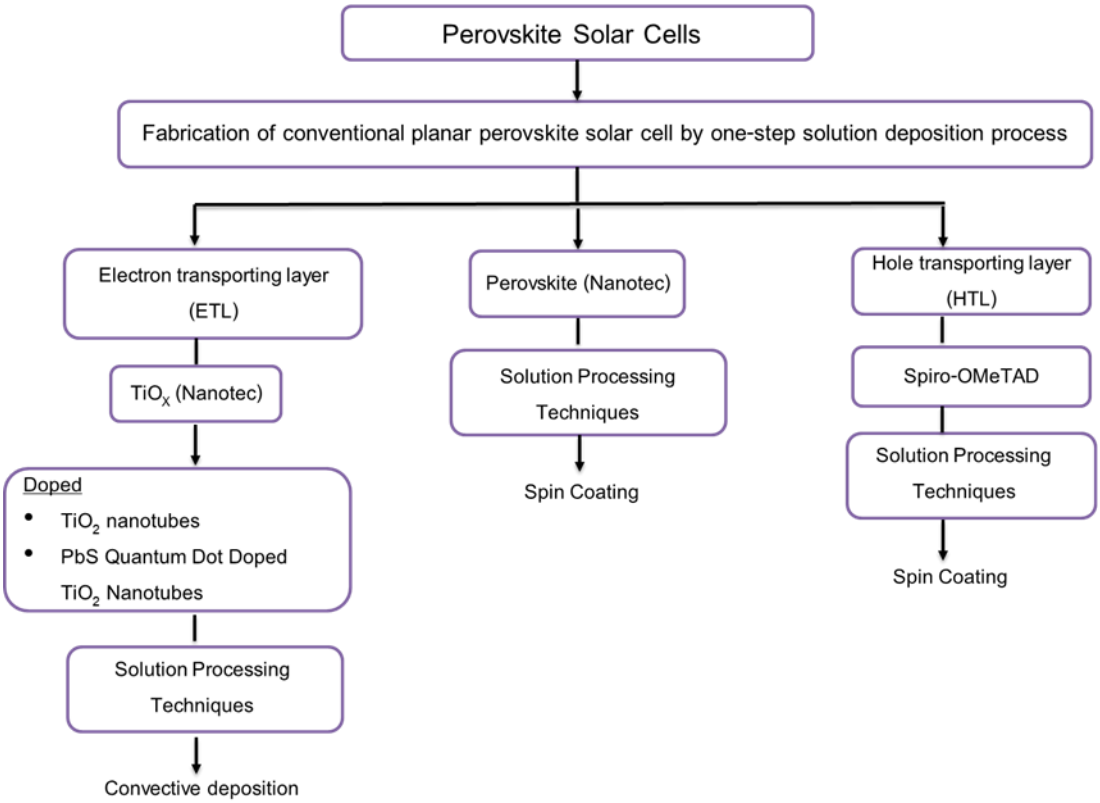

Figure 1.3 Scope of research.

จุฬาลงกรณ์มหาวิทยาลัย

This research is focused on the study of fabrication of perovskite solar cells using one-step deposition solution process. According to figure 1.3, the effects of fabrication process parameters on power conversion efficiency (PCE) will be investigated, including types of electron transporting layer, different precursors to prepare electron transporting layer and concentration of TiO_2 nanotubes (TNTs) and PbS quantum dot (PbS QDs) doped TNTs, which will be added in TiO_X as the electron transporting layer. The followings describe the fabrication method of each layer of perovskite solar cell, including film characterization and device performance.

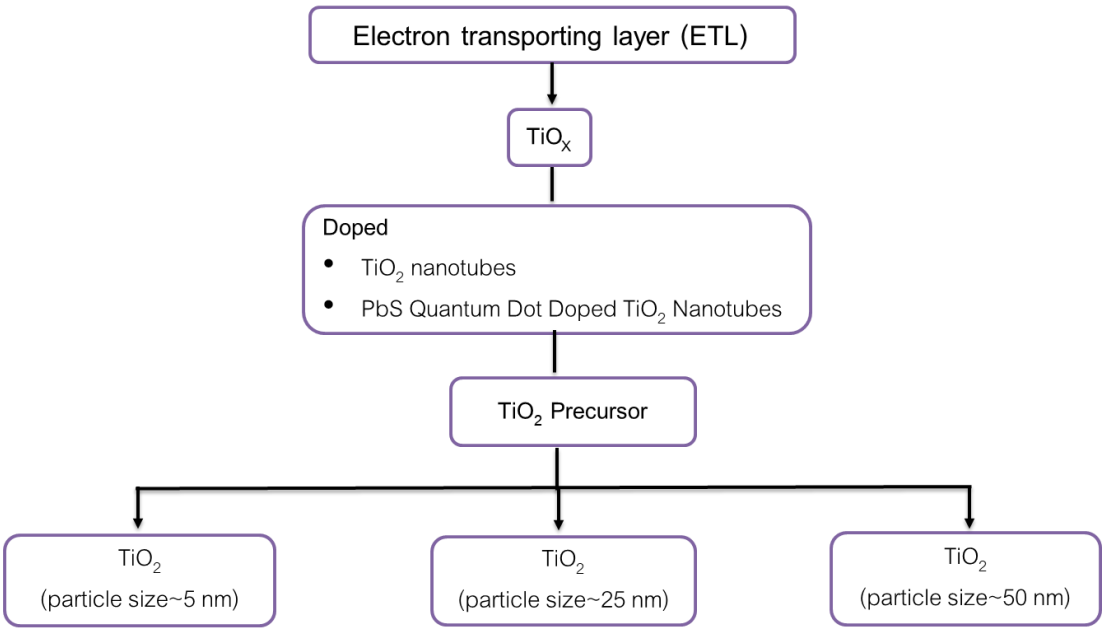

Figure 1.4 Preparation of electron transporting layer.

According to figure 1.4, the effects of preparation of electron transporting layer for perovskite solar cell on power conversion efficiency (PCE) will be investigated, which can be described as follows:

1. Investigate the effect of different sizes of TiO_2 precursors, *i.e.* 5, 25 and 50 nm, to prepare TNTs which will be added in TiO_X as the electron transporting layer.

2. Investigate the effect of PbS QDs doped TNTs with the highest surface area and suitable energy band gap obtained from the first step, which will be added in TiO_X as the electron transporting layer.

1.3.1 Characterization of TNTs.

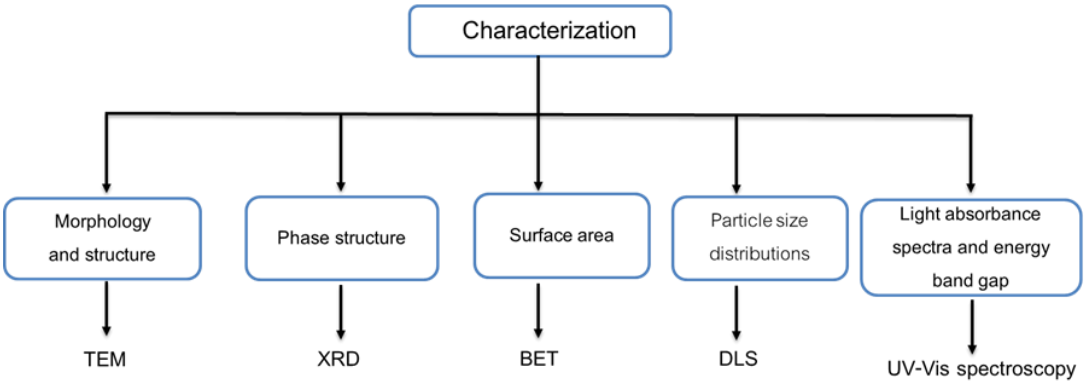

Figure 1.5 Characterization of TiO_2 nanotubes.

Figure 1.5 demonstrates all of the characterization methods required for the investigation of the obtained TNTs, which can be described as follows:

1. Transmission electron microscopy (TEM): Observe morphology and structure.
2. X-ray diffraction (XRD): Analyse the phase structure.
3. Brunauer-Emmett-Teller (BET) : Measure the surface area
4. Dynamic light scattering (DLS): Analyse the particle size distribution.
5. UV-Vis spectroscopy: Measure the light absorbance spectra and energy band gap.

1.3.2 Characterization of PbS QDs doped TNTs.

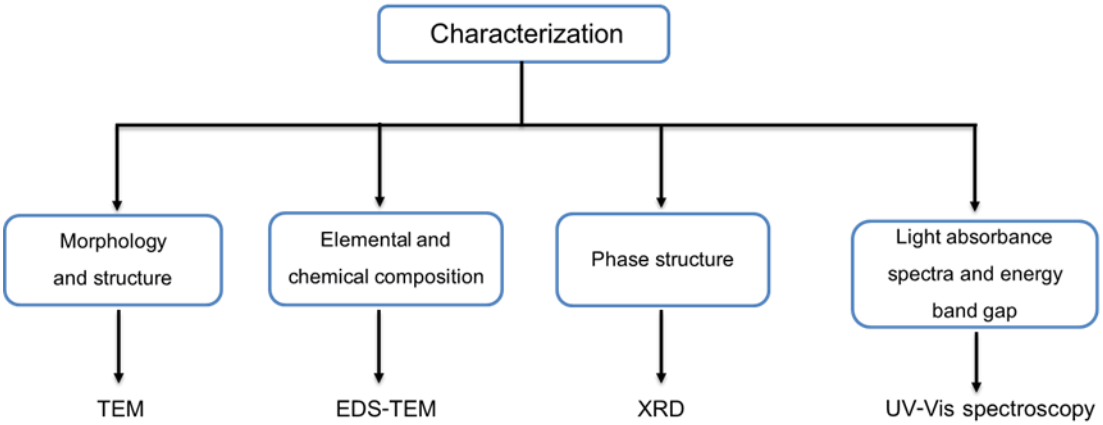

Figure 1.6 Characterization of PbS QDs doped TNTs.

According to figure 1.6, the characterization of PbS QDs doped TNTs, which can be described as follows:

1. Transmission electron microscopy (TEM): Observe morphology and structure.
2. Energy dispersive x-ray spectroscopy (EDS) in the TEM: Analyse the elemental and chemical composition.
3. X-ray diffraction (XRD): Analyse the phase structure.
4. UV-Vis spectroscopy: Measure the light absorbance spectra and energy band gap.

1.3.3 Characterization of perovskite solar cells.

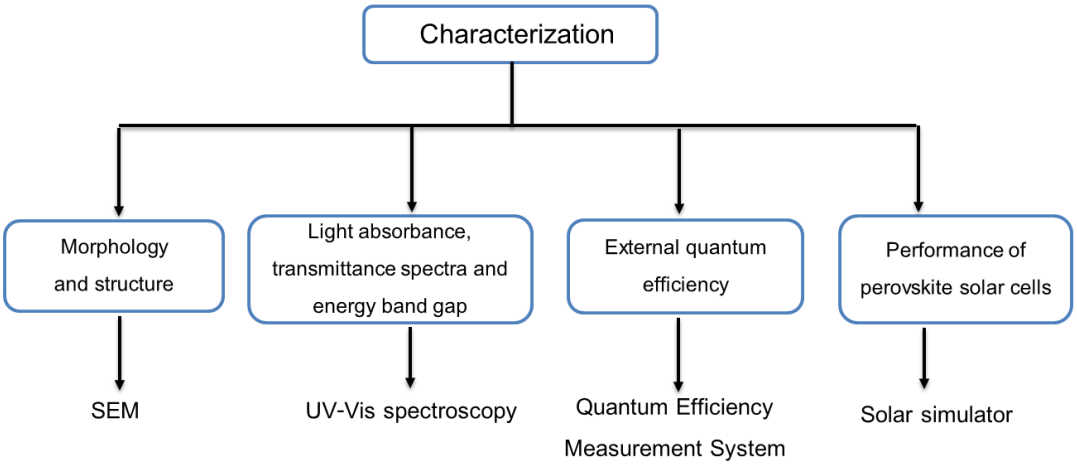

Figure 1.7 Characterization of perovskite solar cells.

As can be seen in figure 1.7, all of the characterization techniques required for the investigation of the solar cell performance, which can be described as follows

1. Scanning electron microscope (SEM): Observe morphology and thickness of perovskite thin films.
2. UV-Vis spectroscopy: Measure the light absorbance, transmittance spectra and energy band gap.
3. Quantum Efficiency Measurement System: Measure the external quantum efficiency.
4. Solar simulator: Measure power conversion efficiency (PCE), Fill factor (FF), open circuit voltage (V_{oc}) and photocurrent density-voltage (J-V) curves.

ALONGKORN UNIVERSITY

CHAPTER 2
THEORY AND LITERATURE REVIEW

2.1 Solar cells.

Solar cells or photovoltaic cells are electrical device, made from semiconductor, can convert solar energy into electrical energy directly by the photovoltaic effect, which is a physical and chemical phenomenon. Assemblies of solar cells are used to make solar modules which generate electrical power from sunlight, as distinguished from a "solar thermal module" or "solar hot water panel". A solar panel will be generate solar power using solar energy, as shown in Figure 2.1 [19].

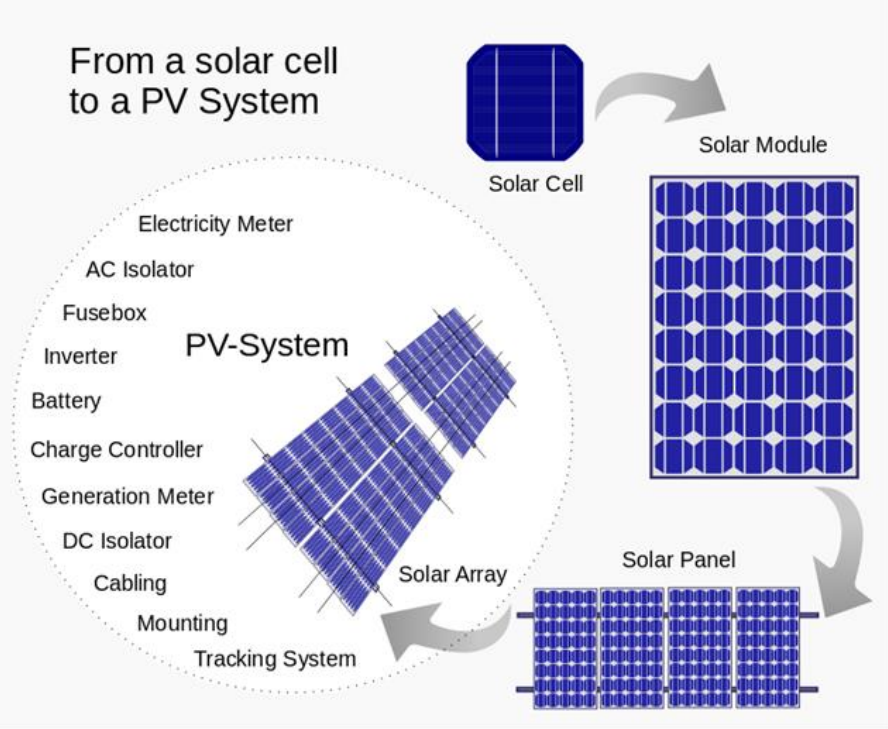

Figure 2.1 A solar cell to a PV system [19].

2.1.1 Principle of solar cells.

In terms of device operation, the most basic structure of solar cell is p-n junction of silicon solar cell, in which its function is built an electric field to separate negative charge (electron) and positive charge (hole). Silicon solar cell composes of a p-type semiconductor with doping boron (B-) which has ability to accept electrons and n-type semiconductor with doping phosphorous (P+) which has ability to donate electrons [20], as shown in Figure 2.2.

When photon contacts with silicon solar cell, three things can occur:

(1) The photon can pass straight through the device.

(2) The photon can reflect back the surface.

(3) The photon can be absorbed on the silicon semiconductor.

In case of the absorbed photon in solar cell, it can produce electrons and holes since the electrons are excited and then they can transport through n-type to front electrode (-). While the holes flow through p-type to back electrode (+). Finally, when the both electrodes of solar cell connect to load, light bulb, they can create direct electric current [21].

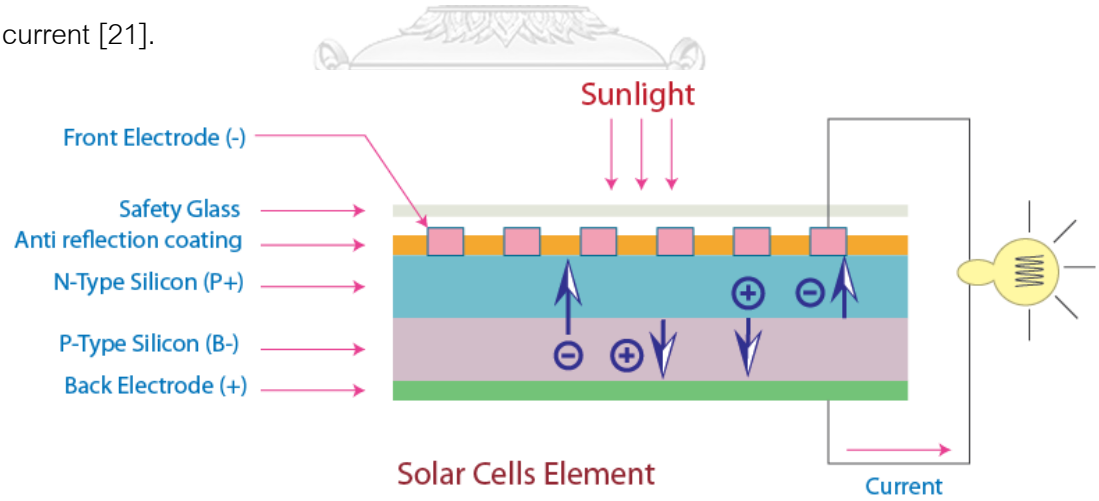

Figure 2.2 Basic operating principle of solar cells [20].

2.1.2 Types of solar cells.

Solar cells can be separated into two groups, mainly based on types of semiconducting material as photoactive layer and charge transporting layer, i.e. organic and inorganic materials. Furthermore, solar cells can be classified into three main generations [19], mainly based on technologies of solar cells, as shown in Figure 2.3. The first generation solar cells are crystalline silicon solar cell made from crystalline silicon materials, in which these cells have been currently the commercial solar cells. Silicon solar cells have high performance, with the power conversion efficiency up to 25%, but these cells are high costs because the production costs of devices are still expensive and hazardous for health and environment [28]. For example, single crystalline (sc-Si) or monocrystalline silicon solar cell and multi crystalline (mc-Si) or polycrystalline silicon solar Cell [22], as shown in Figure 2.4.

The second generation solar cells are thin film solar cell made from amorphous silicon materials and compound semiconductors such as amorphous silicon solar cell (a-Si) which is the non-crystalline form of silicon, requires low process temperature, enabling module production on flexible and low cost substrates, efficiency achieved ~ 15 % in lab scale and it is abundant and non-toxic, copper indium gallium diselenide solar cells (CIGS) which is manufactured by depositing a thin layer of copper, indium, gallium and selenide on glass or plastic backing, along with electrodes on the front and back to collect current and the highest efficiency achieved about 20.4%, cadmium telluride solar cells (CdTe) which is based on the use of cadmium telluride, a thin semiconductor layer designed to absorb and convert sunlight into electricity and the highest efficiency achieved about 21% and copper zinc tin sulphur solar cells (CZTS) which is compound semiconductor made of copper, zinc, tin and sulphur. The second generation solar cell has high power conversion efficiency (PCE) and stability, but these cells are still too expensive, complicated process to produce with high technology and hazardous for health and environment because of some toxic material (cadmium) and some rare earth material (indium) [23].

จุฬาลงกรณ์มหาวิทยาลัย
Chulalongkorn University

From the previous problems, the researchers are searching and developing the third generation solar cells, which are produced from organic materials such as dye sensitized solar cell (DSSC) is based on a semiconductor formed between a photo-sensitized anode and an electrolyte, a photo electrochemical system [24], polymers in organic solar cells (OPVs) is a type of photovoltaic that uses organic electronics, a branch of electronics that deals with conductive organic polymers or small organic molecules for light absorption and charge transport to produce electricity from sunlight by the photovoltaic effect [25], quantum dot solar cell is a solar cell design that uses quantum dots as the absorbing photovoltaic material and hybrid materials solar cell [26]. The DSSC and OPV have low cost of materials and a simple fabrication process but they have low power conversion efficiency as compared to those of the first and second generation solar cells. Furthermore, they have long-term stability and durability is still limited [27].

Consequently, the hybrid materials solar cells have been developed, which are fabricated from a combination of organic and inorganic semiconducting materials. Organic materials can absorb light as the electron donors and hole-transporters and inorganic materials can use as the electron acceptors and transporters in the hybrid solar cell structure. Advantages of these solar cells have high power conversion efficiency, low cost, lightweight and easy fabrication [28]. Recently, the hybrid organic-inorganic perovskite solar cells (PSCs) as new generation solar cells, due to their high power conversion efficiency, low cost, light weight, superb light-harvesting characteristics, easy improve energy band gap and simple fabrication process at low temperature [29].

จุฬาลงกรณ์มหาวิทยาลัย
Chulalongkorn University

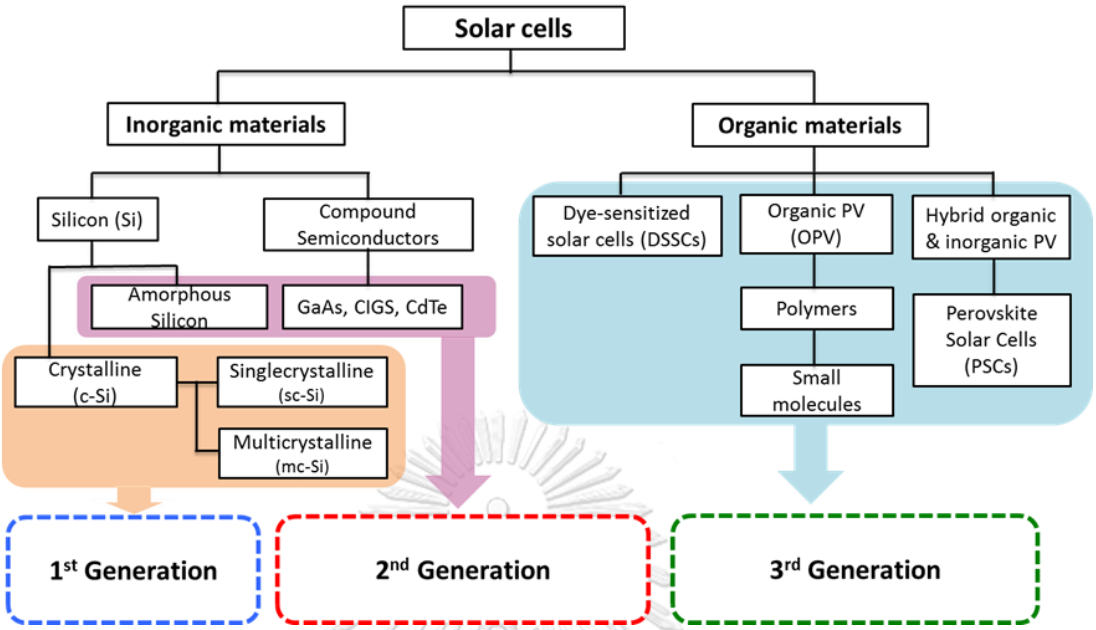

Figure 2.3 Diagram of type of solar cells classified by generation.

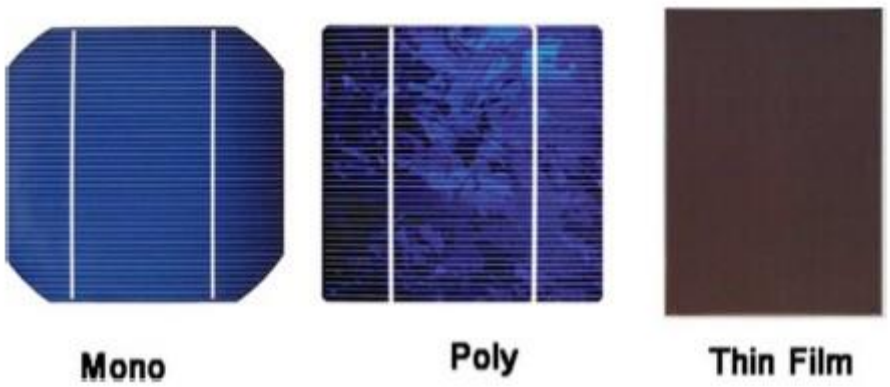

Figure 2.4 Crystalline and amorphous silicon solar cell [5].

2.2 Perovskite Solar Cells and device structure.

Perovskite solar cell is a type of solar cell that has been attracting a prominent attention in recent years due to its progress in power conversion efficiency in comparison to other types of solar cells, ease of fabrication by a low-temperature solution technique, low cost, superb light-harvesting characteristics and easy to improve energy band gap [30].

2.2.1 Perovskite crystal structure.

Perovskite is a calcium titanium oxide mineral composed of calcium titanate, with the chemical formula $CaTiO_3$. The mineral was named after the Russian mineralogist Lev-Perovski. Compounds which have the same type of crystal structure as $CaTiO_3$, i.e., ABX_3 are called perovskites, as shown in Figure 2.5, where A is a large cation, such as Cs^+ $CH_3NH_3^+$, or $NH_2CHNH_2^+$, B is small metal cation, such as Pb^{2+}, Sn^{2+} and X is halide anions, such as Cl^-, Br^-, or I^-. In organic–inorganic hybrid perovskite compounds, the advantages of organic materials, such as the functional versatility, mechanical flexibility, low-cost process ability, can be well combined with the inorganic components by interacting with weak bond [31].

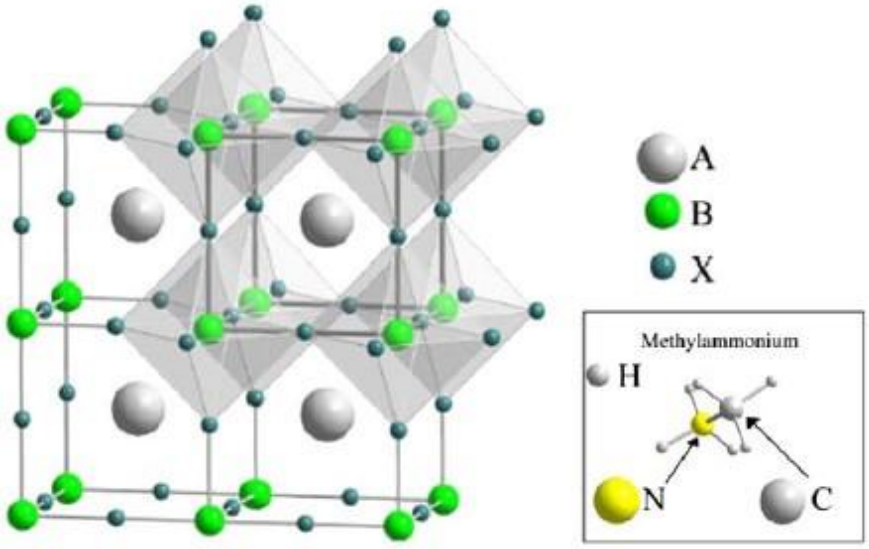

Figure 2.5 Unit cell of basic ABX_3 perovskite structure [31].

ABX_3 perovskite materials have revolutionized solar cells due to their ease of processing and outstanding electronic and optical properties. Thus the standard compound is methyl ammonium lead triiodide ($CH_3NH_3PbI_3$), with mixed halides $CH_3NH_3PbI_{3-X}Cl_X$ and $CH_3NH_3PbI_{3-X}Br_X$ also being important [32].

Mostly, the common hybrid organic–inorganic perovskite material, applied in the field of photovoltaics, is $CH_3NH_3PbI_3$ perovskite as light harvester. This perovskite material consists of a large organic cation (methylammonium CH_3NH^{3+}), lead (Pb) as the smaller metal cation, and iodine as the halide anion. $CH_3NH_3PbI_3$ is a direct band gap semiconductor with a band gap of 1.55 eV, which determines its absorption offset up to 800 nm, high V_{OC} value (1.15 V) and the weak photo generated exciton binding energy of merely 0.03 eV facilitates the charge separation at ambient temperature [33].

2.2.2 Planar structure of Perovskite Solar Cells.

The device structures of perovskite solar cell are respectively depicted in Figure 2.6, where the transparent conductive oxide (TCO) layer usually coated on a substrate such as glass, make the transparent electrode of the solar cells and also used in optoelectronic devices and displays, for instance, Indium tin oxide (ITO) and fluorine-doped tin oxide (FTO). These two types are similar in application and performance, but different in surface roughness and resistance, which can result in different surface wettability and electrical conductivity, respectively. Electron transporting layer (ETL) is a semiconductor that has a thin film coating on substrate which helps to transfer electrons to perovskite layer. Perovskite layer or absorber layer is a layer which absorbs sun light and transfers electron. Hole transporting layer (HTL) is another important layer for preventing the contact between metal and perovskite layer so, it can reduce the problem of recombination between electron and hole. Also, it helps to transfer a hole. Metal is a counter electrode which have a high-work function and will receive hole and make completely electric circuits. Normally, Au, Ag and Al have been employed widely in perovskite solar cells [12, 34].

จุฬาลงกรณ์มหาวิทยาลัย
Chulalongkorn University

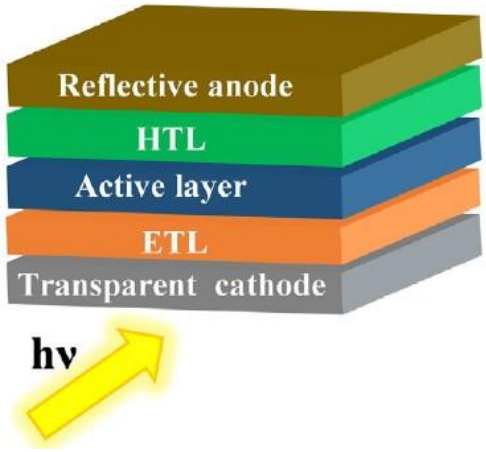

Figure 2.6 The device structure of perovskite solar cell [35].

In planar structure, the heterojunction architecture can divide in two devices, i.e., conventional “n-i-p” and inverted “p-i-n” planar perovskite solar cells, depending on the direction of electric current. The “n-i-p” planar architecture, as shown Figure 2.7 (a), inherits from the features of the mesoscopic perovskite solar cells, so its term is conventional structure. First layer, the n-type interlayer (or compact oxide layer as an electron collection layer) is deposited on a transparent conductive substrate, which common substrate uses in this structure is FTO, since it can endure to annealed device at high temperature (500°C). Then it sequentially follows with coating of hybrid perovskite layer as light absorber, p-type interlayer (hole selective layer), and top metal contact. In device operation, photon first passes through the bottom electron selective layer and then the photon is absorbed in the perovskite material. Exciton (electron-hole pair) is then created and this electron-hole pair can be dissociated at a donor-acceptor interface of perovskite layer. Once separated, the electron can transfer to the n-type, electron-transporting layer, and be transported to the cathode (FTO) for charge collection. Meanwhile hole moves pass through p-type, hole-transporting layer, and then be collected at the anode (Au). For instance, the common “n-i-p” conventional device is FTO/ TiO_2/perovskite/spiro-OMeTAD/Au [11, 36] .

In inverted architecture, the “p-i-n” devices, as shown in Figure 2.7 (b), based on solution processing of organolead (Pb) halide perovskite sandwiched between p-type

conducting polymer (PEDOT:PSS) and an n-type fullerene derivative ($PC_{61}BM$). The PEDOT:PSS layer deposited directly on the transparent conductive substrate (ITO), which the inverted planar perovskite configuration is ITO/PEDOT:PSS/perovskite/$PC_{61}BM$/Al. Initially, the first assumption of this structure was the perovskite has good p-type characteristics and heavily influenced by the p-n heterojunction concept in organic solar cells. In operation principle, after the exciton is generated, the electron-hole pair can be dissociated at a donor-acceptor interface. To opposite the electron-hole pathway of conventional device, the electron can transfer to the n-type, electron-transporting layer, and then be transported to the cathode (Al) for charge collection. Meanwhile hole moves pass through p-type, hole-transporting layer, and then be collected at the anode (FTO) [11, 36].

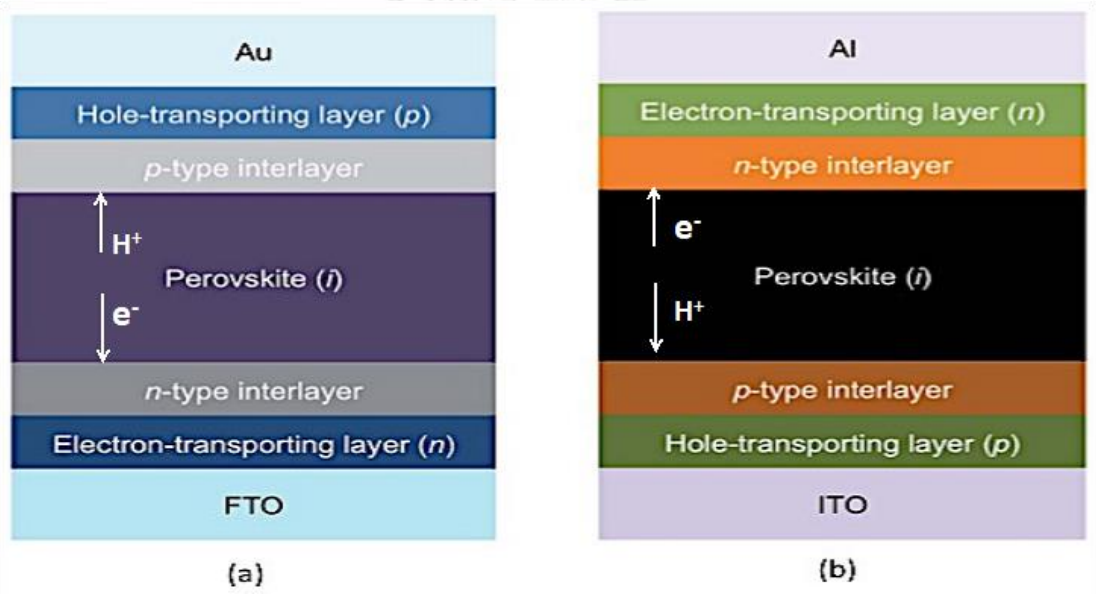

Figure 2.7 Schematic diagram of planar heterojunction solar cells with (a) conventional “n-i-p” and (b) inverted “p-i-n” configurations [36]. “

In this work, we will be fabricated and developed conventional “n-i-p perovskite solar cells by one-step solution processes. The structure of this hybrid compound is consisted of FTO/ TiO_X (Nanotec)/ perovskite solution (Nanotec)/ Spiro-OMeTAD/Au solar cell.

2.2.3 Principles of Perovskite Solar Cells.

The device positive charges are contacted by transparent bottom electrode (cathode). Besides, the active layer is contacted with n-type material for electron extraction and a p-type material for hole extraction. In working principle of this architecture, when the photons are absorbed by coated perovskite material, the photo generated electrons are transferred from perovskite active layer to the mesoporous scaffold TiO_2 layer through n-type contact and then transported to the electrode (FTO). Meanwhile, the holes are transported through p-type contact and collected at counter electrode [37], as shown in Figure 2.8.

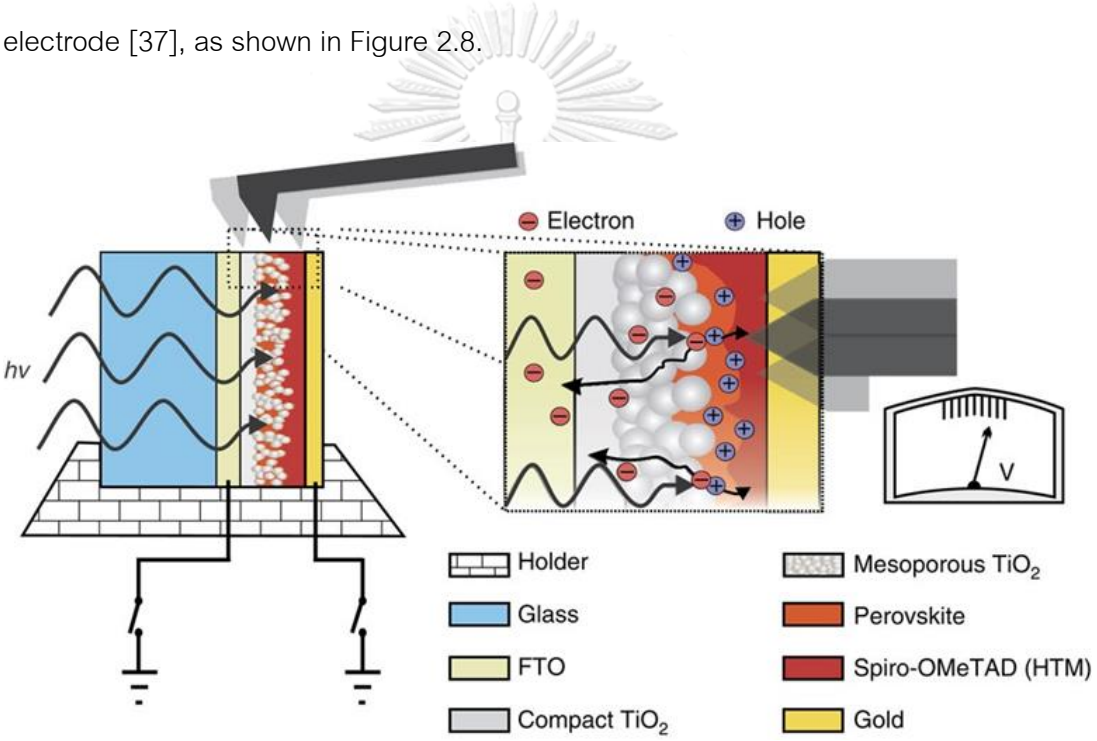

Figure 2.8 Principles of Perovskite Solar Cells [38].

A range of device strategies yielding high efficiencies has been reported: the regular and inverted electrical geometries with or without mesoporous oxide supports and using a variety of transport materials. The energy band gaps levels of commonly used organometallic perovskite materials as light absorbers, which its band gap can be tuned in the range of 1.48 - 2.23 eV by replacing the methylammonium cation with the slightly larger formamidinium cation. Moreover, various commercially available electron transport materials such as TiO_2, ZnO, PCBM, etc. While hole transport materials have various commercially, for examples, spiro-OMeTAD, P3HT, NiO, etc, [39] as shown in Figure 2.9.

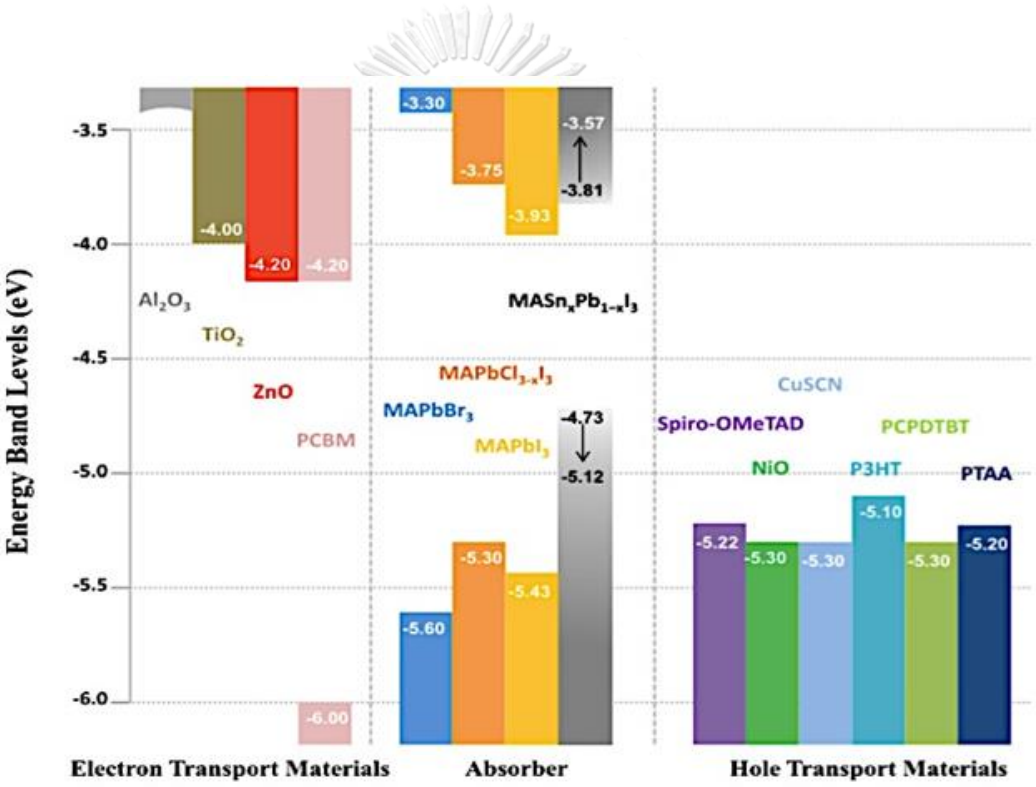

Figure 2.9 Energy level diagram of the materials used in perovskite solar cells [39].

2.2.4 Solution processing techniques.

The solution processing techniques for the perovskite layer, electron and hole transporting layer can be broadly classified into various groups, more commonly used spin-coating methods and dip-coating [40]. Moreover, rapid convective deposition is new solution processing techniques, which has been attracting a prominent attention in recent years due to its low cost, simple adjustment and less solution lost in comparison to other solution processing techniques [41].

2.2.4.1 Spin-coating technique.

Spin coating is one of the most common techniques for applying thin films to substrates. Spin-coating process can deposition of perovskite solution and other solution such as PEDOT: PSS, spiro-OMeTAD, TiO_2, etc. onto a substrate, including glass, plastic, quartz, silicon and sapphire. According to Figure 2.10, the solution is dropped on the substrate and then it is rotated at high speed in order to spread the fluid by centrifugal force. Finally, it is dried in order to evaporate residual solvent and improve crystallinity, resulting in a formation of thin film. Thickness and uniformity are sensitive to viscosity of the solution, temperature and spinning velocity. The advantages of spin coating are low-cost, fast processing, relative ease with a process can be set up and small quantities of solution needed for covering large substrate area. In contrast, disadvantages compose of significant losses of coating material (over 90%), sensitivity to the rate of evaporation, and non-uniform film thickness [40, 42].

จุฬาลงกรณ์มหาวิทยาลัย
Chulalongkorn University

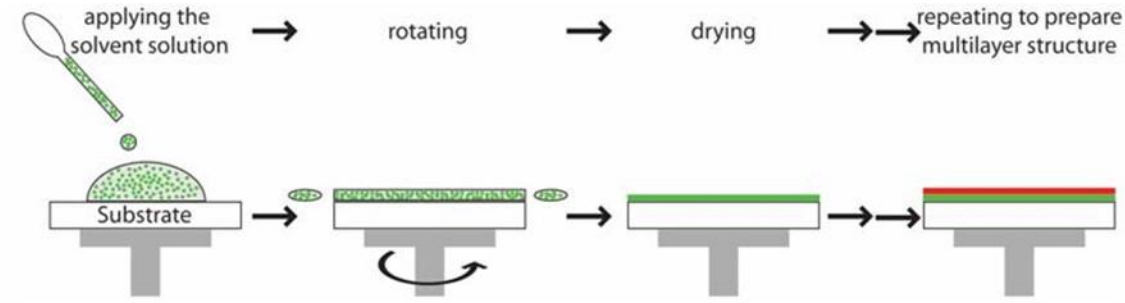

Figure 2.10 Schematic of the spin-coating process [43].

2.2.4.2 Dip-coating technique.

Dip coating is very simple by producing film formation through immersion of substrate in coating solution because it can provide easy and fast deposition of polymer films over a large area [44]. Dip coating is a process where the substrate to be coated is immersed in a liquid and then withdrawn with a well-defined withdrawal speed under controlled temperature and atmospheric conditions, as shown in Figure 2.11. Several parameters, such as precise speed control and minimal vibration of the substrate and fluid surface could be controlled an accurate and uniform coating thickness [45]. The advantages of dip coating are low-cost and simple process. While the disadvantages are non-uniform film surface and no patterning [40].

จุฬาลงกรณ์มหาวิทยาลัย
CHULALONGKORN UNIVERSITY

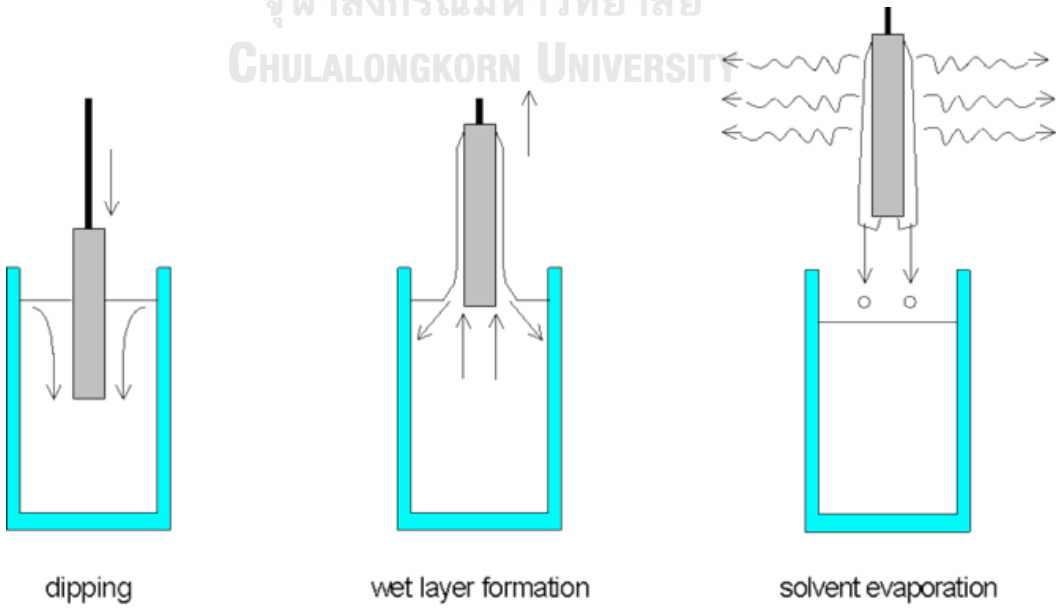

Figure 2.11 Schematic of the dip-coating process [46].

2.2.4.3 Rapid convective deposition.

Convective deposition is a well-known technique for depositing microspheres into closed packed structures and has proven very useful tool in fields like coatings for LED's and solar cells, membranes, cell capture devices, and in functionalizing Janus particles, as shown in Figure 2.13. Convective deposition, the evaporation-driven flow and capillary-driven assembly of colloidal particles on a substrate in the thin film following the receding meniscus, not unlike the "coffee ring effect" [41]. Advantages of Rapid convective deposition, surfaces with controlled roughness, low cost, easy adjustment of film thickness and uniform layer thickness. On the other hand, disadvantages compose of limited to highly wet substrate and must coat onto hydrophilic substrate.

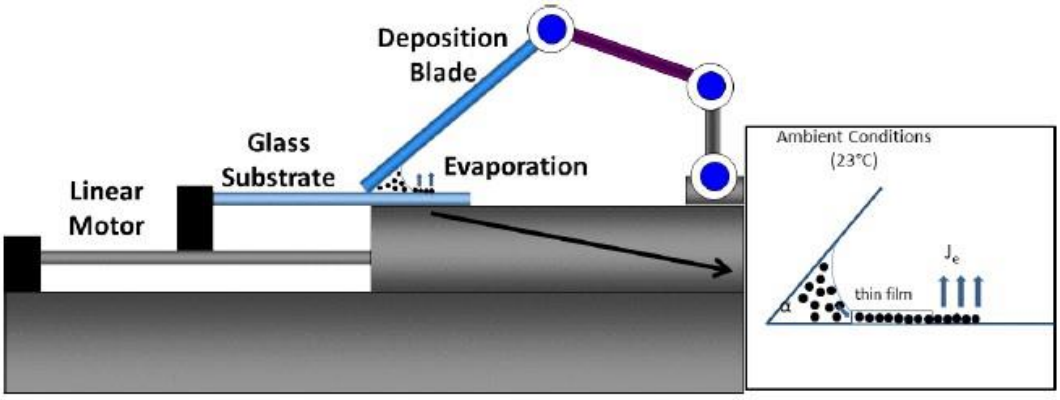

Figure 2.12 Schematic showing rapid convective deposition experimental setup with the inset highlighting the evaporating meniscus and thin film. The deposition blade is stationary while the glass substrate translates to the right [47].

2.2.5 Solution process fabrication of perovskite layer.

The deposition methods for the perovskite layer onto substrates are followed by solution deposition methods, either based on one-step deposition or two-step deposition (sequential deposition) by employing mixture of two precursors. Perovskite thin film can be formed either by spin coating a mixed CH_3NH_3I (MAI) and PbI_2 solution (one-step coating) or by spin-coating PbI_2 followed by deposition of CH_3NH_3I (two-step coating) [48], as shown in Figure 2.13.

For the one-step solution deposition process, a precursor solution is prepared by mixing CH_3NH_3I (MAI) or $CH(NH_2)_2I$ (FAI) and PbI_2 or $PbCl_2$ in polar aprotic solvents such as Dimethylacetamide (DMA) or gamma-butyrolactone (GBL). After that spin-coating the precursor solution on the substrate, then drying and heating at low temperatures (70°C ~ 170°C). The result of perovskite film coverage relies on annealing temperature during solution processing, which it should be optimum annealing temperature. The higher annealing temperatures result in degraded active layer while lower an annealing temperature leads to poor film coverage [39].

For two-step deposition method, a precursor solution is prepared by mixing PbI_2 and N,N –dimethylformamide (DMF), which is first coated on the substrate by spin-coating and then a Iso-propyl alcohol (IPA) of CH_3NH_3I (MAI) or $CH(NH_2)_2I$ (FAI) is spun on the PbI_2 film, then dry and heat at low temperatures (70°C ~ 170°C) [13] .

จุฬาลงกรณ์มหาวิทยาลัย
Chulalongkorn University

This process is expected to be benefit for preparation of organometallic film system, which organic and inorganic components have incompatible solubility characteristics, or for systems in which the organic component is difficult to evaporate. Furthermore, the two-step solution process gives the great result of film with significantly large surface roughness that was frequently peeled off from the substrate. Also, this process has been greatly achievable in films with solid-state mesoscopic solar cells [49].

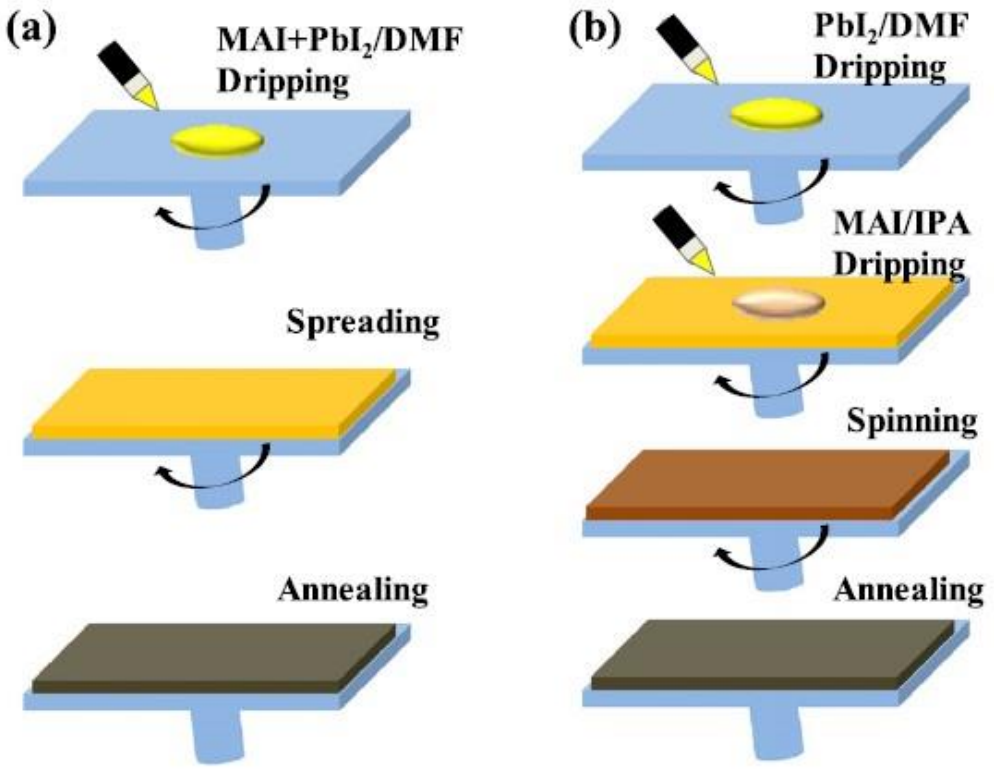

Figure 2.13 Two general deposition methods for preparing perovskite active layers. (a) One-step coating deposition method, (b) Two-step coating deposition method [2].

2.3 Titanium dioxide (TiO_2)

One of the key efforts to improve power conversion efficiency (PCE) of planar perovskite solar cells has been directed toward the enhancement of surface area of titanium dioxide (TiO_2), representing as an electron transporting layer (ETL).

2.3.1 Properties and applications of Titanium dioxide.

Titanium dioxide (TiO_2) is a very well-known semiconductor material and versatile material due to its superior photo-reactivity, available in low cost, non-toxicity and long term stability. It has a great potential in many applications, including photo-catalysis to degrade the pollutants in water, solar cells, environmental purification, and gas sensors, etc. [50] It has been developed and used in in recent years with photocatalysis being

used in a variety of products across a broad range of research areas, including especially environmental and energy-related fields [51], as shown in Figure 2.14.

Moreover, TiO_2 as a semiconductor with photocatalytic activities and using as electron transporting layer for perovskite solar cells which helps to transfer electrons to perovskite layer due to suitable energy band gap, light sensitive materials and high electron mobility [52].

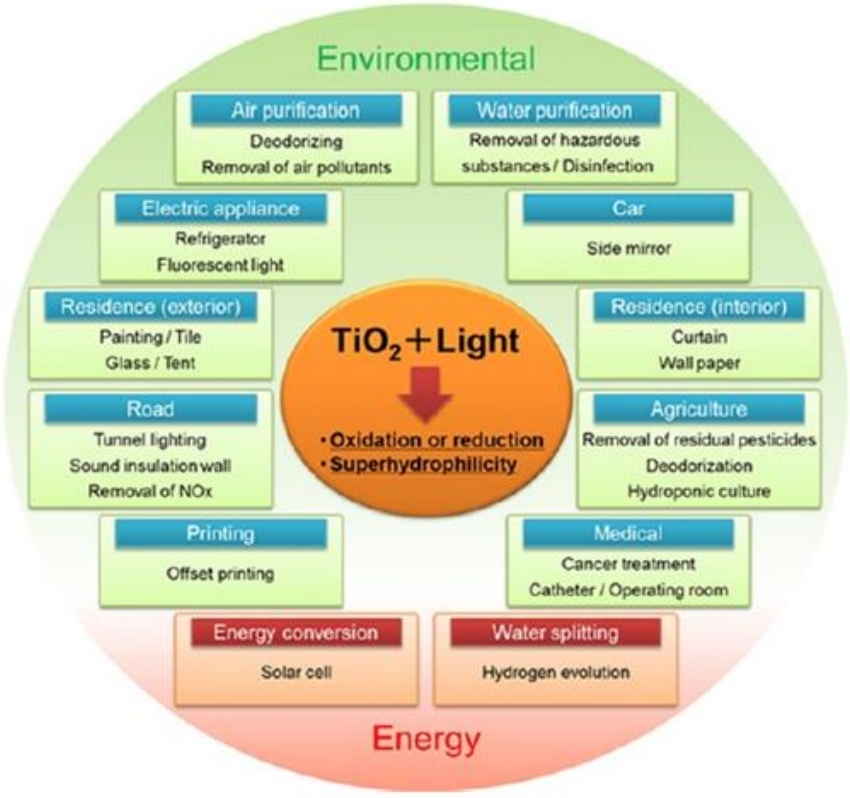

Figure 2.14 Applications of TiO_2 photo catalysis [53].

Semiconductor molecules contain a valence band (VB) occupied with stable energy electrons and empty higher energy conduction bands (CB). The photocatalytic properties of TiO_2 are derived from the formation of photogenerated charge carriers (hole and electron) which occurs upon the absorption of ultraviolet (UV) light corresponding to the band gap. The electrons in the valence bands are excited by UV light and energy (hv) to conduction bands and the mechanism of the electron and hole pair formation when the TiO_2 particle is irradiated with light of adequate energy [53, 54], as shown in Figure 2.15.

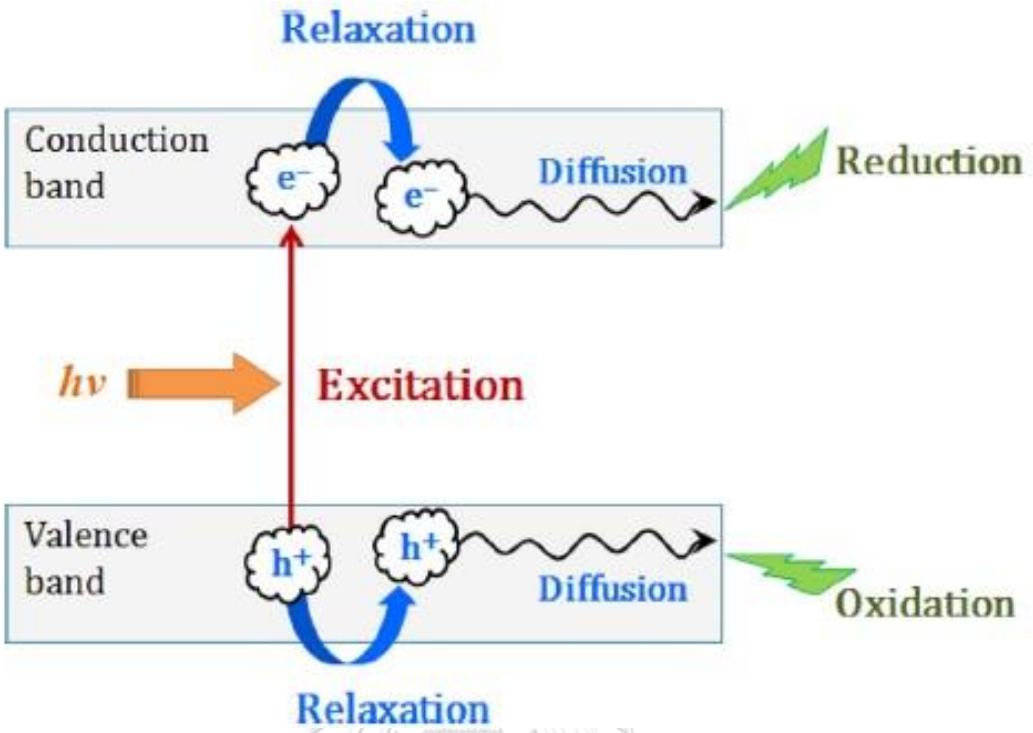

Figure 2.15 Schematic illustration of the formation of photogenerated charge carriers (hole and electron) on absorption of ultraviolet (UV) light [54].

2.3.2 Phases structure of Titanium dioxide.

Titanium dioxide can be separated into three phases, mainly based on crystalline phases, i.e. anatase (tetragonal), rutile (tetragonal) and brookite (orthorhombic), as shown in Figure 2.16. The primary source and the most stable form of TiO_2 is rutile, whereas anatase and brookite phases can be transformed to rutile phase when heated under high temperature exceeding in the range 600–800 °C (1,112–1,472 °F) [55]. Titanium dioxide is an n-type wide energy band gap semiconductor due to oxygen deficiency. The energy band gap of about 3.20, 3.00 and 3.20 eV of, anatase, rutile and brookite [56], respectively. Anatase and rutile TiO_2 are most often reported as photocatalysts and their physical properties are summarized in Table 2.1.

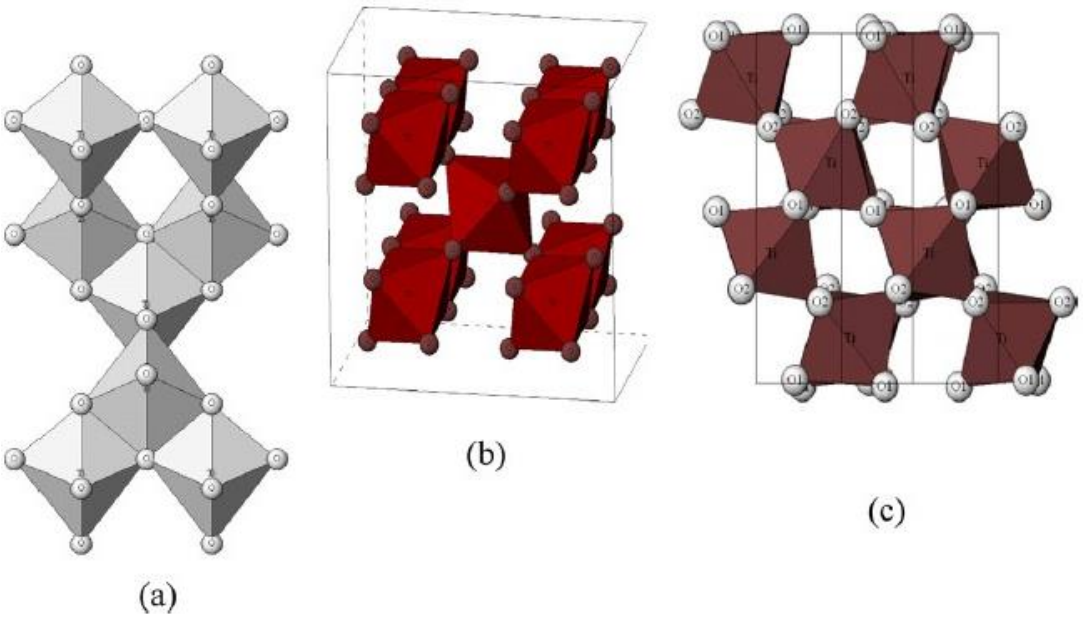

Figure 2.16 Crystalline structures of titanium dioxide (a) anatase, (b) rutile and (c) brookite [56].

Anatase TiO_2 has been used as a catalyst for photodecomposition and solar energy conversion due to its high photo activity.

จุฬาลงกรณ์มหาวิทยาลัย
CHULALONGKORN UNIVERSITY

Table 2.1 Physical properties of crystal structure of Titanium dioxide [56].

Property	Anatase	Rutile
Molecular weight (g/mol)	79.88	79.88
Melting point (°C)	1825	1825
Boiling point (°C)	2500-3000	2500-3000
Light absorption (nm)	<390	<415
Mohr's Hardness	5.5	6.5-7.0
Refractive index	2.55	2.75
Dielectric constant	31	114
Crystal structure	Tetragonal	Tetragonal
Lattice constants (A˚)	a=3.78	a=4.59
	c=9.52	c=2.96
Density (g/cm^3)	3.79	4.13
Ti-O bond length (A˚)	1.94 (4)	1.95 (4)
	1.97 (2)	1.98 (2)

จุฬาลงกรณ์มหาวิทยาลัย
CHULALONGKORN UNIVERSITY

2.3.3 Morphologies and Nanostructures of Titanium dioxide.

The disadvantages of TiO_2 nanoparticles photocatalyst include the requirement of large amount of catalysts, difficulty in catalyst recycling and problematic agglomeration of TiO_2 nanocrystals into large particles. Currently, the researchers are searching and developing the others one-dimensional (1D) nanostructured TiO_2 such as nanotubes, nanorods, nanofibers, nanosheets, ect, as shown in Figure 2.17, in order to enhance photocatalytic activity, facilitate catalyst separation after photocatalytic reaction and charge recombination probability [57].

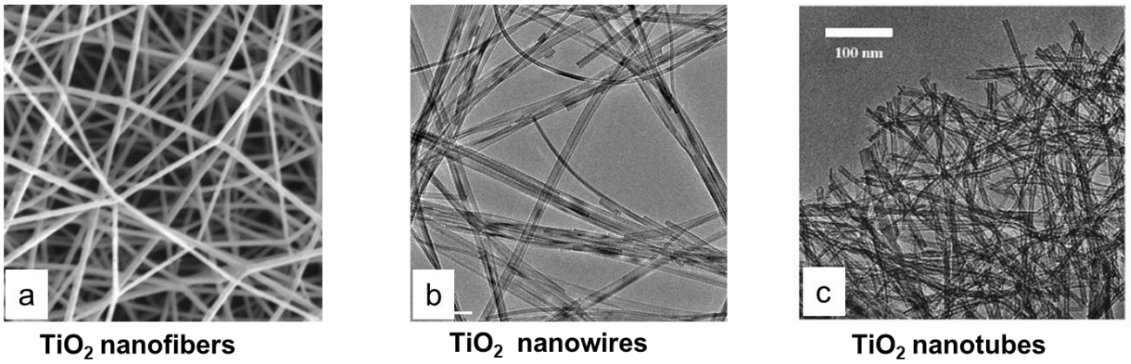

Figure 2.17 TEM images of TiO_2 nanostructures: (a) nanofibers, (b) nanowires and (c) nanotubes [58, 59].

From previous study, TiO_2 nanotubes, nanofibers and nanowires were prepared by the hydrothermal treatment of TiO_2Degussa P-25 as TiO_2 precursors. Table 2.2 shows the results of the surface area, pore volume, average pore diameter and band gap of the different TiO_2 nanostructure. The surface areas of the nanostructured NP, NT, NF, and NW samples were increased after using the sol–gel and alkaline hydrothermal methods, in comparison with the conventional TiO_2 Degussa P-25 [60].

จุฬาลงกรณ์มหาวิทยาลัย
Chulalongkorn University

Table 2.2 BET surface areas and band gap for TiO_2 nanoparticle (NP), nanotube (NT), nanofiber (NF), nanowire (NW) and Degussa P-25 nanostructured samples [60].

Sample	Surface area, S_{BET} (m^2/gr)	Average pore size, D_p (Å)	Pore volume, V_p (cm^3/gr)	Band gap (eV)
Nanoparticles	228	44	0.34	3.18
Nanotubes	354	45	0.34	3.00
Nanofibers	219	67	0.44	3.10
Nanowires	189	60	0.30	3.09
Degussa P-25	58	120	0.36	3.21

From Table 2.2, TiO_2 nanotubes have the highest surface areas and the least band gap. Therefore, TiO_2 nanotubes can be used as an electron transporting material for solar cell, resulting in the enhanced efficiency.

จุฬาลงกรณ์มหาวิทยาลัย
Chulalongkorn University

2.3.4 Typical methods to synthesize TiO_2 nanotubes.

In reviewing the synthesis of TiO_2 nanotubes are presented to developed methods of fabricating TiO_2-based nanotubes including the template-assisted method, the sol–gel process, electrochemical anodic oxidation and hydrothermal treatment [61].

2.3.4.1 Template-assisted method.

The dimensions (diameter and length) of TiO_2nanotubes formed through hard template approach membranes can be controlled easily by the dimension of templates.

Template can be divided into two types: positive and negative templates as shown in Figure 2.18. Positive template synthesis is employed when oxide materials are coated on the outer surface of the template. While negative template synthesis involved oxide materials which are deposited inside the template channel space [57]. However, the template-assisted method has disadvantage being difficult to separate the nanotubes product from template material and complicated fabrication process.

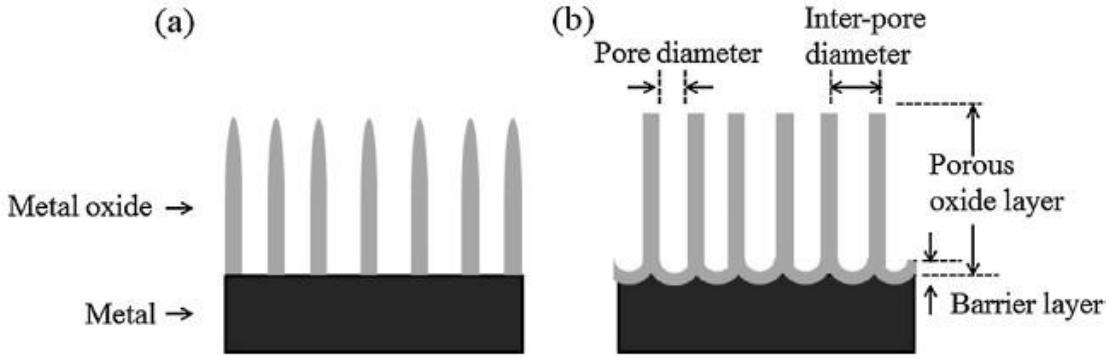

Figure 2.18 Illustration of two different types of hard templates: (a) positive template and (b) negative template [57].

2.3.4.2 Sol–gel process.

The sol–gel method has generated a large scope of interest in the preparation of inorganic ceramic and glass materials. It has many advantages, including simple, cost effective and low temperature synthesis procedure. The underlying principal of sol–gel method is the transition of a system from a colloidal particles (sol for nanoscale particle) into a solid gel phase (integrated network). The sol–gel procedure includes the process of hydrolysis, water condensation and alcohol condensation during which process M–OH–M or M–O–M bridges are established between the metallic atoms M of the precursor molecules such as Si, Zr, Ti, Sn and Alkyl group. Specifically for TiO_2, titanium alkoxides (such as titanium isopropoxide, titanium n-butoxide), alcohol, and acid/water are introduced into the reaction system [55]. Extra steps of drying and subsequent calcinations of gel are usually carried out for densification of films and burn out organic residues coming from the solution.

จุฬาลงกรณ์มหาวิทยาลัย
Chulalongkorn University

2.3.4.3 Electrochemical anodic oxidation.

Electrochemical anodization method can be produced highly ordered arrangement, high aspect ratio and crystallized array films of TiO_2 immobilized on a titanium foil surface. Basically, TiO_2 nanotubes grow on the surface of the anode of titanium foils or thin sheets. The dimensions of nanotubes formed in various electrolytes can be controlled by applying different electrolyte composition, applied voltage, pH and anodizing time [57]. Electrochemical anodization method has many advantages, including controllable pore size, good uniformity and conformability over large areas, which is applied in electrochemistry, photocatalysis and self-cleaning surfaces. Nevertheless, this process suffers from an environmental concern, as the anodization of Ti foil must be processed in highly toxic hydrofluoric acid aqueous solutions [62] .

2.3.4.4 Hydrothermal treatment.

Hydrothermal treatment is an important tool and widely used to prepare advanced nanostructural material processing, covering the processing of electronics, ceramics and catalysis zeolite catalysts in industry. Hydrothermal treatment is defined as any heterogeneous chemical reaction in the presence of an aqueous solvent above room temperature and at a pressure greater than 1 atm in a closed system. In generally, hydrothermal synthesis is conducted in steel autoclaves with or without Teflon liners under controlled temperatures ($T < 200°C$) and/or pressures ($p < 10$ MPa) with the reactions in aqueous solutions in order to covers the process of crystal growth, crystal transformation and phase equilibrium [55]. Hydrothermal method is the most popular to synthesize high yields of slender TiO_2 nanotubes (diameter<10 nm.) with vast pore and unique nanotubular structures due to the simple control of the aqueous solution, cost-effective, high reactivity, low energy requirement and environmental friendly method for largescale production of nanotubes [60]. However, this synthesis method has the main disadvantages such as long reaction duration in concentrated sodium hydroxide (NaOH), which lead to the excessive intercalation of sodium ions in the produced nanotubes and difficult in achieving uniform size of nanotubes [57].

จุฬาลงกรณ์มหาวิทยาลัย
Chulalongkorn University

2.3.5 Formation mechanism of TiO_2 nanotubes.

The formation mechanisms of TiO_2 nanotubes can be explained as Figure 2.19. The TiO_2 nanoparticles are dissolved by NaOH in the hydrothermal treatment; on the other hand, NaOH can react with TiO_2 to form layered alkali titanate nanosheets, as shown in Reaction (1). Then, with time going on, the lamellar nanosheets begin to curl, forming nanotubes little by little. After the hydrothermal treatment, the obtained precipitate should be washed with HCl solution and DI water, in which process, H^+ will exchange with Na^+, as shown in Reaction (2). After calcination, TiO_2 nanotubes are formed finally as shown in Reaction (3).[55]

$$TiO_2 + 2NaOH \longrightarrow Na_2TiO_3 + H2O \qquad (1)$$

$$Na_2TiO_3 + 2H^+ \longrightarrow H_2TiO_3 + 2Na^+ \qquad (2)$$

$$H_2TiO_3 \longrightarrow TiO_2 + H_2O \qquad (3)$$

According to Figure 2.19, the currently most widely accepted formation mechanism of TNTs during the hydrothermal process involves four steps[62]:

Step 1: Dissolution of TiO_2 precursor and breaking of Ti-O-Ti bonds in the concentrated alkaline solution in the primary stage of hydrothermal treatments.

Step 2: Formation and growth of layered nanosheets of sodium titanates.

Step 3: Subsequently, nanosheets are exfoliated.

Step 4: Growing of nanosheets with the increasing tendency of curling and scrolling lead to the nanotube formation.

จุฬาลงกรณ์มหาวิทยาลัย
Chulalongkorn University

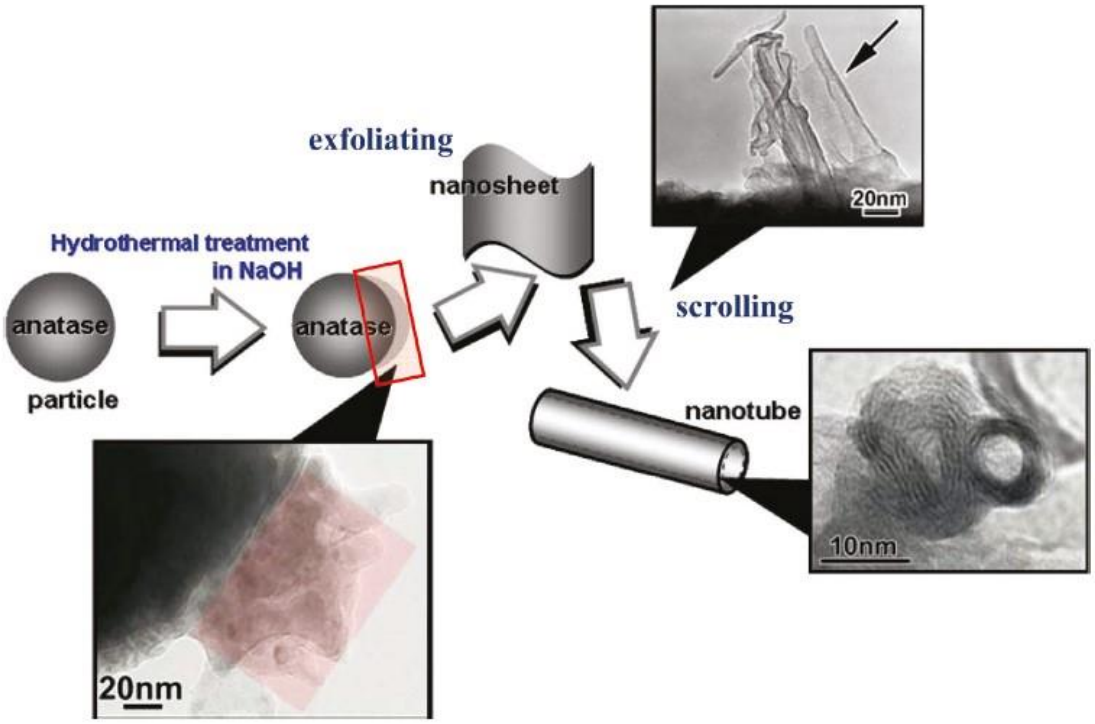

Figure 2.19 Schematic drawing of the exfoliation and scrolling mechanism of nanotubes formation [63].

2.4 Lead Sulfide Quantum Dots (PbS QDs).

Quantum dots (QD) are very small semiconductor particles composed of II-VI, III-V or IV-VI group elements, only several nanometres in size, so small that their optical and electronic properties differ from those of larger particles. Quantum dots are synthesized in such a way that the diameter is below the characteristic exciton Bohr radius of the material and can be adsorbed on nanostructured wide band gap semiconductors using two general in situ synthesis methods: chemical bath deposition (CBD) and successive ionic layer adsorption and reaction (SILAR). Quantum dots exhibit properties that are intermediate between those of bulk semiconductors and those of discrete molecules. Their optoelectronic properties change as a function of both size and shape [18].

2.4.1 PbS QDs doped TNTs.

Many semiconductors have been employed to sensitize TiO_2, including CdS, CdSe, PbSe, PbS, etc. Lead sulfide (PbS) is an attractive semiconductor for this approach because of its small band gap (0.41 eV) in the IR region and its large exciton Bohr radius of 18 nm and the multiple exciton generation effect, which leads to extensive quantum size effects and their high absorption coefficient [64]. In addition, due to the narrow band gap of PbS quantum dots, they could be utilized as a surface blocking layer between the nanocrystalline TiO_2 photoanode and the $MAPbI_3$ light absorber, which is similar to Sb_2S_3, and thus could reduce electron recombination between the two. PbS quantum dots (PbS QDs) can further improve the photocatalytic activity of TiO_2 because of multiple exciton generation (MEG) and efficient spatial separation of photogenerated charge, preventing electron-hole recombination [65] .

The formation mechanisms of PbS quantum dots doped TiO_2 nanotubes can be explained as Figure 2.20. The TiO_2 nanotubes were modified with PbS QDs by using a bifunctional thiolactic acid linker. The carboxylic group of thiolactic acid reacts with the surface of TNTs and leaves the thiol group to bind with Pb^{2+}. The growth of PbS nanocrystals occurs after adding a Na_2S solution [66].

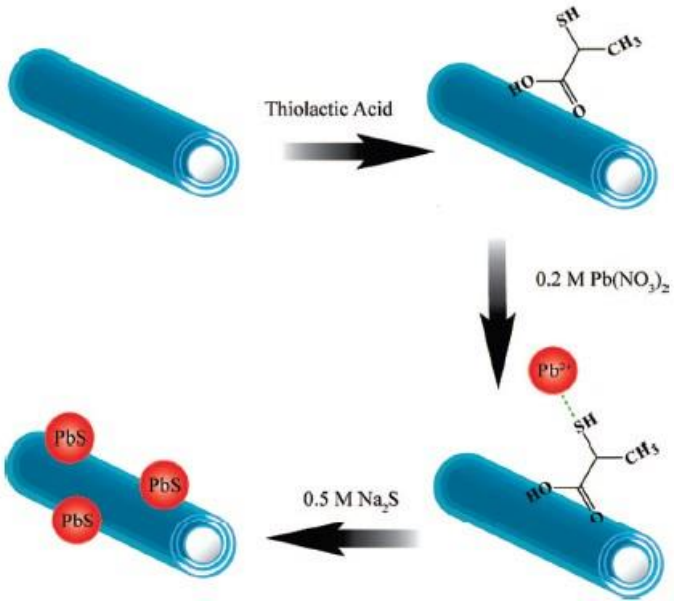

Figure 2.20 Preparation of PbS QDs on TiO_2 nanotubes [66].

2.5 Performance Characteristics.

2.5.1 Current-voltage (I-V) characteristics.

In terms of the solar cell performance characteristics, the power conversion efficiency (PCE) of a solar cell is defined as

$$Power\ conversion\ efficiency\ (PCE) = \frac{Jsc \cdot Voc \cdot FF}{Pin} \quad (1)$$

Where, Jsc is short-circuit current density (mA/cm^2), Voc is open-circuit voltage (V), FF is fill factor, and Pin is incident input power

From Figure 2.21, Current-Voltage (I-V) Curve, I_{SC} (short circuit current) is maximum intensity that can generate a photovoltaic cell or module when measuring the current if performing a short circuit (output voltage of 0 volts), V_{OC} (open circuit voltage) is maximum voltage that can generate a photovoltaic cell or module when measuring the voltage if not flowing current (current of 0 amps), P_{MAX} (Maximum power) is maximum power that can generate a photovoltaic cell or module and it's the product of maximum voltage and current, V_{MAX} (Maximum Voltage) is the voltage at maximum power (around 80% of open circuit voltage) and I_{MAX} (Maximum Current) is the current at maximum power.

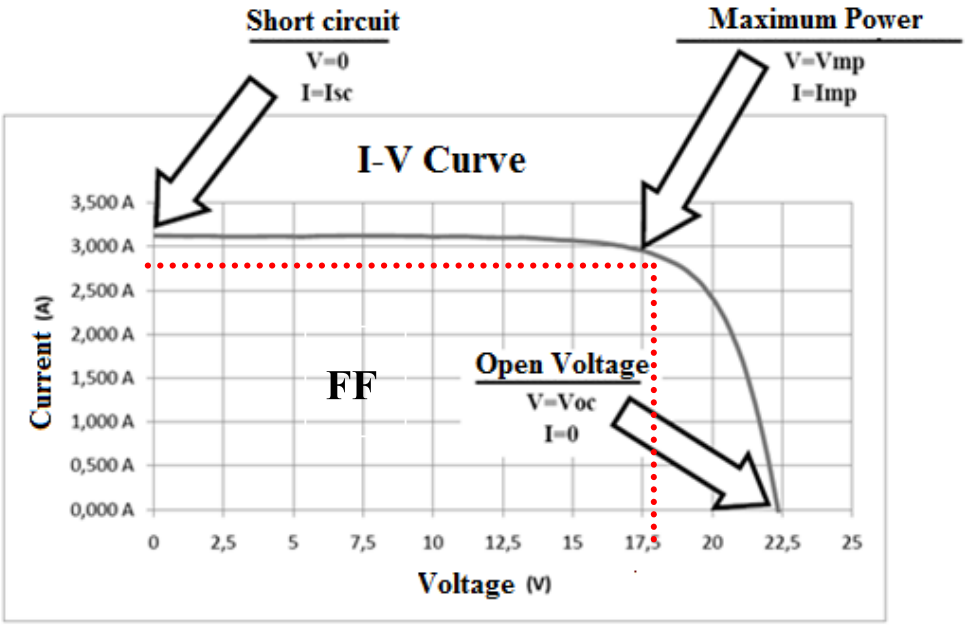

Figure 2.21 I-V characteristics of photovoltaic module [67].

In addition, the fill factor (FF) describes the 'squareness' of the J-V curve, which is largest rectangular area under the curve. Its practical value is less than the ideal value of 1. It is defined as:

$$FF = \frac{Jm \cdot Vm}{Jsc \cdot Voc} \qquad (2)$$

Where, J_m and V_m are the maximum power point current density and voltage, respectively.

2.5.2 External quantum efficiency (EQE).

The term quantum efficiency (QE) may apply to incident photon to converted electron (IPCE) ratio of a photosensitive device or it may refer to the TMR effect of a Magnetic Tunnel Junction. The QE is the ratio of the number of carriers collected by the solar cell to the number of photons of a given energy incident on the solar cell. The quantum efficiency may be given either as a function of wavelength or as energy. If all photons of a certain wavelength are absorbed and the resulting minority carriers are collected, then the quantum efficiency at that particular wavelength is unity. The quantum efficiency for photons with energy below the band gap is zero. A quantum efficiency curve for an ideal solar cell as shown in Figure 2.22. QE can be separated into two types.

External Quantum Efficiency (EQE) is the ratio of the number of charge carriers collected by the solar cell to the number of photons of a given energy shining on the solar cell from outside (incident photons), includes the effect of optical losses such as transmission and reflection. Internal quantum efficiency (IQE) refers to the efficiency with which photons that are not reflected or transmitted out of the cell can generate collectable carriers. By measuring the reflection and transmission of a device, the external quantum efficiency curve can be corrected to obtain the internal quantum efficiency curve. The external quantum efficiency therefore depends on both the absorption of light and the collection of charges. Once a photon has been absorbed and has generated an electron-hole pair, these charges must be separated and collected at the junction. A "good"

material avoids charge recombination. Charge recombination causes a drop in the external quantum efficiency [68].

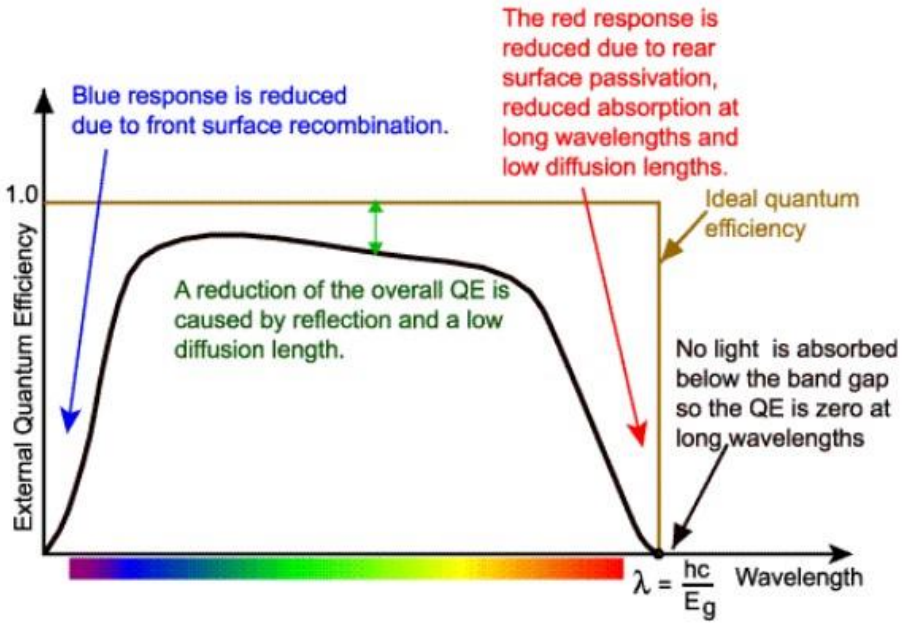

Figure 2.22 The quantum efficiency of a silicon solar cell. Quantum efficiency is usually not measured much below 350 nm as the power from the AM1.5 contained in such low wavelengths is low [69].

2.6 Literature review.

Yu-Zhen Zeng et al. (2014) synthesize nanosized titanium dioxide with tubular structure for the photocatalytic applications, and self-prepared anatase TiO_2 powder is the precursor. We investigated the influence of different pH values of acid washing on the crystalline-structure, optical absorption range, porosity, specific surface area, and photo-catalytic activity of nanotubes. The results show that TiO_2 nanotubes had been proved to be generated with acid washing pH value of 1.3, the outer diameter and length of the nanotube is about 10 nm and 1μm respectively. Moreover, it possesses the largest surface area of 381.2 m^2/g, band gap of 3.12eV and the best photocatalytic activity[69].

Ratanatawanate et al. (2009) were prepared PbS quantum dots on to the inside and outside surfaces of TiO_2 nanotubes (TNTs) by using thiolactic acid as an organic linker in order to modify the band gap of TiO_2 to match with the solar spectrum for the

photodegradation of organic dyes. The photoactivity of the PbS/TNTs was maintained even when irradiated at longer wavelengths than the absorption wavelength of TNTs. The PbS QDs decorated TNTs were superior catalysts for the photodegradation of cationic dyes compared with the commercial P25 catalyst and we are currently exploring the oxidation of more challenging organic pollutants [65].

Kang Du et al. (2015) improved the efficient absorption of solar energy from sunlight and modified energy band gap of TiO_2 nanotubes by depositing PbS QDs into anodized TiO_2 nanotube via ultrasonic-assisted dip coating technique in different concentration solutions. Resulted in the absorptive spectra of TNTs decorated with PbS QDs have been extended to the visible light and enhanced the photocurrent of TiO_2 nanotubes. The band gap energy (E_g) of the PbS QDs decorated TNTs were determined from 3.05~3.12eV, which are slightly smaller than that of the anatase phase (E_g=3.23eV). It is possible that incorporation of PbS QDs makes the band gap narrower [17].

In 2009, Miyasaka and colleagues incorporated perovskite semiconductors into photovoltaic devices. A photovoltaic cell was constructed by combining the $CH_3NH_3PbX_3$-deposited TiO_2 electrode ($CH_3NH_3PbX_3/TiO_2$) as the photoelectrode (anode) and a Pt-coated FTO glass as the counter electrode (cathode) with insertion of a 50 μm thick separator film, where X was halide anions, such as Br^-, or I^-. The perovskite iodide, $CH_3NH_3PbI_3/TiO_2$ resulted in a power conversion efficiency (PCE) of 3.81% and the perovskite bromide, $CH_3NH_3PbBr_3/TiO_2$ resulted in a PCE of 3.13% [10] .

Im et al. (2014) studied and compared the photovoltaic performances of perovskite $CH_3NH_3PbI_3$ light absorber, which is deposited on the mesoporous TiO_2 layer via one-step and two-step coating methods. Average short-circuit current density (J_{sc}), open-circuit voltage (V_{oc}), fill factor (FF), and power conversion efficiency (PCE) of 19.15 mA/cm^2, 0.828 V, 0.470, and 7.5% are observed from the one-step deposited perovskite solar cells, while higher values of 21.47 mA/cm^2, 1.024 V, 0.634, and 13.9% are obtained from the two-step deposited ones. The electron life time of two-step deposited perovskite is about one order of magnitude longer than that of one-step implying that the recombination kinetics highly depends on the perovskite structure determined by

deposition method. In conclusion, the PCE of $CH_3NH_3PbI_3$ using two-step coating methods more than the PCE of $CH_3NH_3PbI_3$ using one-step coating methods [70] .

Dongqin Bi's group. (2013) used a two-step deposition methods for preparing $CH_3NH_3PbI_3$ perovskite solar cells onto ZrO_2 and TiO_2 mesoporous layer, resulting in a power conversion efficiency (PCE) of 10.8% and 9.5%, respectively. The ZrO_2 based solar cell shows higher photovoltage and longer electron lifetime than the TiO_2 based solar cell because the J_{sc} can be higher because of a larger amount of perovskite that can be deposited by two-step deposition method because of better solubility and V_{oc} for the solar cell based on ZrO_2 is higher, which is the reason for the higher efficiency [16].

Xianfeng Gao's group. (2014) studied and compared to photo conversion efficiency (PCE) and morphology of perovskite solar cell with TiO_2 nanotube, TiO_2 nanoparticle and different thickness of TiO_2 nanotube film. Freestanding TiO_2 nanotube (TNTs) arrays were prepared by a two-step anodization process and using iodide liquid electrolytes to control the nanotube thickness. Perovskite precursors as 1 M PbI_2 and 0.1887 M CH_3NH_3I (MAI), TiO_2 nanotube and TiO_2 nanoparticle as electron transporting layer (ETL). Perovskite solar cells based on freestanding TiO_2 nanotube arrays improved light absorption with more than 90% of light absorbed in the whole visible range and a reduced charge recombination rate, leading to a significant improvement of the photocurrent and efficiency. The photovoltaic performance increases with a decrease of the TiO_2 nanotube film thickness, attributing to the different photo excited charge extraction and collection efficiencies [71] .

Yan Huang's group. (2015) studied and compare to the photo conversion efficiency and morphology of perovskite solar cell with TiO_2 nanotubes in different lengths using of a two-step deposition method. Resulting in a the photovoltaic performance of devices was found to be significantly dependent on the length of the TiO_2 nanotubes, and the power conversion efficiency decreased as the length of the TiO_2 nanotubes increased from~ 0.40 μm to ~0.65 and then to ~0.93 μm. The highest power conversion efficiency of the perovskite device prepared from ~0.40 μm-long anatase TiO_2 nanotube arraysis

จุฬาลงกรณ์มหาวิทยาลัย
Chulalongkorn University

11.3% and fill factor of 0.68 under illumination of 100 mW/cm^2 AM 1.5G simulated sunlight [72].

Ying Yang and Wenyong Wang. (2015) studied the effects of incorporating PbS QDs in hybrid perovskite solar cells based on $MAPbI_3$ and improved light absorption after incorporating PbS QDs and photovoltaic performance of PbS QDs-modified perovskite solar cells. TiO_2 film was deposited by spin coating a TiO_2 paste on FTO substrate and then, PbS quantum dots (QDs), prepared by the successive ionic layer adsorption and reaction (SILAR) method, After that, $MAPbI_3$ precursor solution and P3HT was deposited by spin coating on the substrate with PbS covered TiO_2 electrode, respectively. In conclusion, the incorporation of PbS QDs between TiO_2 and $MAPbI_3$ could improve the crystallization of $MAPbI_3$ film and enhance light absorption, it is also found that the long-term stability of the PbS QD-modified perovskite solar cells, as measured over 97 h under ambient conditions without sealing, is much better than that of the cell without PbS QDs [73].

จุฬาลงกรณ์มหาวิทยาลัย
Chulalongkorn University

CHAPTER 3
EXPERIMENTAL

This chapter describes the experimental procedures for materials, fabrication methods, including the preparation of TNTs, deposition of PbS QDs onto TNTs and fabrications of perovskite solar cells by one-step deposition solution processes, as well as characterizations of PbS QDs doped TNTs and of perovskite solar cell devices.

3.1 Preparation of TNTs.

In this work, TNTs were synthesized via hydrothermal process from different particle sizes of TiO_2 nanoparticle precursors as follows: 5 nm, 25 nm, and 50 nm.

3.1.1 Materials.

1). Sodium hydroxide anhydrous (CARLO ERBA, 98%, ACS reagent)

2). Hydrochloric acid (CARLO ERBA, 37%)

3). Deionized water (DI water)

TiO_2 Precursors

4). TiO_2 (DK-NANO, 99.9% Anatase, particle size~5 nm)

5). TiO_2 (Sigma-Aldrich, 99.7% trace metals basis, particle size~25 nm)

6). TiO^2 (Sigma-Aldrich, ≥99.5% trace metals basis, particle size~50 nm)

จุฬาลงกรณ์มหาวิทยาลัย
Chulalongkorn University

3.1.2 Synthesis of TNTs.

1). TiO_2 Precursors were baked at 500°C for 1 hr.

2). 0.5 g of TiO_2 precursors were mixed with 30 mL of 10 M NaOH aqueous solution in a 50 ml hydrothermal autoclave.

3). The solution was stirred at room temperature for 10-15 min and then heated at 150°C for 24 hr.

4). The obtained white precipitates were washed and centrifuged with 0.1 M HCl and DI water until a pH became 7 (Neutralization).

5). The sample was dried at 90°C for 10 hr, and then annealed at 350°C for 75 min.

3.2 Deposition of PbS QDs onto TNTs.

Materials.

1). TNTs (synthesis via a hydrothermal process).

2). Thiolactic acid (Sigma-Aldrich, 95%).

3). Lead nitrate (Sigma-Aldrich, <99%, ACS reagent).

4). Sodium sulfide nonahydrate (CARLO ERBA, <98%, ACS reagent).

Experimental methods.

1). 0.25 g of TNTs were treated with a 25 mL of 0.3 M thiolactic acid aqueous solution for 30 min, and then dried at 50oC overnight.

2). A 25 mL of 0.2 M Pb(NO3)2 aqueous solution was then added into the pretreated TNTs for 30 min, and then dried at 50oC overnight.

3). A 25 mL of 0.5 M Na2S aqueous solution was added into the pretreated TNTs for 30 min.

4). Gray precipitates were obtained and were washed and centrifuged with DI water.

5). The samples were dried at 50oC overnight.

3.3 Fabrications of perovskite solar cells.

The perovskite solar cells were fabricated on FTO glass substrates with the following device configuration: FTO/ electron transporting layer/perovskite/ hole transporting layer/cathode, by solution processing techniques, including spin coating and rapid convective deposition, as shown in Figure 3.1. Spiro-OMeTAD is used as a hole transporting material and helps to transfer a hole to the next layer.

จุฬาลงกรณ์มหาวิทยาลัย
Chulalongkorn University

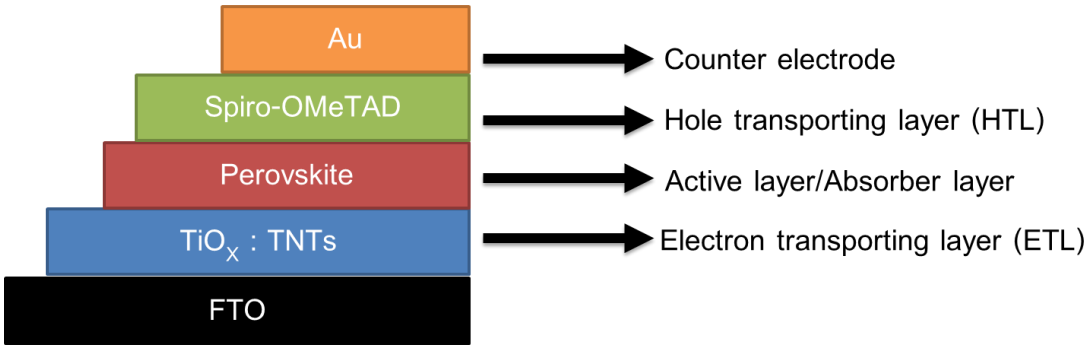

Figure 3.1 The conventional (n-i-p) planar perovskite solar cells.

TNTs = TiO_2 nanotubes.

PbS QDs = Lead (II) sulfide quantum dots.

Spiro-OMeTAD = 2,2',7,7'-Tetrakis[N,N-di(4-methoxyphenyl)amino]-9,9'-spirobifluorene.

3.3.1 Device Preparation.

3.3.1.1 Transparent Conducting Oxides Substrate.

Fluorine doped tin oxide coated (FTO,15 **Ω**) glass substrates were purchased from Lumtec and were cleaned by sequential ultrasonic treatment in a detergent, deionized water, and isopropyl alcohol (IPA) at 60°C for 15 min and dried by a flow of nitrogen gas.

3.3.1.2 TiO_X solution (Nanotec).

A mixture of 1 ml of TiO_X and 8 ml of Iso-propyl alcohol (IPA) was stirred at room temperature for 1 hr.

จุฬาลงกรณ์มหาวิทยาลัย
Chulalongkorn University

3.3.1.3 Perovskite precursor solution (Nanotec).

3.3.1.4 Preparation of PbS QDs doped TNTs suspension.

1). PbS QDs doped TNTs were dispersed in anhydrous 2-butanol. (Concentration: 1.0, 3.0, 5.0, 7.0 and 9.0 mg/ml)

2). Using ultrasonic bath for 30 min.

3). 100 µl of PbS QDs doped TNTs suspension were mixed with 900 µl of TiO_X (Nonotec).

3.3.2 Fabrication of conventional planar perovskite solar cell by one-step deposition.

1). 20 µl of TiO_X or TiO_X : PbS QDs doped TNTs solution was coated on FTO substrate (Cleaned with alconox, deionized water and 2-propanol by ultrasonic treatment) by rapid convective deposition, at a deposition speed of 3000 µm/s for two layers.

2). The TiO_X coated sample was heated at 500°C for 1 hr, and cooled down at room temperature.

3). 50 µl of perovskite solution (Nanotec) was spin coated at a speed of 1,000 rpm,10 S on top of the sample prepared in the previous step, and 150 µl of chlorobenzene solution was spin coated at a speed of 3,500 rpm,30 S.

4). Then, the perovskite coated sample was heated at 100 °C for 1.30 hr and cooled down at room temperature for 15 min.

5). Lastly, 40 µl of Spiro-OMeTAD solution was spin coated at 4,000 rpm on top of the sample prepared from the previous step.

6).Then, the sample was aged overnight under vacuum conditions.

7).An electrode of Au was performed by thermal evaporation technique to complete a cell device.

จุฬาลงกรณ์มหาวิทยาลัย
Chulalongkorn University

3.4 Analytical instruments.

1). Transmission electron microscopy (TEM; JEOL-2100Plus).

2). X-ray diffraction (XRD; Bruker, Germany).

3). Surface area analyser based on nitrogen adsorption (BET, BelSorp-Mini II).

4). Particle size analyser based on dynamic light scattering (DLS; Zetasizer nano size, ZEN 3600, Malvern).

5). UV-Vis spectroscopy (Perkin Elmer, Lambda 950).

6). Energy dispersive x-ray spectroscopy ((EDS; FE-SEM with EDS (Hitachi SU8230)).

7). Scanning electron microscope (SEM; FE-SEM with EDS (Hitachi SU8230))

8). Solar simulator (model SN 258, ABET)

9). ORIEL Intelligent Quantum Efficiency (IQE) 200TM Measurement system.

3.4.1 Characterization of TNTs.

TNTs were characterized by transmission electron microscopy (TEM) operating at 200 kV to observe the morphology and structure. The phase structure was investigated by X-ray diffraction (XRD) with 2θ ranging from 5^{O} to 55^{O} for 5^{O} min^{-1} of scan speed with 40 kV operating voltage and 30 mA current and by using a Cukα radiation source at ambient temperature. The surface area of the TiO_2 nanotube was measured by the Brunauer-Emmett-Teller (BET) method. The particle size distributions were characterized with dynamic light scattering (DLS). UV-vis light absorbance spectra and energy band gap were recorded by UV-vis spectrophotometer in the range of 200 to 700 nm.

3.4.2 Characterization of PbS QDs doped TNTs.

PbS QDs doped TNTs were characterized by a transmission electron microscopy (TEM) to observe morphology and structure. The elemental and chemical composition were characterized by energy dispersive x-ray spectroscopy (EDS) in the TEM. The phase structure was investigated by an X-ray diffraction (XRD) with 2θ range from 5^{O} to 55^{O} of scan speed with 40 kV operating voltage and 30 mA current and by using a Cukα radiation source at ambient temperature. The optical absorption spectra and energy band gap of PbS QDs doped TNTs were measured from 200 to 700 nm on a UV-vis spectrophotometer.

จุฬาลงกรณ์มหาวิทยาลัย
Chulalongkorn University

3.4.3 Characterization of Perovskite Solar Cells.

Perovskite thin films were characterized by a scanning electron microscope (SEM) to observe morphology, structure and film thickness. The optical absorption, transmission spectra and energy band gap of TiO_X : PbS QDs doped TNTs thin film were measured from 300 to 800 nm on a UV-vis spectrophotometer. EQE efficiency were measured by

EQE spectra. The measurement was done in air using an Quantum Efficiency 200TM Measurement System established with the tunable light source. Power conversion efficiency (PCE) fill factor (FF), open circuit voltage (V_{oc}) and photocurrent density-voltage (J-V) curves were measured under an ambient atmosphere and simulated solar light, AM 1.5, 100 mW/cm^2 by using a solar simulator with a xenon lamp.

จุฬาลงกรณ์มหาวิทยาลัย
CHULALONGKORN UNIVERSITY

CHAPTER 4
RESULTS AND DISCUSSION

In this work, we investigated the effect of different particle sizes of TiO_2 precursors used for preparing TNTs that results in a variation of surface area. The obtained TNTs with highest surface area will be applied with PbS QDs and deposited onto the perovskite layer as the electron transporting layer (ETL), in order to achieve the enhanced power conversion efficiency of perovskite solar cell.

4.1 Synthesis of TNTs via hydrothermal process

TNTs were synthesized via hydrothermal process from different particle sizes of TiO_2 nanoparticle precursors as follows: 5 nm, 25 nm, and 50 nm.

4.1.1 Morphology and structure of TNTs.

The formation and morphology of TNTs prepared via NaOH hydrothermal treatment from different particle sizes of TiO_2 nanoparticle precursors after annealing at 350 °C were observed by Transmission electron microscopy (TEM), as shown in Figure 4.1- 4.3.

จุฬาลงกรณ์มหาวิทยาลัย

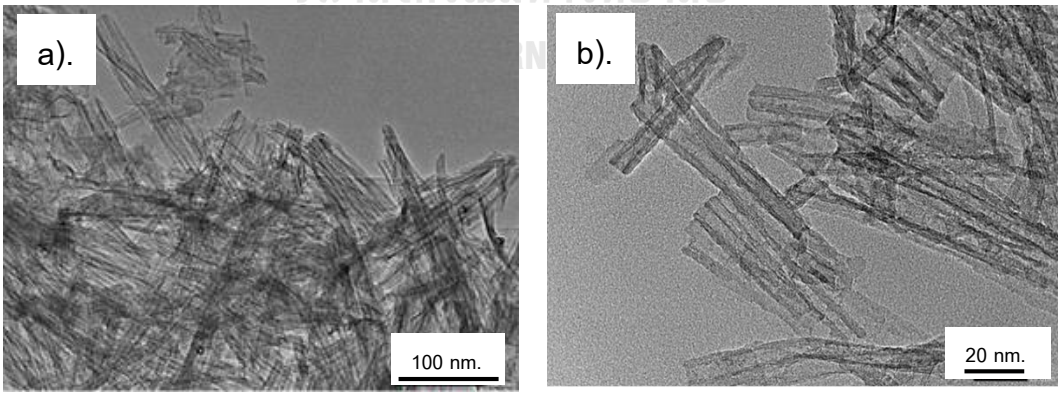

Figure 4.1 TEM images of TNTs synthesized via hydrothermal process from TiO_2 precursor with particle size of 5 nm. a) Magnification of 100,000 times and b) Magnification of 300,000 times.

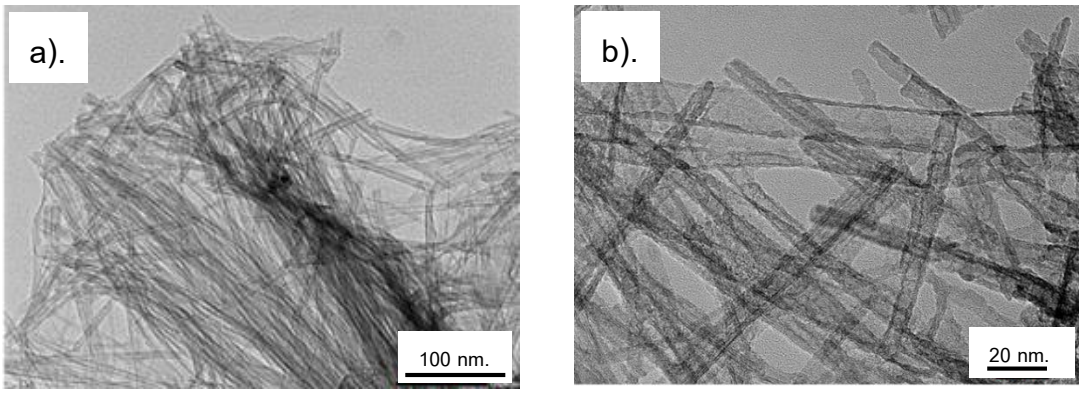

Figure 4.2 TEM images of TNTs synthesized via hydrothermal process from TiO_2 precursor with particle size of 25 nm. a) Magnification of 100,000 times and b) Magnification of 300,000 times.

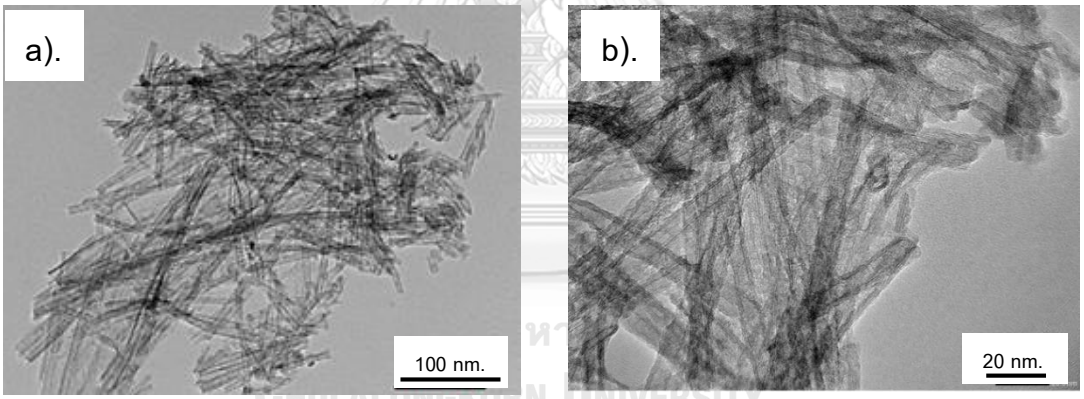

จุฬาลงกรณ์มหาวิทยาลัย
Chulalongkorn University

Figure 4.3 TEM images of TNTs synthesized via hydrothermal process from TiO_2 precursor with particle size of 50 nm. a) Magnification of 100,000 times and b) Magnification of 300,000 times.

As can be seen in the figures, TNTs prepared from 25 nm of TiO_2 precursor are in long tubular structures with a uniform morphology. While TNTs prepared from 5 and 50 nm of TiO_2 precursors have a combination of short and long tubular structures grouping in small bundles and exhibiting non-uniform morphologies, which can be seen in Figure 4.1, and Figure 4 .3, respectively. According to the formation mechanism of TNTs synthesized via hydrothermal process, as previously shown in Figure 2.19, TiO_2 precursor

with particle size of 5 nm has a very small particle size, causing a collapse of lamellar structure of the nanosheets in step 3 and subsequently leading to TNTs with a short tubular structure bunching up in small bundles. While TiO_2 precursor with particle size of 50 nm is larger than TiO_2 precursor with particle size of 5 nm, causing the breakage of curling and rolling of nanosheets in step 4 which subsequently leading to a combination of short and long tubular structure of TNTs. On the other hand, TiO_2 precursor with particle size of 25 nm, which is between the sizes of 5 and 50 nm, has a suitable particle size for the transformation of the TiO_2nanosheets into TNTs, followed in step 3 and 4, which consequently leads to TNTs with a uniform long tubular structures [74].

Based on TNTs prepared from the TiO_2 precursor with particle size of 25 nm, it can be seen in Figure 4.4 that the average outer diameter and inner diameter of the nanotubes are about 10-15 nm and 5-8 nm, respectively. The length is ranging from several tens to several hundreds of nanometers. The obtained samples are in uniform morphology, which should be proper as a site for doping with PbS QDs and consequently suitable to transport electrons continuously within the electron transporting layer without recombination in perovskite solar cells.

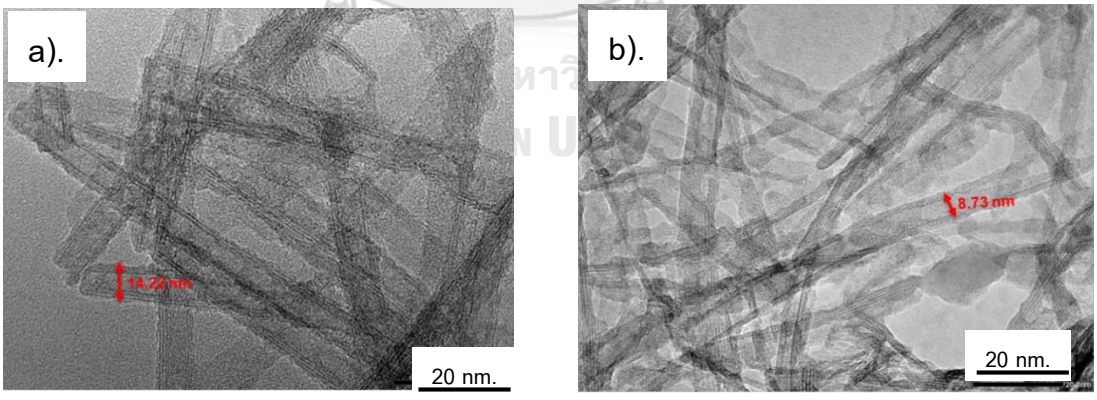

Figure 4.4 TEM images of a). High magnification of about 500,000 times of outer diameter and b). High magnification of 500,000 times of inner diameter of the TNTs synthesized via hydrothermal process from TiO_2 precursor with particle size of 25 nm.

4.1.2 Phase structure of TNTs.

The phase structure of TNTs synthesized via NaOH hydrothermal treatment from different particle sizes of TiO_2 nanoparticle precursors after annealing at 350 °C, was examined by XRD, which is demonstrated in Figure 4.5. All the samples present the major XRD peaks observed at 25.6, 37.9, and 48,2°, indicating the formation of the TiO_2 anatase phase. All the peaks are assigned to (101), (004) and (200) planes of tetragonal crystal structure, respectively (JCPDS number: 21-1272) [75]. TNTs with anatase phase were successfully synthesized which is suitable for use as ETL due to its high stability.

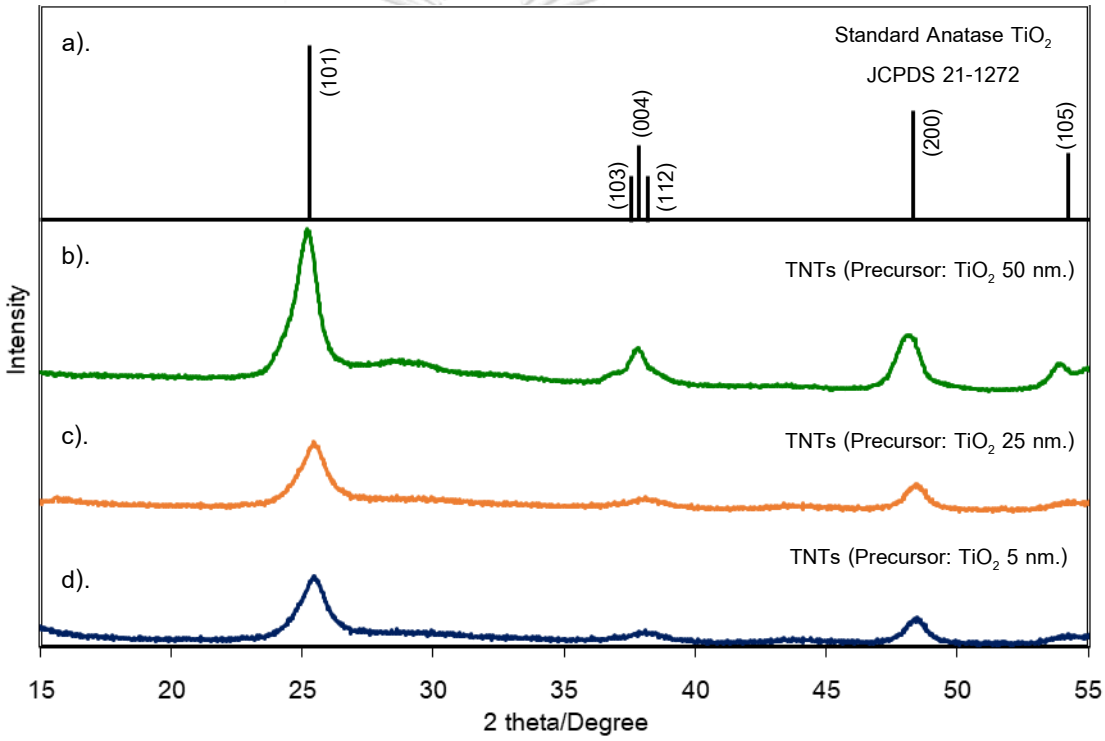

Figure 4.5 XRD patterns of TNTs synthesized via hydrothermal process from different particle sizes of TiO_2 nanoparticle precursors: (a) standard TiO_2 with crystal structure of anatase from JCPDS 21-1272, (b) TiO_2 50 nm, (c) TiO_2 25 nm, and (d) TiO_2 5 nm.

4.1.3 Particle size distributions of synthesized TNTs.

The particle size distribution of TNTs was examined by dynamic light scattering (DLS) analyses, as shown in Figure 4.6. TNTs prepared from TiO_2 precursors of 5 nm and 50 nm exhibited a relatively broad size distribution and non-uniform size of nanotubes. This is attributed to a mixture of short and long tubular structure, presented in the previous section. While TNTs prepared from 25 nm of TiO_2 precursor exhibited a narrow particle size distribution, corresponding to the uniform structure previously shown in TEM result.

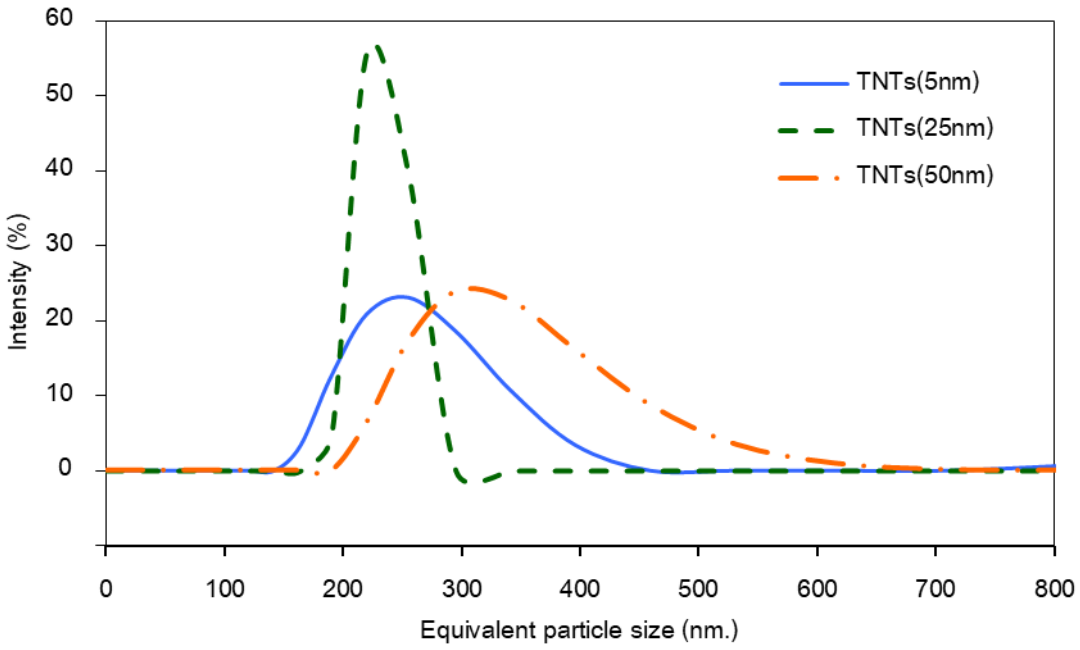

Figure 4.6 Particle size distributions from DLS measurement of TNTs prepared from NaOH hydrothermal treatment with different sizes of TiO_2 precursors.

4.1.4 Surface area of TNTs.

To investigate and select the most appropriate structure of TNTs for using as a site for doping with PbS QDs which were prepared from different sizes of precursors, a measurement of surface area was performed. According to the Brunauer–Emmett–Teller (BET) results, a variation in the average surface area obtained from different particles size of TiO_2 nanoparticles and TNTs was observed, which is presented in Table 4.1. It indicates that the surface area of TNTs prepared from different sizes of precursors are about 5-7 times higher than those of TiO_2 nanoparticles. The largest surface area of TNTs (312 m^2/g) was obtained from TiO_2 precursor with particle size of 25 nm. Therefore, TNTs samples derived from this condition will be used for doping with PbS QD and as ETL in the next step.

Table 4.1. The average surface area of TiO_2 nanoparticles and TiO_2 nanotubes (TNTs) prepared from different sizes of TiO_2 precursors.

sample	Surface area (m^2/g)
TiO_2 (5 nm.)	34.78 ± 0.34
TNTs (5 nm.)	258.35 ± 0.53
TiO_2 (25 nm.)	62.81± 0.33
TNTs (25 nm.)	312.39 ± 0.54
TiO_2 (50 nm.)	48.10± 0.28
TNTs (50 nm.)	280.44 ± 0.57

จุฬาลงกรณ์มหาวิทยาลัย
Chulalongkorn University

4.1.5 UV-vis absorption spectrum and energy band gap of TNTs.

To apply TNTs as the ETL in perovskite solar cells, the optical properties of TNTs were investigated. The absorption spectra of TNTs prepared from different particle sizes of TiO_2 precursors were examined by UV-Vis spectrophotometer, which are shown in Figure 4.7. It can be seen that all samples of TNTs absorb UV light radiation at the wavelength below 400 nm. No difference in optical properties was observed from TNTS obtained from different particle sizes of TiO_2 nanoparticles. Moreover, the energy band gaps of TNTs synthesized from TiO_2 nanoparticle precursors of 5, 25 and 50 nm, could be determined by Kubelka Munk function [76], as shown in Figure 4.8.

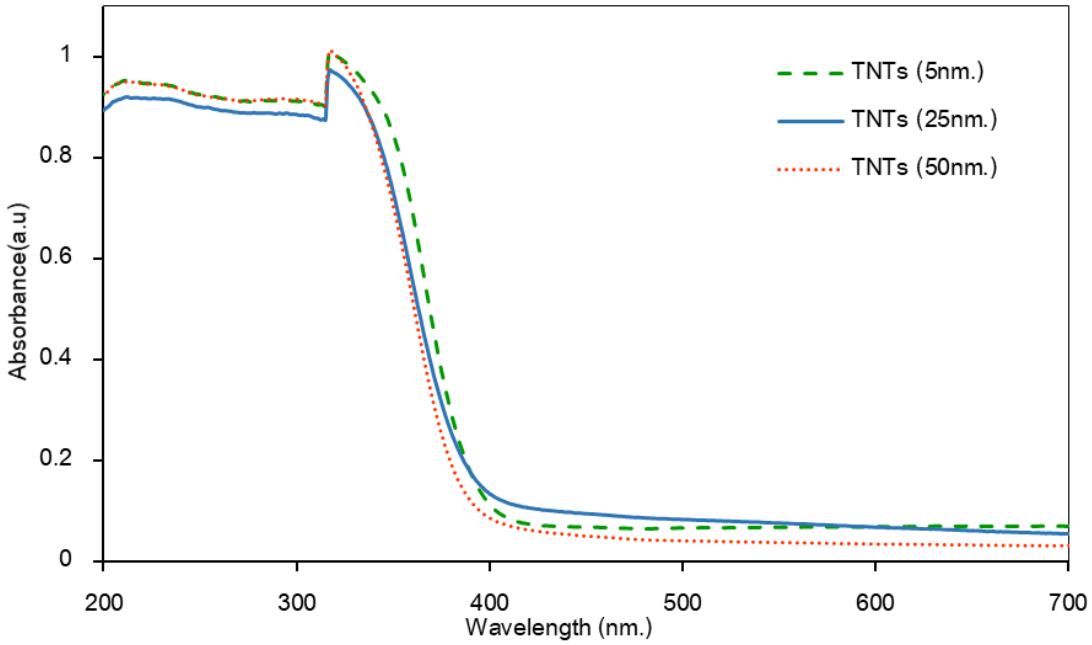

Figure 4.7 UV-vis absorption spectra of as-prepared TNTs via hydrothermal process from different particle sizes of TiO_2 nanoparticle precursors 5, 25 and 50 nm.

Note: the sharp peak at the wavelength about 330 nm comes from a change in light sources, which changes from a UV source to a visible source during a continuous detection.

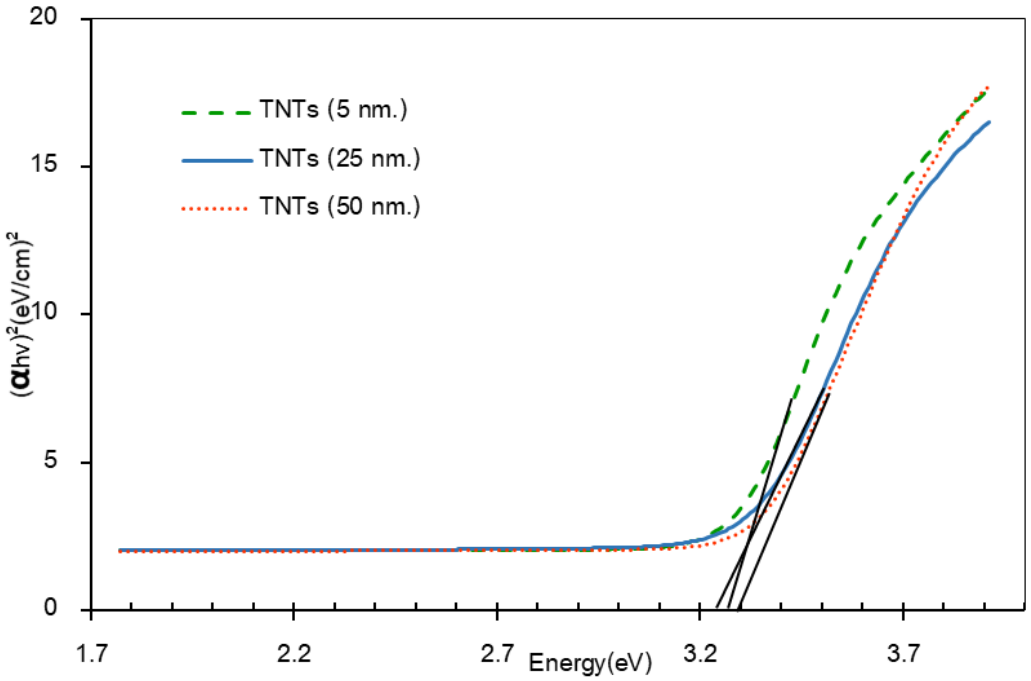

Figure 4.8 The energy band gaps of TNTs as-prepared via hydrothermal process from different particle sizes of TiO_2 nanoparticle precursors 5, 25 and 50 nm.

Table 4.2 summarizes the results of energy band gaps of TNTs prepared from different sizes of TiO_2 precursors. The energy band gaps of about 3.27, 3.24 and 3.30 eV were obtained from TNTs synthesized from TiO_2 precursors of 5, 25 and 50 nm, respectively. This range of band gaps is suitable to be used as the ETL in perovskite solar cells. Although the band gaps derived from various precursors are not significantly different, based on previous study, TNTs prepared from 25 nm of TiO_2 precursor with the highest surface area was selected to be doped with PbS QDs in the next step.

จุฬาลงกรณ์มหาวิทยาลัย
Chulalongkorn University

Table 4.2 The energy band gap of TNTs prepared from different sizes of TiO_2 precursors.

Samples	Energy band gap (eV)
TNTs (5 nm.)	3.27
TNTs (25 nm.)	3.24
TNTs (50 nm.)	3.30

According to all investigated studies and obtained results, TNTs synthesized from different particle sizes of TiO_2 precursors show no big difference in terms of phase structure, absorption and energy band gap. However, in terms of the surface area, TNTs prepared from 25 nm of precursor have the highest surface area, which was expected to be the most suitable for doping with PbS QDs with a good distribution.

4.2 Deposition of PbS QDs onto TNTs.

The highest surface area of TNTs of 312.39 m^2/g with uniform structure, obtained from TiO_2 precursor with particle size of 25 nm, was applied with PbS QDs and deposited onto the perovskite layer as the electron transporting layer (ETL), in order to achieve the enhanced power conversion efficiency of perovskite solar cell.

4.2.1 Morphology and structure of PbS QDs doped TNTs.

The formation and morphology of PbS QDs doped TNTs were observed by Transmission electron microscopy (TEM).

The TEM image with low magnification in Figure 4.9a shows open-ended TNTs without PbS QDs. While that with high magnification in Figure 4.9b shows several of PbS QDs with a few nanometers in size scattering all over TNTs.

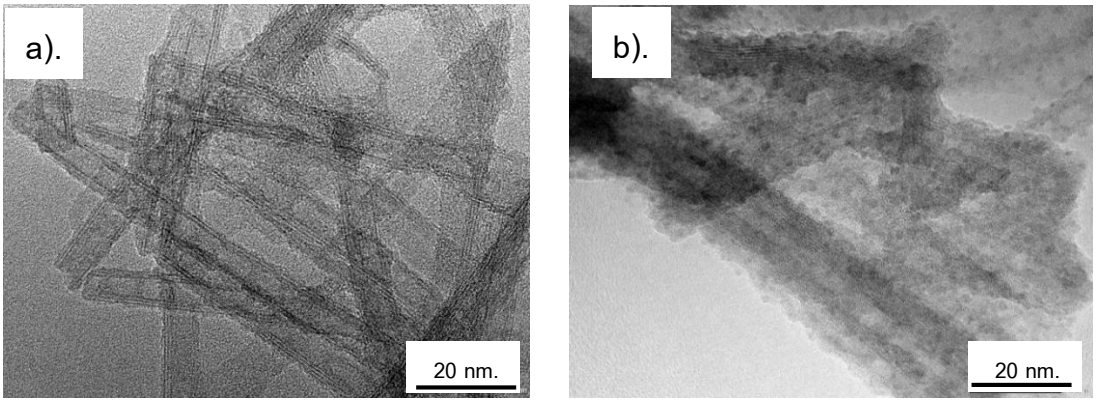

Figure 4.9 a). Low magnification of TEM image of TNTs synthesized from TiO_2 precursor with particle size of 25 nm. b). High magnification of TEM image of PbS QDs on TNTs.

PbS QDs were attached well onto TNTs on both inside and outside surfaces of the TNTs, as a result of thiolactic acid as an organic linker, as shown in Figure 4.10a. The TEM image in Figure 4.10b shows the average size of PbS QDs of about 3-4 nm, which was calculated based on the measurement from TEM images (high magnification about of 800,000 times).

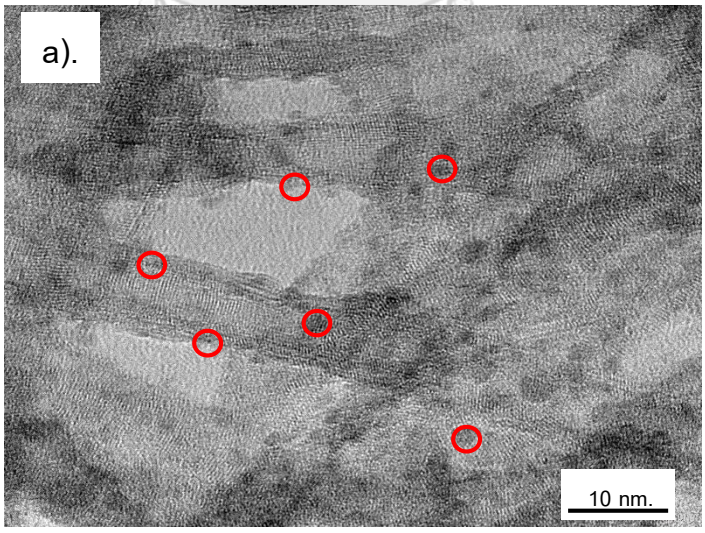

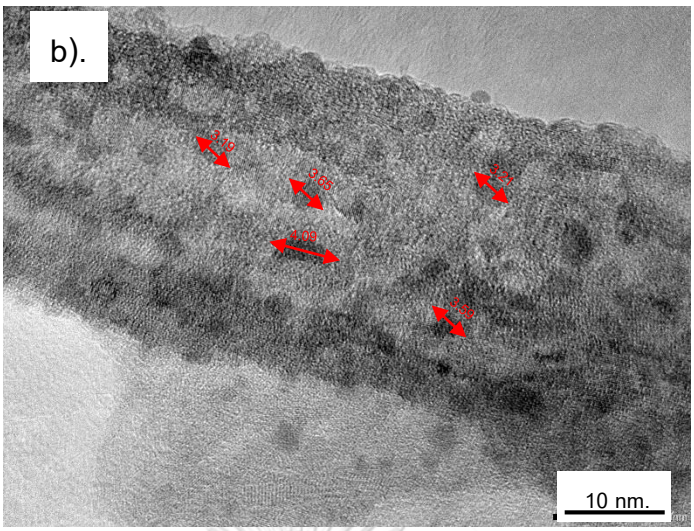

Figure 4.10 TEM images of a). PbS QDs inside and outside TNTs b). The average size of PbS QDs.

4.2.2 Phase structure of PbS QDs doped TNTs.

The XRD patterns of the TNTs synthesized via hydrothermal process and PbS QDs doped TNTs, were demonstrated in Figure 4.11. As shown in figure, both XRD patterns derived from pure TNTs and PbS QDs doped TNTs after annealing at 350 °C show the anatase phase of TiO_2, where the diffraction peaks appear at 2θ = 24.9, 28.7, and 48.6° (JCPDS 71-5576). No distinct difference in diffraction patterns between these two samples was observed. Moreover, no peaks of PbS are presented, according to a reference pattern from JCPDS 05-0592. It could be due to a very small size of quantum dot structure, therefore the diffraction patterns of PbS QDs could be submerged in the background noise. [17].

จุฬาลงกรณ์มหาวิทยาลัย
Chulalongkorn University

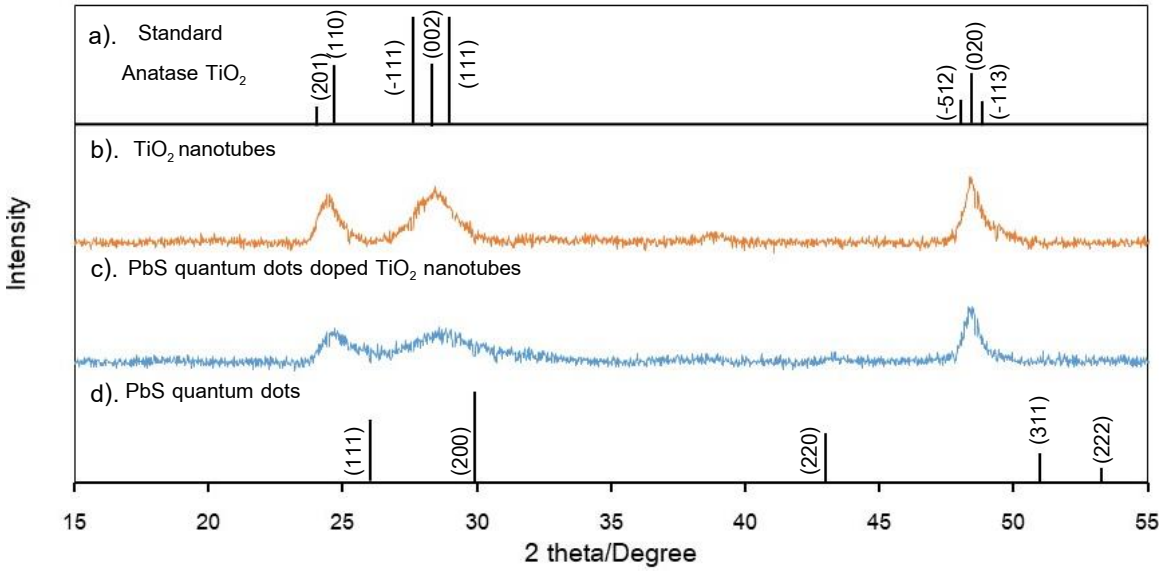

Figure 4.11 XRD patterns of (a) standard TiO_2 with crystal structure of anatase from JCPDS 71-5576, (b) TNTs synthesized via hydrothermal process after annealing, (c) PbS QDs doped TNTs and (d) Galena (PbS) from JCPDS 05-0592.

4.2.3 The elemental and chemical composition of PbS QDs doped TNTs.

Table 4.3 shows the results of the elemental and chemical composition of PbS QDs doped TNTs from area scan of energy dispersive x-ray spectroscopy (EDS) in the transmission electron microscopy (TEM). The result confirms the presence of Pb and S doping onto the TiO_2 nanotubes, even though the ratio of Pb:S does not correspond to the stoichiometric ratio of PbS. The average atomic percentage of Pb and S elements are about 2.33% and 0.11%, respectively.

จุฬาลงกรณ์มหาวิทยาลัย
Chulalongkorn University

Table 4.3 The elemental and chemical composition of the synthesized PbS QDs doped TNTs.

Element	Mass%	Atom%
O	54.73	84.40
S	0.14	0.11
Ti	25.57	13.17
Pb	19.56	2.33
Total	100.00	100.00

4.2.4 Comparison of UV-vis absorption spectra and energy band gap of pure TNTs and PbS QDs doped TNTs.

The absorption spectra of pure TNTs prepared from NaOH hydrothermal treatment is compared with that of PbS QDs doped TNTs. As seen in Figure 4.12, pure TNTs absorb UV light radiation at the wavelength below 400 nm, while the absorption spectrum of PbS QDs doped TNTs has been extended towards the visible light region from 400 nm to 700 nm. This behavior is due to the energy band gap of about 0.5 – 2.0 eV of PbS QDs, therefore it can absorb all light in the UV, VIS and NIR of the electromagnetic spectrum [77].

Furthermore, the energy band gaps of pure TNTs and PbS QDs doped TNTs were determined by Kubelka Munk function [76], as shown in Figure 4.13.

จุฬาลงกรณ์มหาวิทยาลัย
Chulalongkorn University

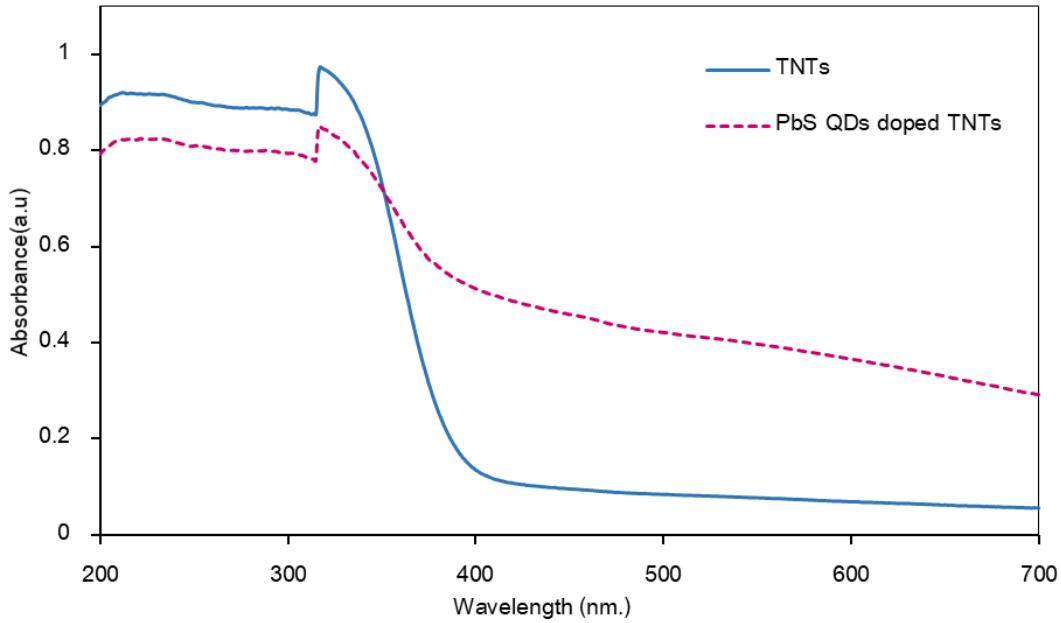

Figure 4.12 UV-vis absorption spectra of TNTs without PbS QDs and PbS QDs doped TNTs.

Note: the sharp peak at the wavelength about 330 nm comes from a change in light sources, which changes from a UV source to a visible source during a continuous detection.

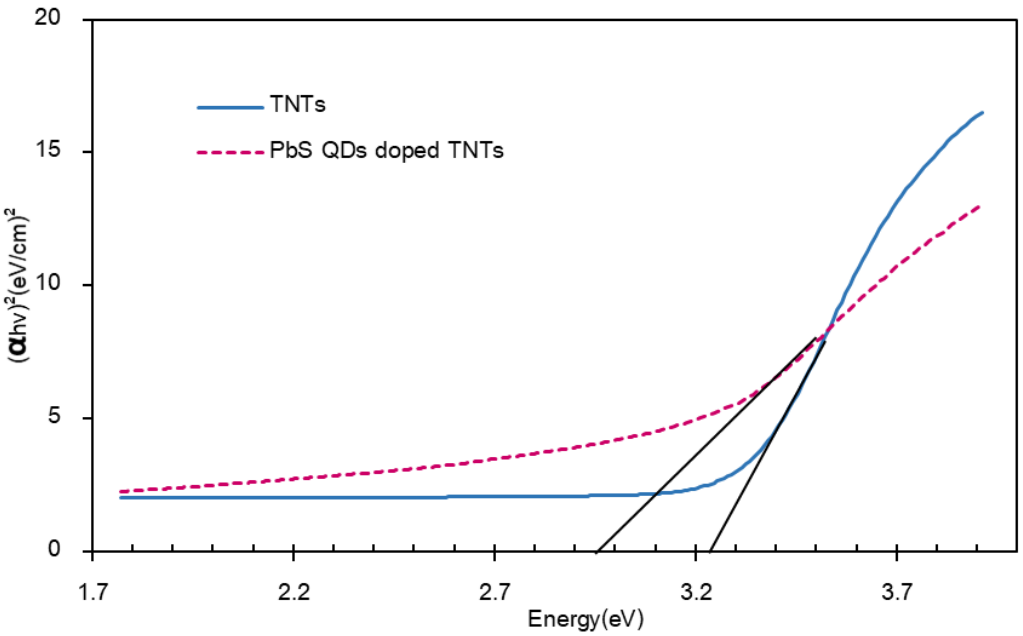

Figure 4.13 The energy band gaps of TNTs without PbS QDs and PbS QDs doped TNTs.

Table 4.4 summarizes the results of energy band gaps of TNTs without PbS QDs and PbS QDs doped TNTs. The energy band gap of about 3.24 eV of pure TNTs synthesized from hydrothermal process was obtained, whereas the energy band gap of PbS QDs doped TNTs was determined to be about 2.97 eV. A slight decrease of energy band gap is observed. Due to a small band gap of PbS QDs of about 0.41 eV, the band gap of PbS QDs doped TNTs did not change significantly. The resulting band gap can be matched well with the solar spectrum which can also act as an efficient light absorbing material [17, 65]. Apparently, PbS QDs doped TNTs are one of the most suitable materials whose energy band gap is appropriate to be used as the electron transporting layer for perovskite solar cells, in order to enhance the power conversion efficiency of the solar cell device for practical use.

Table 4.4. The energy band gaps of TNTs without PbS QDs and PbS QDs doped TNTs.

Samples	Energy band gap (eV)
TNTs without PbS QDs	3.24
PbS QDs doped TNTs	2.97

จุฬาลงกรณ์มหาวิทยาลัย
Chulalongkorn University

4.3 Fabrications of perovskite solar cells by one-step deposition solution processes.

Among the obtained results in terms of physical, chemical and optical properties of TNTs, described in previous sections, TNTs prepared from 25 nm of TiO_2 precursor was apparently the most suitable for using as electron transporting layer for perovskite solar cells due to its suitable energy band gap, uniform morphology and the highest surface area.

Moreover, even though TNTs were doped with PbS QDs, the energy band gap remained suitable for transporting electrons from perovskite layer to the electrode in perovskite solar cell.

Next, both pure TNTs and PbS QDs doped TNTs were applied and deposited onto the perovskite layer as the ETL, as can be seen in Figure 3.1.

4.3.1 Morphology and microstructure of perovskite film with PbS QDs doped TNTs as ETL.

The surface morphology and microstructure of perovskite film with PbS QDs doped TNTs as ETL using the one-step solution processes via spin coating and rapid convective deposition processes, was characterized by scanning electron microscope (SEM), as shown in Figure 4.14.

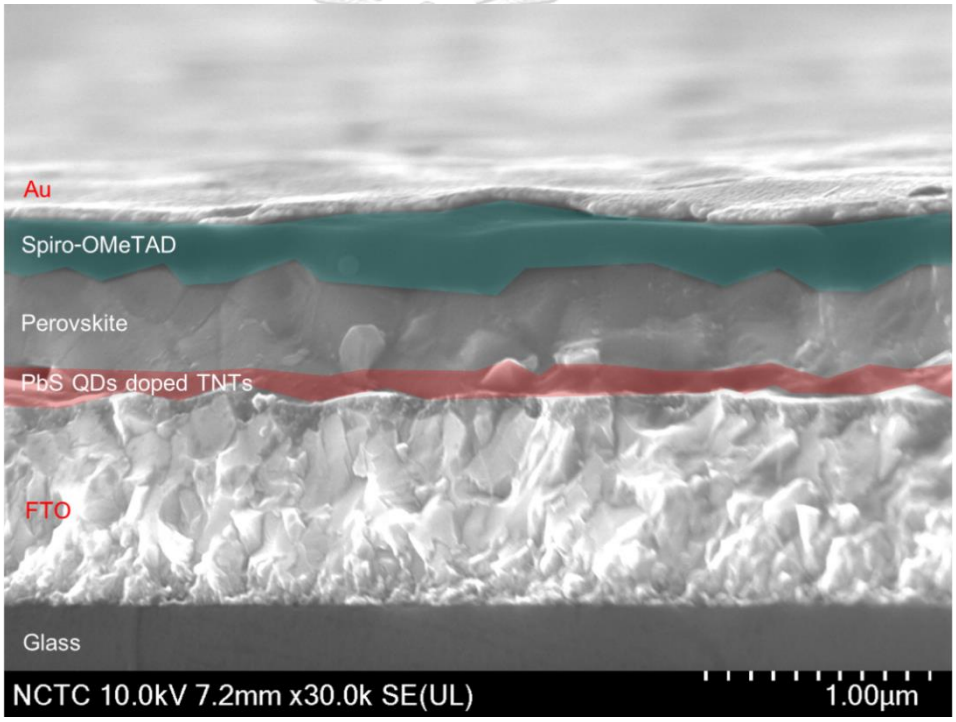

Figure 4.14 Cross-sectional SEM image of perovskite solar cell using one-step deposition method.

Figure 4.14 shows the device structure of the hybrid compound, consisting of glass /FTO / TiO_x : PbS QDs doped TNTs as ETL / perovskite as absorber layer / Spiro-OMeTAD as HTL/ Au as counter electrode. It was observed that perovskite layer was formed all over the surface of ETL. The Spiro-OMeTAD layer is in between the capping layer from perovskite films and the top layer of Au electrode. The formation of each layer

is a close-packed film structure with highly uniform crystalline structures. For this reason, the deposition methods such as convective deposition and spin coating, including the operating parameters are suitable for fabrication of perovskite solar cells [78].

Moreover, as seen in Figure 4.14, the thickness of ETL, perovskite and Spiro-OMeTAD layers are about 80-100 nm, 350-400 nm and 250-300 nm, respectively, which are in the optimal thicknesses for each layer for perovskite solar cells, reported in previous work [79].

4.3.2 UV-Vis spectrum and energy band gap of TiO_X : PbS QDs doped TNTs thin film with various concentrations.

In order to investigate the optical properties of ETL of perovskite solar cell, transmittance (T) of this layer was measured by UV–Vis-NIR spectrophotometer in the wavelength ranging from 300 to 800 nm. The transmittance of ETL films prepared from a solution of TiO_X in 2-butanol with different concentrations of PbS QDs doped TNTs in TiO_X as follows: 0.1, 0.3, 0.5, 0.7 and 0.9 mg/ml, are shown in Figure 4.15. It can be seen that transmittance of the films is above 71%, indicating that the light can transmit through ETL into the perovskite layer. The high transmittance region on a wide range of wavelength in the visible region (from 390 to 700 nm) has been observed and is suitable in the applications of solar cells [80].

จุฬาลงกรณ์มหาวิทยาลัย
Chulalongkorn University

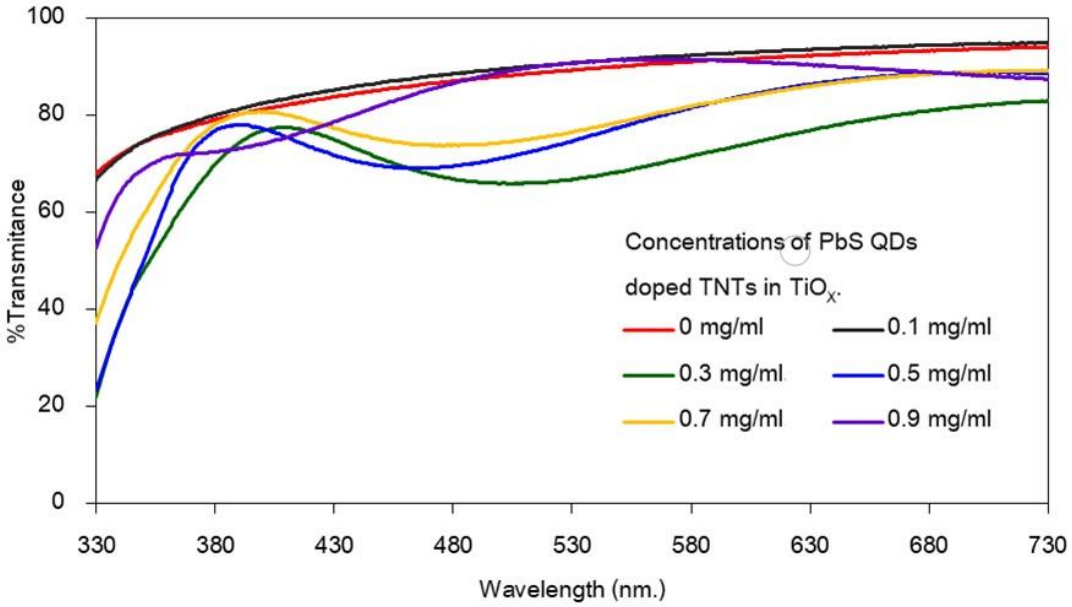

Figure 4.15 Transmittance spectra of ETL with various concentrations of PbS QDs doped TNTs in TiO_X.

The absorption spectra of TiO_X : PbS QDs doped TNTs layers with various concentrations of PbS QDs doped TNTs in TiO_X, as follows: 0.1, 0.3, 0.5, 0.7 and 0.9 mg/ml, are shown in Figure 4.16. It can be seen that the layers prepared from TiO_X in 2-butanol with 0.1 and 0.9 mg of PbS QDs doped TNTs absorbs UV light radiation at the wavelength below 400 nm, while for those with 0.3, 0.5 and 0.7 mg of PbS QDs doped TNTs, the absorption spectra are extended to the visible light region from 380 nm to 600 nm.

Moreover, the energy band gaps of ETL layer with various concentrations of PbS QDs doped TNTs in TiO_X, could be determined by Kubelka Munk function [76], as shown in Figure 4.17.

จุฬาลงกรณ์มหาวิทยาลัย
CHULALONGKORN UNIVERSITY

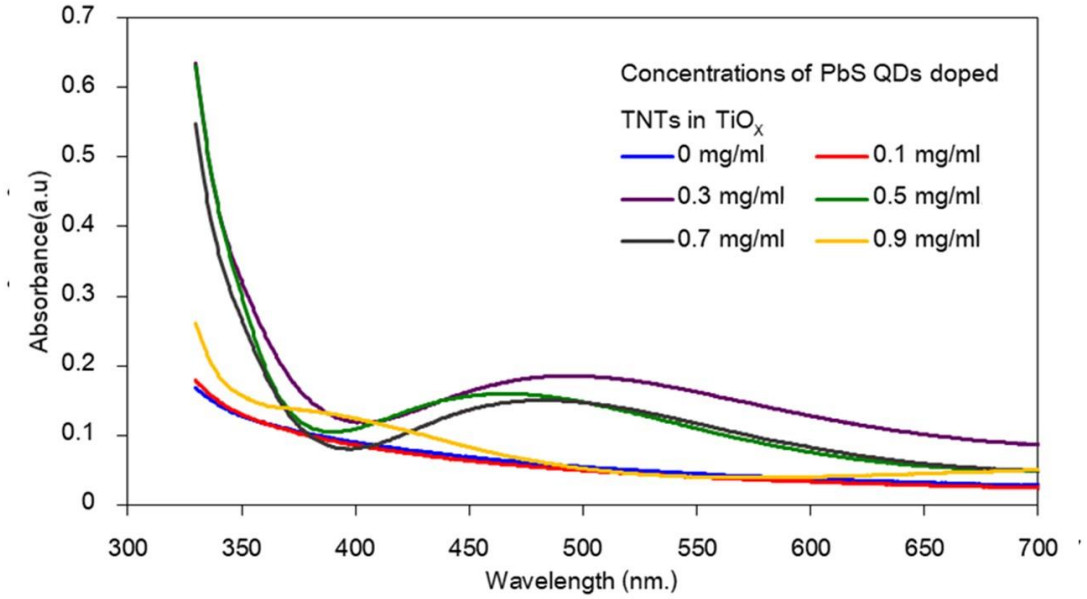

Figure 4.16 UV-Vis absorption spectra of ETL with various concentrations of PbS QDs doped TNTs in TiO_X.

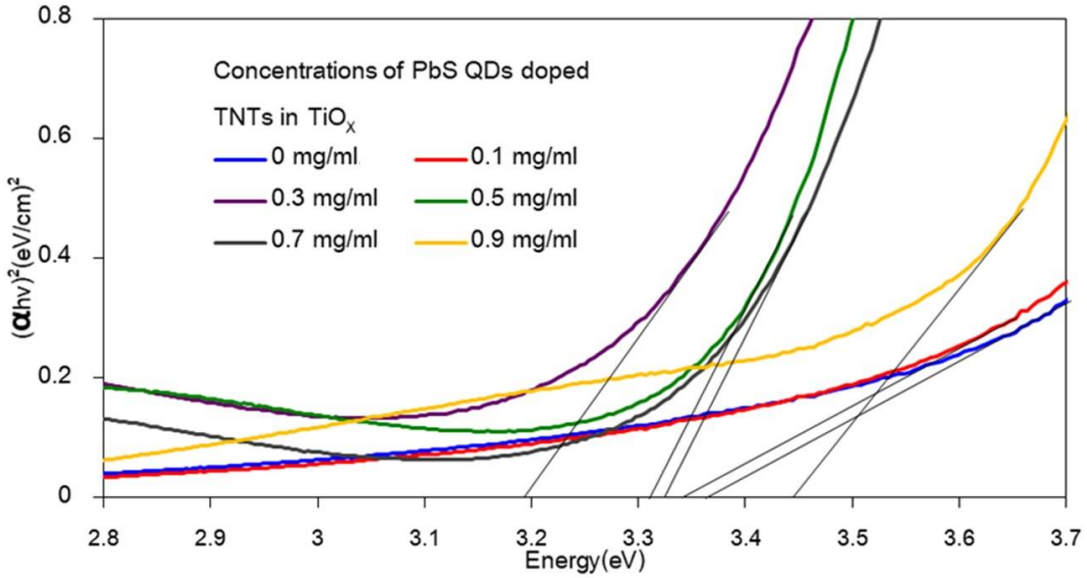

Figure 4.17 Energy band gaps of ETL with various concentrations of PbS QDs doped TNTs in TiO_X.

Table 4.5 summarizes the results of energy band gaps of ETL with various concentrations of PbS QDs doped TNTs in TiO_X, corresponding to Figure 4.17. Energy band gaps of about 3.37, 3.34, 3.19, 3.31, 3.33 and 3.44 eV of ETL prepared with concentrations of PbS QDs doped TNTs in TiO_X, as follows: No doping, 0.1, 0.3, 0.5, 0.7 and 0.9 mg/ml, respectively. Apparently, the concentration of 0.3 mg/ml of PbS QDs doped TNTs in TiO_X exhibits the most suitable electron transporting layer for perovskite solar cells due to its least energy band gap. It can be explained that, the low energy band gap leads to a high electron mobility because the gap between the conduction band and the valence band decreases [81]. According to Figure 4.18 which shows the energy level alignment of perovskite solar cell with TiO_2 as ETL and PbS as interlayer between perovskite and TiO_2, it can be seen that the presence of a PbS layer between TiO_2 and perovskite is expected to facilitate electron transfer from perovskite to TiO_2 [82].

So, the concentration of 0.3 mg/ml of PbS QDs doped TNTs in TiO_X is the optimized condition to fabricate ETL whose energy band gap is appropriate to be used as electron transporting layer for perovskite solar cells in order to enhance the power conversion efficiency of the solar cell device.

In this work, the conduction band and valence band of PbS QDs doped TNTs were not investigated but from previous study, carbon quantum dots (CQDs) were doped into TiO_2 in order to improve the efficiency of charge carrier extraction and injection between the TiO_2 and perovskite layers in perovskite device. According to Figure 4.19, the energy level alignment of the perovskite solar cell structure with the CQDs doped TiO_2 as ETL compared to TiO_2 as ETL is shown. It can be seen that the presence of the valence bands of TiO_2 and CQDs doped TiO_2 was calculated to be -7.25 and -7.35 eV, respectively. The conduction bands of TiO_2 and CQDs doped TiO_2 were calculated to be -3.95 and -4.05 eV, respectively. A higher conduction band of CQDs doped TiO_2 increases the driving force for electron injection from the conduction band of perovskite to its layer which results in enhancing the power conversion efficiency of the solar cell device [83]. Therefore, it is expected in our work that the behavior of PbS QDs doped TNTs as ETL is similar to that of the previous study.

จุฬาลงกรณ์มหาวิทยาลัย
Chulalongkorn University

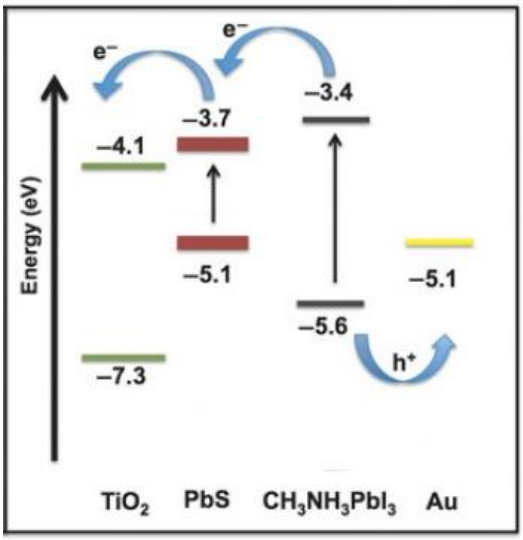

Figure 4.18 The energy level alignment in the hybrid perovskite solar cell [82].

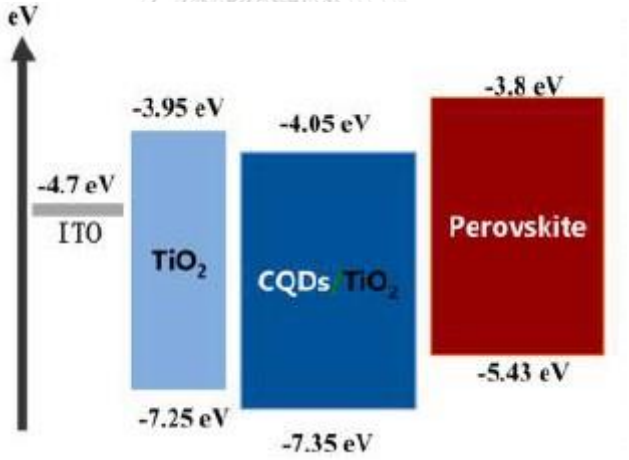

Figure 4.19 Energy diagram of TiO_2 and CQDs/TiO_2 as ETL in perovskite solar cells [83].

Table 4.5. Energy band gaps of ETL with various concentrations of PbS QDs doped TNTs in TiO_X.

Concentrations of PbS QDs doped TNTs in TiO_X (mg/ml)	Energy band gap (eV)
0	3.37
0.1	3.34
0.3	3.19
0.5	3.31
0.7	3.33
0.9	3.44

4.3.3 Photovoltaic properties of perovskite solar cells

Generally, perovskite solar cell structure is composed of an active layer between electrodes. To increase the PCE of perovskite solar cell, an electron transporting layer and a hole transporting layer are added before and after the active layer, respectively. For electron transporting layer, TiO_X (Nanotec; TiO_2) is commonly used as electron transporting material (ETM) but TiO_2 possesses a large band gap which limits the efficiency of energy conversion and low surface area. In this study, TNTs, synthesized via hydrothermal process from TiO_2 precursor with particle size of 25 nm, were applied and deposited onto the perovskite layer as the ETL, as can be seen in Figure 3.1, in order to achieve the enhanced power conversion efficiency of perovskite solar cell. Moreover, TNTs thin films were deposited with various concentrations of TNTs in TiO_X, as follows: 0, 0.1, 0.3, 0.5, 0.7 and 0.9 mg/ml.

จุฬาลงกรณ์มหาวิทยาลัย
Chulalongkorn University

Current density-voltage (J-V) curves of perovskite devices with a TNTs layer deposited at various concentrations of TNTs in TiO_X compared to the reference cell with TiO_X (Nanotec) layer as an ETL were measured under illumination of a solar simulator in air are shown in Figure 4.20. The photovoltaic parameters including open-circuit voltage (V_{oc}), short-circuit current (J_{sc}), fill factor (FF), and power conversion efficiency (PCE) of perovskite devices are also shown in Table 4.6. Among TNTs films deposited at different concentrations of TNTs in TiO_X, the concentrations of 0.3 mg/ml gives the best performance device. The PCE of perovskite device with concentrations of TNTs in TiO_X of 0.3 mg/ml is 12.82% which was calculated from V_{oc} of 1.12 V, J_{sc} of 20.94 mA/cm^2, and fill factor of 54.64%, which shows a better performance compared to the un-doped TNTs based solar cell was found to be V_{oc} of 1.12 V, J_{sc} of 18.56 mA/cm^2, fill factor of 58.52% and PCE of 12.18%. As the doping concentration of TNTs in TiO_X increases the J_{sc} and PCE are also increased due to the fact that TNTs has a high surface area leading to increasing of contact between the perovskite layer and electron transporting layer and its longer electron life time. Nevertheless, increasing the doping concentration of TNTs in TiO_X to 0.5, 0.7 and 0.9 mg/ml, the cell performance gradually decreases, respectively, as shown in Figure 4.21. This is attributed to the aggregation and precipitation of TNTs at high concentration, leading to a poor size distribution in which the particles start to agglomerate to increase in the particle sizes, resulting in a non-uniform film thickness [84]. According to Figure 4.22, it can be observed that the as-prepared solution of TNTs in TiO_X becomes slightly more cloudy with increasing concentration.

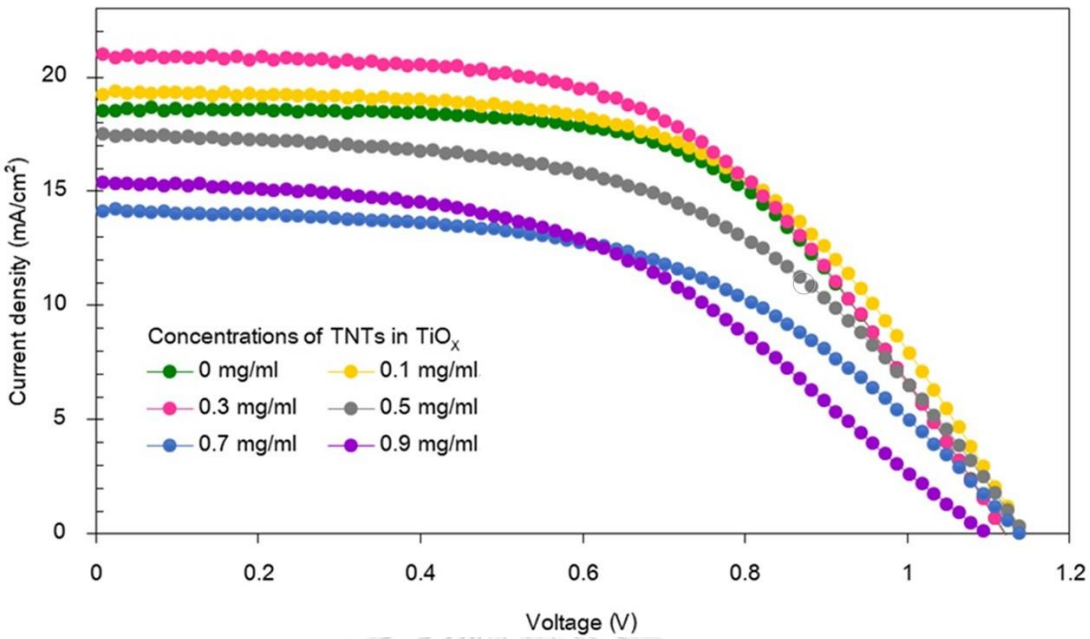

Figure 4.20 Photovoltic performance of perovskite devices with various concentrations of TNTs in TiO_X as ETL.

Table 4.6. The performance of perovskite devices with difference concentrations of TNTs in TiO_X as ETL.

Concentrations of TNTs in TiO_X as ETL. (mg/ml)	J_{sc} (mA/cm^2)	V_{oc} (V)	Fill Factor (%)	PCE (%)
0	18.56	1.12	58.52	12.18
0.1	19.32	1.14	56.51	12.49
0.3	20.94	1.12	54.64	12.82
0.5	17.49	1.14	52.27	10.47
0.7	14.18	1.13	51.80	8.37
0.9	15.42	1.09	46.73	7.91

จุฬาลงกรณ์มหาวิทยาลัย
Chulalongkorn University

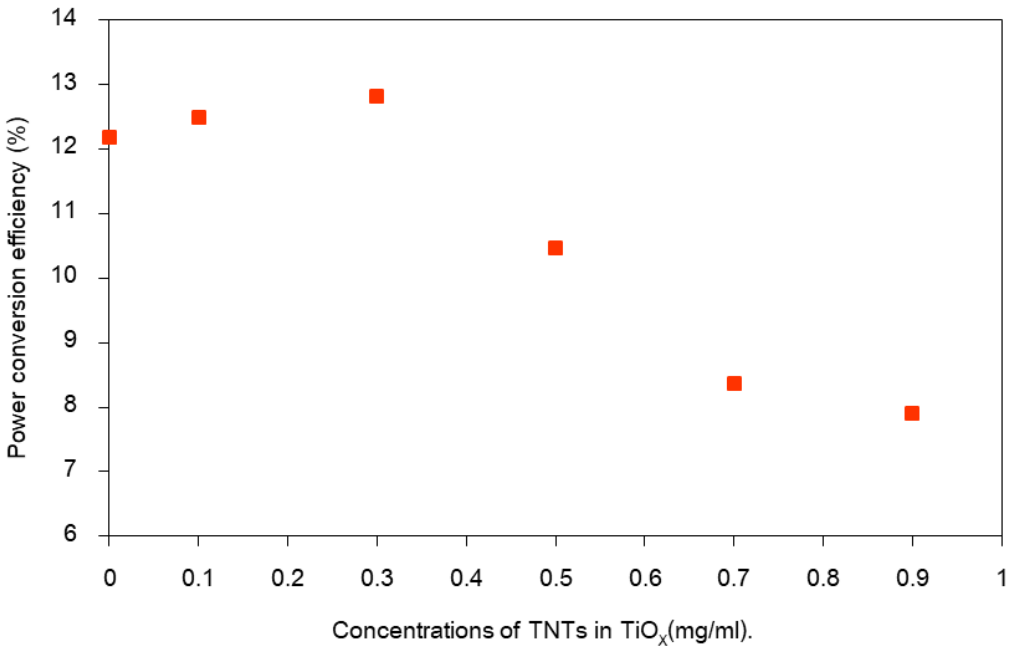

Figure 4.21 Power conversion efficiency of perovskite devices with various concentrations of TNTs in TiO_X as ETL.

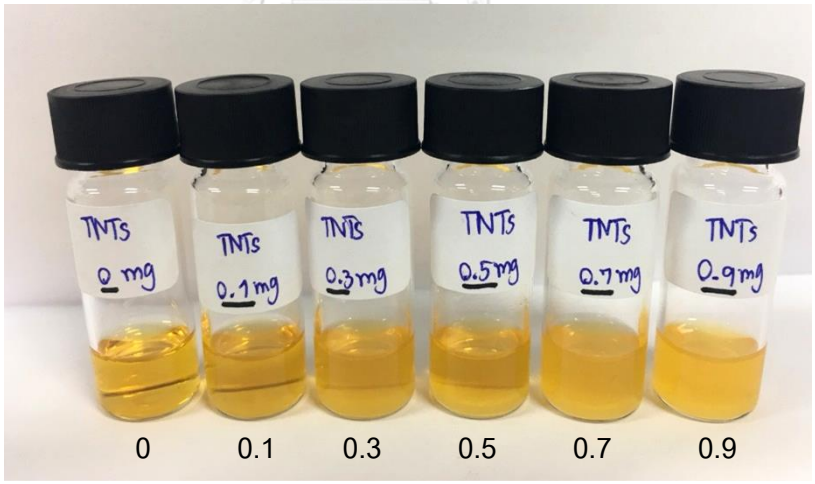

Figure 4.22 TNTs suspension with various concentrations of TNTs in TiO_X (mg/ml).

Furthermore, PbS QDs doped TNTs were applied and deposited onto the perovskite layer as the electron transporting layer (ETL), as can be seen in Figure 4.23, in order to achieve the enhanced power conversion efficiency of perovskite solar cell. PbS QDs doped TNTs thin films were deposited at various concentrations of PbS QDs doped TNTs in TiO_X, as follows: 0, 0.1, 0.3, 0.5, 0.7 and 0.9 mg/ml.

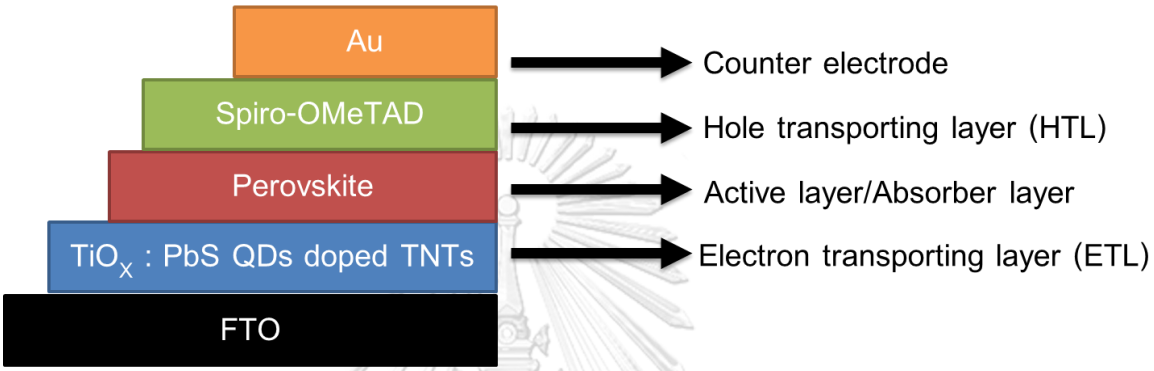

Figure 4.23 The conventional (n-i-p) planar perovskite solar cells.

The current density-voltage (J-V) characteristic of perovskite devices with a PbS QDs doped TNTs layer deposited at various concentrations of PbS QDs doped TNTs in TiO_X compared to the reference cell with TiO_X (Nanotec) layer as a ETM were acquired under illumination of a solar simulator in air are shown in Figure 4.24. The photovoltaic parameters including open-circuit voltage (V_{oc}), short-circuit current (J_{sc}), fill factor (FF), and power conversion efficiency (PCE) of perovskite devices are summarized in Table 4.7. It was observed that the concentrations of 0.3 mg/ml of PbS QDs doped TNTs in TiO_X base perovskite devices achieved the highest PCE of 14.95%, V_{oc} of 1.14 V, J_{sc} of 23.38 mA/cm^2, and fill factor of 56.03%. Whereas the un-doped PbS QDs doped TNTs (0 mg/ml) based perovskite devices shows less performance compared to the PbS QDs doped TNTs in TiO_X. Photovoltaic parameters for the devices with un-doped PbS QDs doped TNTs are PCE of 13.01%, V_{oc} of 1.14 V, J_{sc} of 20.98 mA/cm^2, and fill factor of 54.10%. However, increasing the doping concentration of PbS QDs doped TNTs in TiO_X to 0.5, 0.7 and 0.9 mg/ml, the cell performance decreases, respectively, as shown in Figure 4.25.

Similarly, this is because of the aggregation and precipitation of PbS QDs doped TNTs at high concentration, leading to a poor size distribution, in which the particles start to agglomerate to increase in the particle sizes, resulting in a non-uniform film thickness [84]. Accordingly, it can be observed in Figure 4.26 that the as-prepared solution of PbS QDs doped TNTs in TiO_X becomes slightly more cloudy with increasing concentration.

From previous sections, the PbS QDs doped TNTs in TiO_X as ETL based perovskite devices achieved the better performance compared to the un-doped and doped pure TNTs due to the effect of the small band gap of PbS QDs of about 0.41 eV, leading to a significant decrease of energy band gap of TNTs for enhancing the power conversion efficiency of the perovskite device.

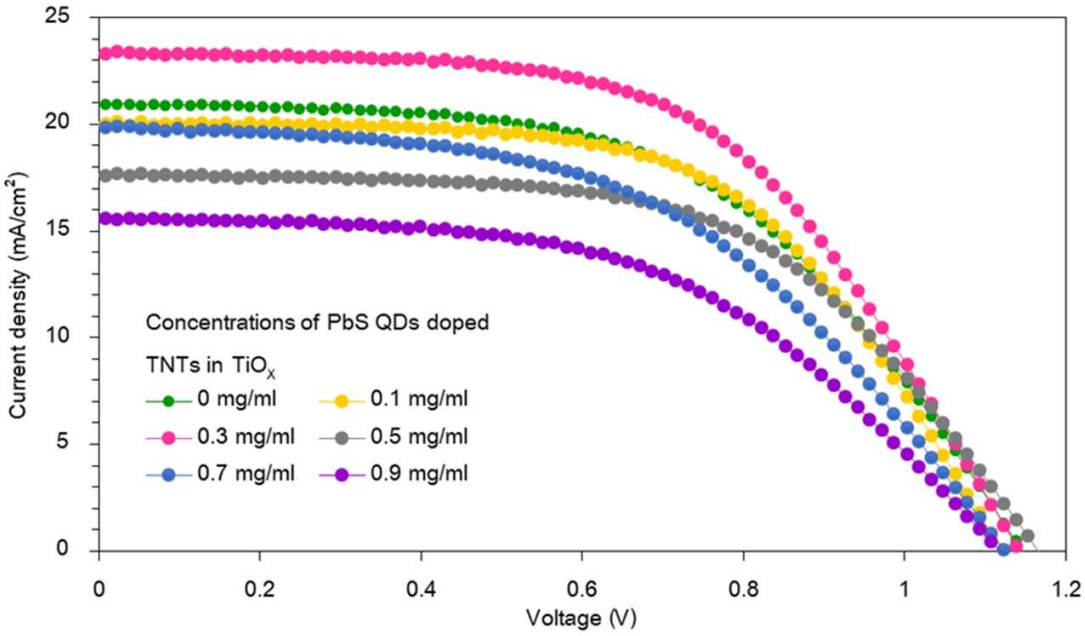

Figure 4.24 Photovoltic performance of perovskite devices with various concentrations of PbS QDs doped TNTs in TiO_X as ETL.

Table 4.7. The performance of perovskite devices with difference concentrations of PbS QDs doped TNTs in TiO_X as ETL.

.

Concentrations of PbS QDs doped TNTs in TiO_X as ETL. (mg/ml)	J_{sc} (mA/cm^2)	V_{oc} (V)	Fill Factor (%)	PCE (%)
0	20.98	1.14	54.10	13.01
0.1	20.07	1.12	58.69	13.21
0.3	23.38	1.14	56.03	14.95
0.5	17.65	1.16	57.61	11.86
0.7	19.91	1.12	50.50	11.31
0.9	15.60	1.11	52.25	9.11

จุฬาลงกรณ์มหาวิทยาลัย
CHULALONGKORN UNIVERSITY

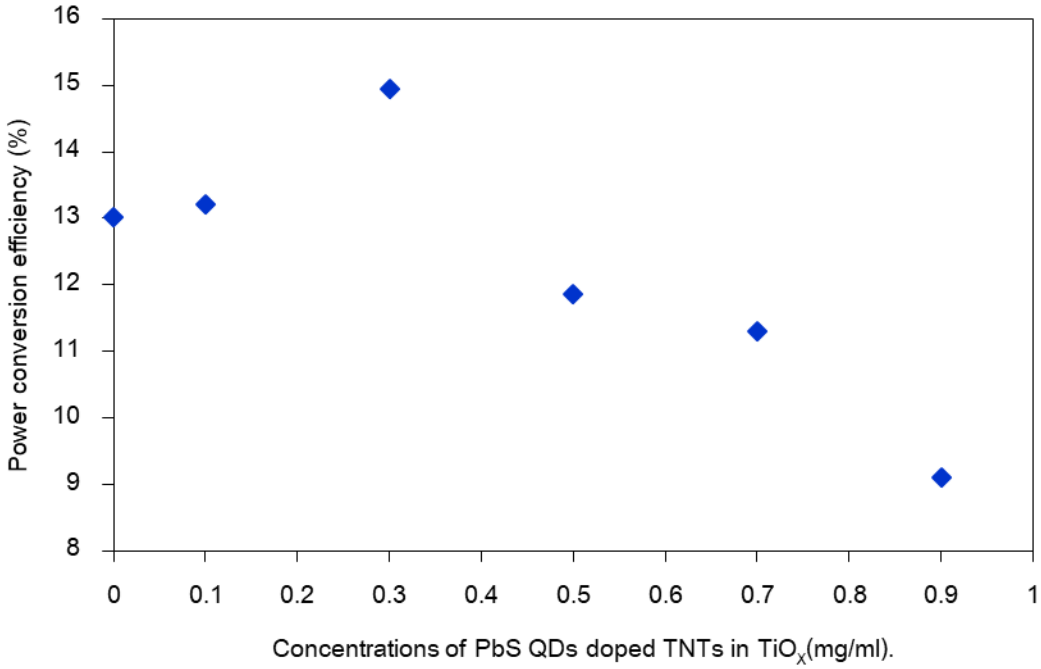

Figure 4.25 Power conversion efficiency of perovskite devices with various concentrations of PbS QDs doped TNTs in TiO_X as ETL.

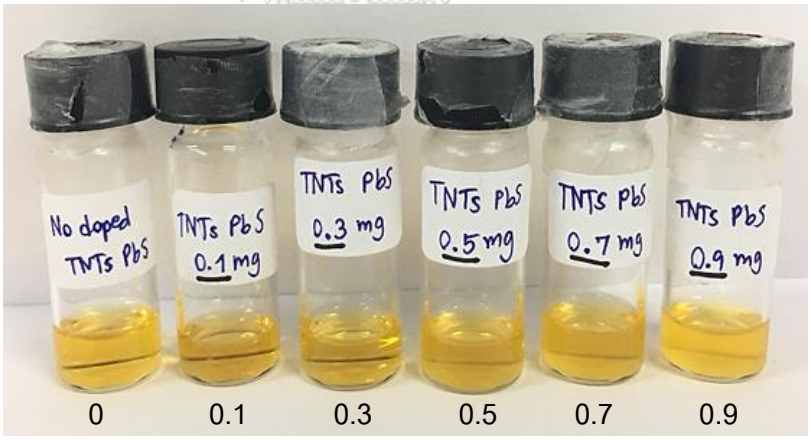

Figure 4.26 PbS QDs doped TNTs suspension with various concentrations of PbS QDs doped TNTs in TiO_X (mg/ml).

In addition, to confirm the accuracy of the PCE results, the external quantum efficiency (EQE) of the best solar cells un-doped, doped pure TNTs and PbS QDs doped TNTs were also measured by ORIEL Intelligent Quantum Efficiency (IQE) 200TM Measurement system established with the tunable light source. According to Figure 4.27, the EQE curve of these devices reveal a significant contribution at wavelength between 310 and 810 nm and a maximum EQE appearing around 510 nm. The perovskite device with PbS QDs doped TNTs prepared from the concentration of 0.3 mg/ml of PbS QDs doped TNTs in TiO_X shows a higher EQE of about 78% in the wavelength of 510-560 nm, which is consistent with its higher J_{SC}, shown in Figure 4.24, compared to the reference cell (un-doped) and doped pure TNTs [85].

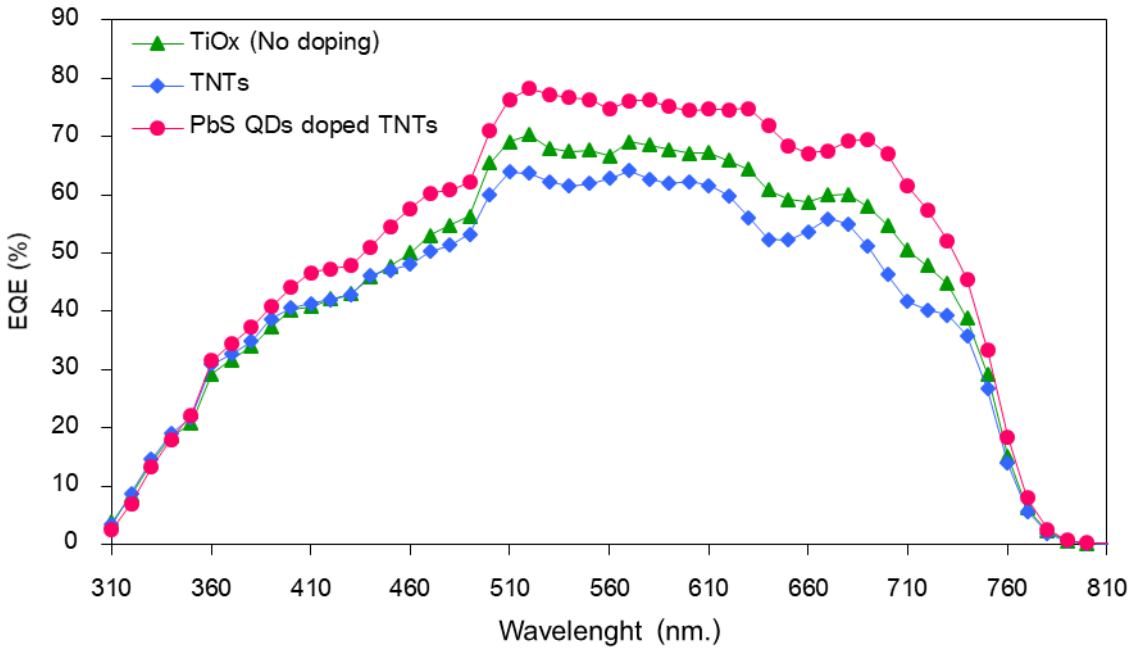

Figure 4.27 External Quantum efficiency curves of the best perovskite solar cells prepared with different in ETL.

In summary, the best power conversion efficiency of the perovskite device obtained from the ETL which was prepared from the concentrations of 0.3 mg/ml of PbS QDs doped TNTs in TiO_X is 14.95%, which is about 15% higher than those with un-doped PbS QDs doped TNTs in TiO_X (Reference Cell), as shown in Figure 4.28.

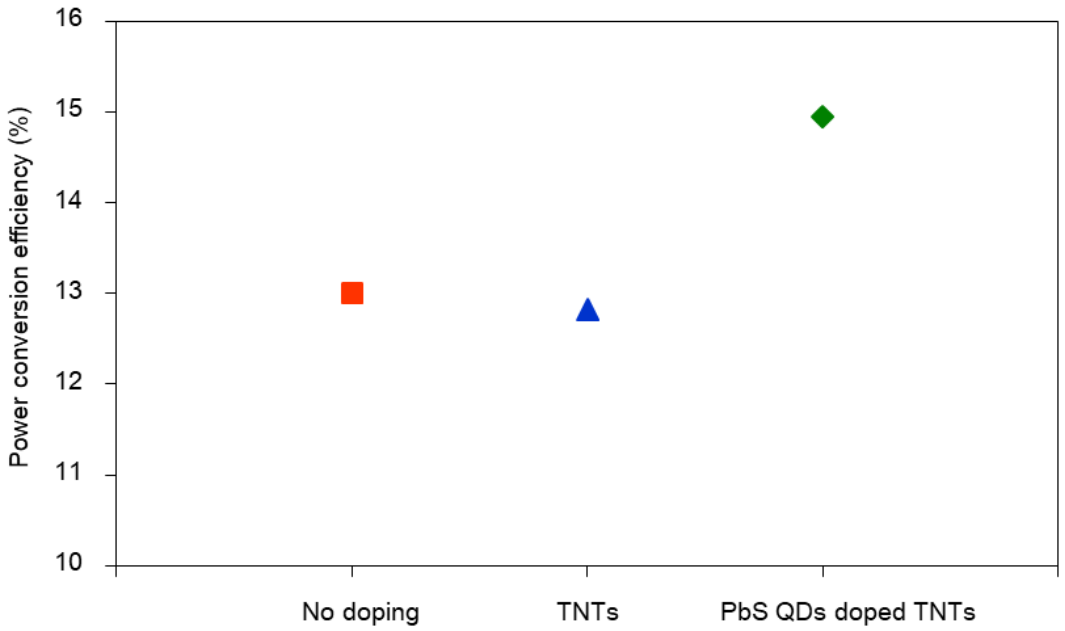

Figure 4.28 Power conversion efficiency of the best perovskite solar cells prepared with different in ETL.

จุฬาลงกรณ์มหาวิทยาลัย
Chulalongkorn University

CHAPTER 5
CONCLUSION

5.1 Conclusions

1. TNTs were successfully synthesized via hydrothermal process from various particle sizes of TiO_2 precursors. The highest surface area of TNTs of 312.39 m^2/g with a uniform morphology was obtained from TiO_2 precursor with particle size of 25 nm, which was suitable for using as the electron transporting layer (ETL). High surface area TNTs offer the enhanced interfacial area for doping of PbS QDs, which ultimately improved the property of ETL and resulted in the enhanced power conversion efficiency of perovskite solar cell.

2. The energy band gap of PbS QDs doped TNTs was determined to be about 2.97 eV, which was slightly decreased from that of pure TNTs. Therefore, doping with PbS QDs did not significantly change the optical property of ETL. A change in valence and conduction energy bands of PbS Qds doped TNTs was expected to enhance the power conversion efficiency of perovskite solar cell.

3. The best power conversion efficiency of the perovskite device obtained in this work is 14.95%, which is about 15% higher than that of perovskite solar cell with un-doped PbS QDs doped TNTs in TiO_X (Reference Cell).

4. The best performance of perovskite solar cell was obtained from PbS QDs doped TNTs ETL which was prepared from the concentration of 0.3 mg/ml of PbS QDs doped TNTs in TiO_X solution.

5.2 Recommendations for the future work.

1. To investigate and find the optimized operating condition based on various ratios of PbS QDs doped TNTs: TiO_X as the electron transporting layer for conventional planar perovskite solar cells in terms of the solar cell performance.

2. Characterization of conduction band and valence band levels by Ultraviolet photoelectron spectroscopy (UPS) should be investigated, in order to observe a change in valence and conduction energy bands of pure TNTs and PbS QDs doped TNTs. This study would help elucidate the mechanism of how the power conversion efficiency is improved.

จุฬาลงกรณ์มหาวิทยาลัย
CHULALONGKORN UNIVERSITY

REFERENCES

1. Lai, C.S., et al., *A comprehensive review on large-scale photovoltaic system with applications of electrical energy storage.* Renewable and Sustainable Energy Reviews, 2017. **78**: p. 439-451.

2. Assadi, M.K., et al., *Recent progress in perovskite solar cells.* Renewable and Sustainable Energy Reviews, 2017.

3. Stuckelberger, M., et al., *Review: Progress in solar cells from hydrogenated amorphous silicon.* Renewable and Sustainable Energy Reviews, 2017. **76**: p. 1497-1523.

4. Yan, J. and B.R. Saunders, *Third-generation solar cells: a review and comparison of polymer:fullerene, hybrid polymer and perovskite solar cells.* RSC Advances, 2014. **4**(82): p. 43286-43314.

5. Mohammad Bagher, A., *Types of Solar Cells and Application.* American Journal of Optics and Photonics, 2015. **3**(5): p. 94.

6. Wright, M. and A. Uddin, *Organic—inorganic hybrid solar cells: A comparative review.* Solar Energy Materials and Solar Cells, 2012. **107**: p. 87-111.

7. *Effect of TiO2 Nanofiber Density on Organic-Inorganic Based Hybrid Solar Cells (RESEARCH NOTE).* International Journal of Engineering, 2014. **27**(7 (A)).

8. Ubani, C.A., M.A. Ibrahim, and M.A.M. Teridi, *Moving into the domain of perovskite sensitized solar cell.* Renewable and Sustainable Energy Reviews, 2017. **72**: p. 907-915.

9. Wang, D., et al., *Stability of perovskite solar cells.* Solar Energy Materials and Solar Cells, 2016. **147**: p. 255-275.

10. Kojima, A., et al., *Organometal halide perovskites as visible-light sensitizers for photovoltaic cells.* J Am Chem Soc, 2009. **131**(17): p. 6050-1.

11. Yin, W., et al., *Recent Advances in Interface Engineering for Planar Heterojunction Perovskite Solar Cells.* Molecules, 2016. **21**(7).

จุฬาลงกรณ์มหาวิทยาลัย
CHULALONGKORN UNIVERSITY

12. Habibi, M., et al., *Progress in emerging solution-processed thin film solar cells – Part II: Perovskite solar cells.* Renewable and Sustainable Energy Reviews, 2016. **62**: p. 1012-1031.

13. Lee, J.-W. and N.-G. Park, *Two-step deposition method for high-efficiency perovskite solar cells.* MRS Bulletin, 2015. **40**(08): p. 654-659.

14. Wang, P., et al., *Planar Heterojunction Perovskite Solar Cells with TiO2 Scaffold in Perovskite Film.* Electrochimica Acta, 2017. **227**: p. 180-184.

15. Im, J.H., et al., *Growth of CH3NH3PbI3 cuboids with controlled size for high-efficiency perovskite solar cells.* Nat Nanotechnol, 2014. **9**(11): p. 927-32.

16. Bi, D., et al., *Using a two-step deposition technique to prepare perovskite (CH3NH3PbI3) for thin film solar cells based on ZrO2 and TiO2 mesostructures.* RSC Advances, 2013. **3**(41): p. 18762.

17. Du, K., et al., *PbS Quantum Dots Sensitized TiO2Nanotubes for Photocurrent Enhancement.* Journal of The Electrochemical Society, 2015. **162**(10): p. E251-E257.

18. Yi, J., et al., *PbS Quantum Dots Sensitized TiO₂ Solar Cells Prepared by Successive Ionic Layer Absorption and Reaction with Different Adsorption Layers.* Journal of Nanoscience and Nanotechnology, 2016. **16**(4): p. 3904-3908.

19. Ranabhat, K., et al., *An introduction to solar cell technology.* Istrazivanja i projektovanja za privredu, 2016. **14**(4): p. 481-491.

20. Kumavat, P.P., P. Sonar, and D.S. Dalal, *An overview on basics of organic and dye sensitized solar cells, their mechanism and recent improvements.* Renewable and Sustainable Energy Reviews, 2017. **78**: p. 1262-1287.

21. Litvinenko, S.V., A.V. Kozinetz, and V.A. Skryshevsky, *Concept of photovoltaic transducer on a base of modified p–n junction solar cell.* Sensors and Actuators A: Physical, 2015. **224**: p. 30-35.

22. Shah, A.V., et al., *Thin-film silicon solar cell technology.* Progress in Photovoltaics: Research and Applications, 2004. **12**(23): p. 113-142.

จุฬาลงกรณ์มหาวิทยาลัย
Chulalongkorn University

23. Lee, T.D. and A.U. Ebong, *A review of thin film solar cell technologies and challenges.* Renewable and Sustainable Energy Reviews, 2017. **70**: p. 1286-1297.

24. Gong, J., et al., *Review on dye-sensitized solar cells (DSSCs): Advanced techniques and research trends.* Renewable and Sustainable Energy Reviews, 2017. **68**: p. 234-246.

25. Antohe, S., et al., *A critical review of photovoltaic cells based on organic monomeric and polymeric thin film heterojunctions.* Thin Solid Films, 2017. **642**: p. 219-231.

26. Kusuma, J. and R. Geetha Balakrishna, *A review on electrical characterization techniques performed to study the device performance of quantum dot sensitized solar cells.* Solar Energy, 2018. **159**: p. 682-696.

27. Kumar Moluguri, N., C. Rama Murthy, and V. Harshavardhan, *Solar Energy System and Design - Review.* Materials Today: Proceedings, 2016. **3**(10): p. 3637-3645.

28. Conibeer, G., *Third-generation photovoltaics.* Materials Today, 2007. **10**(11): p. 42-50.

29. Ali, N., et al., *Advances in nanostructured thin film materials for solar cell applications.* Renewable and Sustainable Energy Reviews, 2016. **59**: p. 726-737.

30. Yin, W.-J., et al., *Halide perovskite materials for solar cells: a theoretical review.* Journal of Materials Chemistry A, 2015. **3**(17): p. 8926-8942.

31. Fan, J., B. Jia, and M. Gu, *Perovskite-based low-cost and high-efficiency hybrid halide solar cells.* Photonics Research, 2014. **2**(5): p. 111.

32. Anaya, M., et al., *ABX 3 Perovskites for Tandem Solar Cells.* Joule, 2017. **1**(4): p. 769-793.

33. Peng, G., X. Xu, and G. Xu, *Hybrid Organic-Inorganic Perovskites Open a New Era for Low-Cost, High Efficiency Solar Cells.* Journal of Nanomaterials, 2015. **2015**: p. 1-10.

34. Song, T.-B., et al., *Perovskite solar cells: film formation and properties.* Journal of Materials Chemistry A, 2015. **3**(17): p. 9032-9050.

จุฬาลงกรณ์มหาวิทยาลัย
Chulalongkorn University

35. Marinova, N., S. Valero, and J.L. Delgado, *Organic and perovskite solar cells: Working principles, materials and interfaces.* J Colloid Interface Sci, 2017. **488**: p. 373-389.

36. Salim, T., et al., *Perovskite-based solar cells: impact of morphology and device architecture on device performance.* Journal of Materials Chemistry A, 2015. **3**(17): p. 8943-8969.

37. Zhou, X., et al., *Recent theoretical progress in the development of perovskite photovoltaic materials.* Journal of Energy Chemistry, 2017.

38. Bergmann, V.W., et al., *Real-space observation of unbalanced charge distribution inside a perovskite-sensitized solar cell.* Nat Commun, 2014. **5**: p. 5001.

39. Cui, J., et al., *Recent progress in efficient hybrid lead halide perovskite solar cells.* Sci Technol Adv Mater, 2015. **16**(3): p. 036004.

40. Petrović, M., V. Chellappan, and S. Ramakrishna, *Perovskites: Solar cells & engineering applications – materials and device developments.* Solar Energy, 2015. **122**: p. 678-699.

41. Kumnorkaew, P. and J.F. Gilchrist, *Effect of nanoparticle concentration on the convective deposition of binary suspensions.* Langmuir, 2009. **25**(11): p. 6070-5.

42. Zheng, J., et al., *Spin-coating free fabrication for highly efficient perovskite solar cells.* Solar Energy Materials and Solar Cells, 2017. **168**: p. 165-171.

43. Kandjani, S.A., S. Mirershadi, and A. Nikniaz, *Inorganic–Organic Perovskite Solar Cells.* 2015.

44. Hu, Z., et al., *Performance of polymer solar cells fabricated by dip coating process.* Solar Energy Materials and Solar Cells, 2012. **99**: p. 221-225.

45. Scriven, L.E., *Physics and Applications of DIP Coating and Spin Coating.* MRS Proceedings, 2011. **121**.

46. Bera, S., et al., *Methodologies of Application of Sol-Gel Based Solution onto Substrate: A Review*. Vol. 3. 2016. 0-0.

47. *<Investigations into Convective Deposition from Fundamental and Ap.pdf>.*

จุฬาลงกรณ์มหาวิทยาลัย
CHULALONGKORN UNIVERSITY

48. Jung, H.S. and N.G. Park, *Perovskite solar cells: from materials to devices.* Small, 2015. **11**(1): p. 10-25.

49. Djurišić, A.B., et al., *Perovskite solar cells - An overview of critical issues.* Progress in Quantum Electronics, 2017. **53**: p. 1-37.

50. Chen, X. and A. Selloni, *Introduction: titanium dioxide (TiO2) nanomaterials.* Chem Rev, 2014. **114**(19): p. 9281-2.

51. Sun, K.C., M.B. Qadir, and S.H. Jeong, *Hydrothermal synthesis of TiO2 nanotubes and their application as an over-layer for dye-sensitized solar cells.* RSC Advances, 2014. **4**(44): p. 23223.

52. Pugazhenthiran, N., S. Murugesan, and S. Anandan, *High surface area Ag-TiO2 nanotubes for solar/visible-light photocatalytic degradation of ceftiofur sodium.* J Hazard Mater, 2013. **263 Pt 2**: p. 541-9.

53. Nakata, K. and A. Fujishima, *TiO2 photocatalysis: Design and applications.* Journal of Photochemistry and Photobiology C: Photochemistry Reviews, 2012. **13**(3): p. 169-189.

54. Lee, S.-Y. and S.-J. Park, *TiO2 photocatalyst for water treatment applications.* Journal of Industrial and Engineering Chemistry, 2013. **19**(6): p. 1761-1769.

55. Wang, Y., et al., *Review of the progress in preparing nano TiO2: an important environmental engineering material.* J Environ Sci (China), 2014. **26**(11): p. 2139-77.

56. Pelaez, M., et al., *A review on the visible light active titanium dioxide photocatalysts for environmental applications.* Applied Catalysis B: Environmental, 2012. **125**: p. 331-349.

57. Pang, Y.L., et al., *A critical review on the recent progress of synthesizing techniques and fabrication of TiO2-based nanotubes photocatalysts.* Applied Catalysis A: General, 2014. **481**: p. 127-142.

58. Jitputti, J., Y. Suzuki, and S. Yoshikawa, *Synthesis of TiO2 nanowires and their photocatalytic activity for hydrogen evolution.* Catalysis Communications, 2008. **9**(6): p. 1265-1271.

จุฬาลงกรณ์มหาวิทยาลัย
CHULALONGKORN UNIVERSITY

59. Viriya-Empikul, N., et al., *A step towards length control of titanate nanotubes using hydrothermal reaction with sonication pretreatment.* Nanotechnology, 2008. **19**(3): p. 035601.

60. Camposeco, R., et al., *Synthesis, characterization and photocatalytic activity of TiO 2 nanostructures: Nanotubes, nanofibers, nanowires and nanoparticles.* Catalysis Today, 2016. **266**: p. 90-101.

61. Ou, H. and S. Lo, *Review of titania nanotubes synthesized via the hydrothermal treatment: Fabrication, modification, and application.* Separation and Purification Technology, 2007. **58**(1): p. 179-191.

62. Liu, N., et al., *A review on TiO2-based nanotubes synthesized via hydrothermal method: Formation mechanism, structure modification, and photocatalytic applications.* Catalysis Today, 2014. **225**: p. 34-51.

63. Nakahira, A., T. Kubo, and C. Numako, *Formation mechanism of TiO2-derived titanate nanotubes prepared by the hydrothermal process.* Inorg Chem, 2010. **49**(13): p. 5845-52.

64. Li, Y., et al., *Efficient inorganic solid solar cells composed of perovskite and PbS quantum dots.* Nanoscale, 2015. **7**(21): p. 9902-7.

65. Ratanatawanate, C., Y. Tao, and K.J. Balkus, *Photocatalytic Activity of PbS Quantum Dot/TiO2 Nanotube Composites.* The Journal of Physical Chemistry C, 2009. **113**(24): p. 10755-10760.

66. Ratanatawanate, C., C. Xiong, and K.J. Balkus, *Fabrication of PbS Quantum Dot Doped TiO2 Nanotubes.* ACS Nano, 2008. **2**(8): p. 1682-1688.

67. Bijl, H.J.v.d., *Theory and Operating Characteristics of the Thermionic Amplifier.* Proceedings of the Institute of Radio Engineers, 1919. **7**(2): p. 97-128.

68. Rothemund, R., et al., *External quantum efficiency analysis of Si solar cells with II-VI nanocrystal luminescent down-shifting layers.* Energy Procedia, 2011. **10**: p. 83-87.

69. Luka, T., S. Eiternick, and M. Turek, *Rapid Testing of External Quantum Efficiency using LED Solar Simulators.* Energy Procedia, 2015. **77**: p. 113-118.

จุฬาลงกรณ์มหาวิทยาลัย
Chulalongkorn University

70. Im, J.-H., H.-S. Kim, and N.-G. Park, *Morphology-photovoltaic property correlation in perovskite solar cells: One-step versus two-step deposition of CH3NH3PbI3*. APL Materials, 2014. **2**(8): p. 081510.

71. Gao, X., et al., *Enhanced photovoltaic performance of perovskite CH3NH3PbI3 solar cells with freestanding TiO2 nanotube array films.* Chemical Communications, 2014. **50**(48): p. 6368-6371.

72. Huang, Y., J. Wu, and D. Gao, *High-efficiency perovskite solar cells based on anatase TiO2 nanotube arrays.* Thin Solid Films, 2016. **598**: p. 1-5.

73. Yang, Y. and W. Wang, *Effects of incorporating PbS quantum dots in perovskite solar cells based on CH3NH3PbI3*. Journal of Power Sources, 2015. **293**: p. 577-584.

74. Tsai, C.-C. and H. Teng, *Regulation of the Physical Characteristics of Titania Nanotube Aggregates Synthesized from HT Treatment*. Vol. 16. 2004.

75. Zeng, Y.-Z., et al., *Study on the Preparation of Nanosized Titanium Dioxide with Tubular Structure by Hydrothermal Method and Their Photocatalytic Activity.* International Journal of Chemical Engineering and Applications, 2014. **5**(3): p. 234-239.

76. Malashchonak, M.V., et al., *Monoclinic bismuth vanadate band gap determination by photoelectrochemical spectroscopy.* Materials Chemistry and Physics, 2017. **201**: p. 189-193.

77. Papagiorgis, P., et al., *The Influence of Doping on the Optoelectronic Properties of PbS Colloidal Quantum Dot Solids*. Scientific Reports, 2016. **6**: p. 18735.

78. Wang, Z., et al., *Enhanced performance of perovskite solar cells by ultraviolet-ozone treatment of mesoporous TiO2.* Applied Surface Science, 2018. **436**: p. 596-602.

79. Li, Y., et al., *Defective TiO2 with high photoconductive gain for efficient and stable planar heterojunction perovskite solar cells.* Nature Communications, 2016. **7**: p. 12446.

80. Sahoo, A., et al., *Optical and electrical properties of sol-gel spin coated titanium dioxide thin films.* IOP Conference Series: Materials Science and Engineering, 2017. **225**: p. 012021.

จุฬาลงกรณ์มหาวิทยาลัย
Chulalongkorn University

81. Zhang, Z.L., et al., *Enhancement of Perovskite Solar Cells Efficiency using N-Doped TiO2 Nanorod Arrays as Electron Transfer Layer.* Nanoscale Res Lett, 2017. **12**(1): p. 43.

82. Etgar, L., *Hole-transport material-free perovskite-based solar cells.* MRS Bulletin, 2015. **40**(08): p. 674-680.

83. Li, H., et al., *Carbon Quantum Dots/TiOx Electron Transport Layer Boosts Efficiency of Planar Heterojunction Perovskite Solar Cells to 19.* Nano Lett, 2017. **17**(4): p. 2328-2335.

84. K, V., M.S. Pandian, and R. P, *Photovoltaic performance of Ag-doped CdS quantum dots for solar cell application.* Materials Research Bulletin, 2017. **94**: p. 371-377.

85. Chen, P.-Y. and S.-H. Yang, *Improved efficiency of perovskite solar cells based on Ni-doped ZnO nanorod arrays and Li salt-doped P3HT layer for charge collection.* Optical Materials Express, 2016. **6**(11): p. 3651.

จุฬาลงกรณ์มหาวิทยาลัย
Chulalongkorn University

APPENDIX

จุฬาลงกรณ์มหาวิทยาลัย
Chulalongkorn University

VITA

Mr.Natthapat Rattanwichai was born on May 24, 1993 in Tak, Thailand. He attended at Takphitthayakhom School, Tak for high school. In 2015, he graduated from Chemical Technology, Chulalongkorn University in Bachelor of Science (Chemical Engineering). After that, he continued to study in Center of Excellence in Particle Technology at Department of Chemical Engineering, Faculty of Engineering, Chulalongkorn University, as a Master's degree student.

จุฬาลงกรณ์มหาวิทยาลัย
CHULALONGKORN UNIVERSITY